1970

Scattering Parameters of VHF Semiconductor Devices

Young Dae Kim

Recommended Citation

Kim, Young Dae, "Scattering Parameters of VHF Semiconductor Devices" (1970). *Electronic Theses and Dissertations*. 3793.
https://openprairie.sdstate.edu/etd/3793

SCATTERING PARAMETERS OF VHF SEMICONDUCTOR DEVICES

BY

YOUNG DAE KIM

A thesis submitted
in partial fulfillment of the requirements for the
degree Master of Science, Department of
Electrical Engineering, South Dakota
State University

January, 1970

SCATTERING PARAMETERS OF VHF
SEMICONDUCTOR DEVICES

This thesis is approved as a creditable and independent investigation by a candidate for the degree, Master of Science, and is acceptable as meeting the thesis requirements for this degree, but without implying that the conclusions reached by the candidate are necessarily the conclusions of the major department.

Thesis Adviser	Date
Head, Electrical Engineering Department	Date

ACKNOWLEDGMENTS

The author wishes to express his appreciation and gratitude to Dr. Virgil G. Ellerbruch and Dr. Franklin C. Fitchen, whose guidance and advice made this investigation possible, and to the National Science Foundation for partial financial support of this investigation.

Y.D.K.

TABLE OF CONTENTS

LIST OF TABLES

LIST OF FIGURES

LIST OF FIGURES (continued)

Figure Page

LIST OF FIGURES (continued)

CHAPTER I

INTRODUCTION

Since Campbell and Foster[1] first used scattering parameters in studying the properties of ideal transformer networks, much work has been done with scattering parameters in the analysis of microwave circuits and general lumped parameter networks. An excellent summary for microwave circuits appears in Montgomery, Dicke, and Purcell.[2] Application of scattering parameters to network synthesis was attempted by Oono and Yasuura.[3] Youla[4] also extended scattering parameter theory by complex normalization. He and Penfield[5] later applied scattering parameters in analyzing negative resistance amplifiers in conjunction with the development of the tunnel diode.

The rapid development of high-frequency technologies in the past decade requires improved high-frequency measurement techniques because of the difficulty in measuring commonly-accepted immittance parameters at frequencies above 100 MHz. This difficulty stemmed from the fact that in measuring the h-, y-, or z-parameters the circuit is either in a short or open condition. The scattering parameter measurement technique is one way of overcoming this problem since the measurement circuit employs finite terminations and therefore provides more stable wide-band measurements.

Along with the introduction of the scattering parameter measurement technique in high-frequency transistor measurements, attempts were made to characterize the transistors with directly measurable scattering parameters. Lange,[6] Weinert,[7] Anderson,[8] Froehner,[9] and Bodway[10] are among those engineers who introduced the use of scattering parameters in transistor circuit design. An excellent analysis of transistor circuit design with generalized 2-port scattering parameters is given by Bodway. At the present time, the scattering parameter technique is one of the standard methods used for high-frequency transistor characterization and design.

The major advantages of the scattering parameter method for high-frequency transistor measurements and characterization are:

1. A very stable wide-band measurement, which allows wide-band swept-frequency measurement, can be made.
2. Matching networks are also measured in terms of scattering parameters for reasons of simplicity at low frequencies, and because of necessity at high frequencies. Thus, unified circuit design is possible with easily measurable scattering parameters.
3. Scattering parameter circuit design is more closely

related to power relations than any other design method. This gives a clearer understanding of amplifier design procedures.

4. The signal flow graph[11] can be easily employed to visualize the scattering parameter design procedures.

In addition to these advantages, the scattering parameter method has a few disadvantages. Since they are parameters derived for traveling waves, voltage and current relationships are not easily seen. Engineers are not as familiar with scattering parameters as they are with immittance parameters. These disadvantages can be overcome when one becomes familiar with scattering parameters and can relate them to existing immittance parameters of the equivalent circuits of the device.

As an effort to fill the gap between conventional methods and the scattering parameter method in high-frequency semiconductor device measurement and characterization, this paper aims at the following goals:

1. To assemble a measuring system to accurately measure 2-, 3-, and 4-port scattering parameters of semiconductor devices at VHF frequencies.
2. To measure scattering parameters of bipolar transistors, single- and dual-gate MOSFETs, and an IC differential amplifier.

3. To explain the behavior of measured scattering parameters of high-frequency semiconductor devices with their equivalent circuits.
4. To apply the scattering parameter method in obtaining equivalent circuit parameters.
5. To analyze mathematically and experimentally the scattering parameter relations between a dual-gate MOSFET and a single-gate MOSFET, and between an IC differential amplifier and its constituent transistors.

Information of this kind has not appeared in the literature. In addition to these, scattering parameters are introduced from the classical transmission line theory and expanded utilizing convenient signal flow graphs. Mixer scattering parameters are also first suggested in this paper as an extension of linear 2-port parameters.

The measurements were made with a modified standard set up[12] at the Microwave Laboratory of the South Dakota State University.

CHAPTER II

SCATTERING PARAMETERS

A. Introduction to S-Parameters[13]

The voltages and currents on a transmission line are generally analyzed as two traveling waves, reflected and incident. These two waves propagate in opposite directions along the line.

When this analysis method is used for a linear n-port network where the access terminals of each port are connected to a transmission line that is equipped with a device designed to sample these two waves, the terminal voltages and currents at each port can be represented by the amplitudes and phase angles.

Voltage and current equations for the ith port can be written as

$$v_i = v_i^+ + v_i^-$$

$$i_i = i_i^+ - i_i^- \qquad (2\text{-}1)$$

The superscripts (+) and (-) stand for inward (toward the network) and outward (away from the network) traveling waves at the ith port, respectively. V_i and i_i are the terminal voltage and current at the ith port. (Refer to Fig. 2-1.)

The characteristic impedance of a transmission line

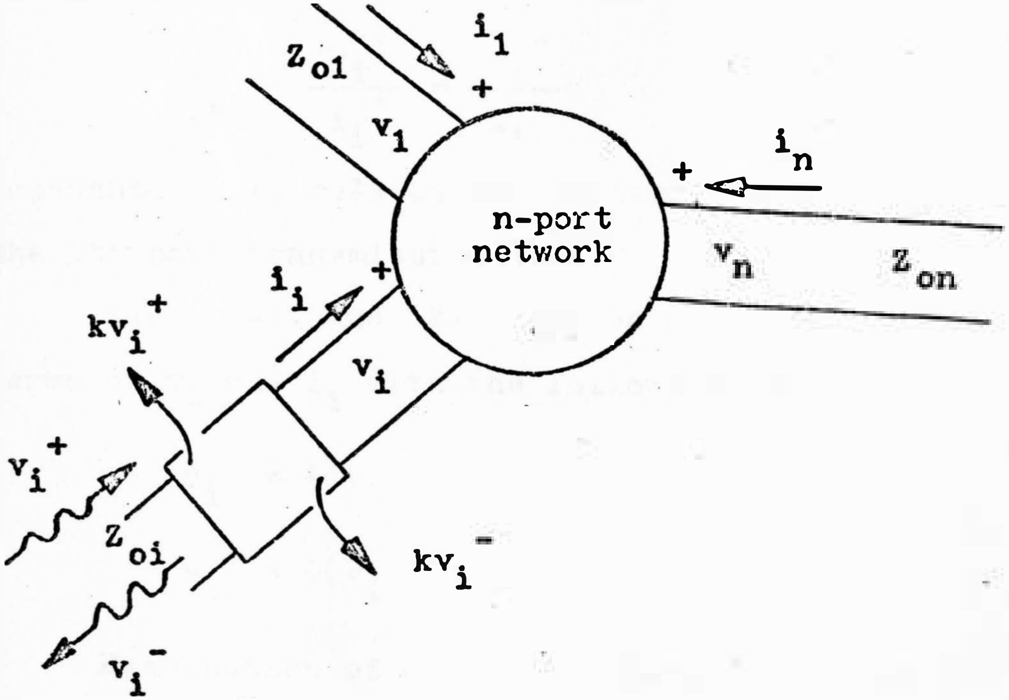

Fig. 2-1. An n-port network.

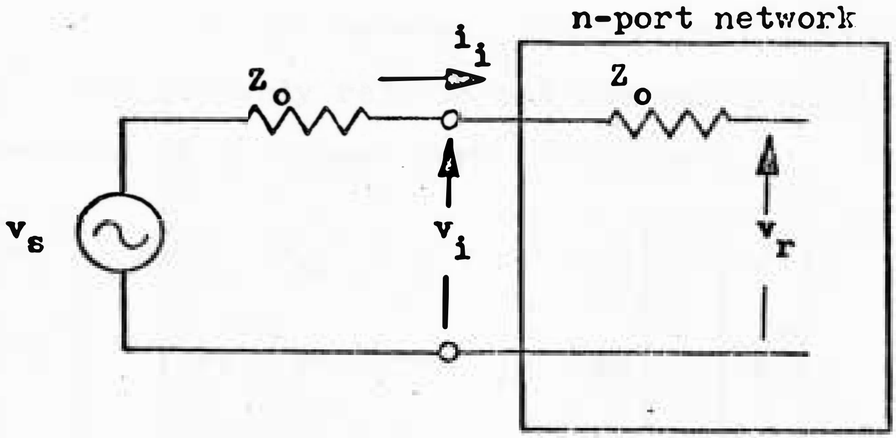

Fig. 2-2. A model for Eq. (2-7).

is defined as

$$Z_{oi} = \frac{v_i^+}{i_i^+} = \frac{v_i^-}{i_i^-} \qquad (2\text{-}2)$$

Impedance, Z_{oi}, relates the voltage and current waves on the ith port transmission line.

Eqs. (2-1) and (2-2) can be simultaneously solved in terms of v_i and i_i with the following results:

$$v_i^+ = \tfrac{1}{2}(v_i + Z_{oi}i_i)$$

$$v_i^- = \tfrac{1}{2}(v_i - Z_{oi}i_i) \qquad (2\text{-}3)$$

Examination of Eqs. (2-3) shows that they are evidently a linear transformation from the terminal variables v_i and i_i to a new set of variables, v_i^+ and v_i^-. Z_{oi} is an arbitrary constant with the dimension of impedance and can be defined as the normalization impedance.

For a linear n-port network, the new port variables, v_i^+ and v_i^-, are linearly related and the relationship can be expressed in a compact form as follows:

$$\begin{bmatrix} v_1^- \\ v_2^- \\ \cdots \\ v_n^- \end{bmatrix} = \begin{bmatrix} S_{11} & S_{12} & S_{13} & \cdots & S_{1n} \\ S_{21} & S_{22} & S_{23} & \cdots & S_{2n} \\ \cdots & \cdots & \cdots & \cdots & \cdots \\ S_{n1} & S_{n2} & S_{n3} & \cdots & S_{nn} \end{bmatrix} \begin{bmatrix} v_1^+ \\ v_2^+ \\ \cdots \\ v_n^+ \end{bmatrix}$$

or $$\bar{V}^- = \bar{S}\,\bar{V}^+ \tag{2-4}$$

$\bar{V}^-$ and $\bar{V}^+$ are column matrices with components v_i^- and v_i^+, respectively, and $\bar{S}$ is a square matrix with components S_{ij}. The S_{ij} components will be defined in the following discussion.

The constant matrix $\bar{S}$ is defined as the scattering matrix and each component in the array is a scattering parameter or simply an S-parameter. Eqs. (2-3) show that the scattering parameters are a function of the network and the impedance Z_{oi}. For practical applications, it is convenient to work with real positive impedances for all ports such that

$$Z_{o1} = Z_{o2} = \ldots = Z_{on} = Z_o \tag{2-5}$$

Furthermore, it turns out to be more natural to normalize $\bar{V}^+$ and $\bar{V}^-$ with respect to $\sqrt{Z_o}$. Later, it is justified that this choice for a normalizing term gives clearer network power relationships without affecting the S-parameters.

These normalized voltage waves, which will be expressed as power waves from now on, have the same form as Eqs. (2-4), i.e.,

$$\bar{B} = \bar{S}\,\bar{A} \tag{2-6}$$

In this equation, $\bar{B}$ and $\bar{A}$ are scattered and incident power wave matrices whose components b_i and a_i are defined by

$$a_i = \frac{1}{2\sqrt{Z_o}}(v_i + Z_o i_i)$$

$$b_i = \frac{1}{2\sqrt{Z_o}}(v_i - Z_o i_i) \qquad (2\text{-}7)$$

Although these relationships are derived from a transmission line voltage wave concept, they can also be verified by lumped-element circuit theory.[14]

By referring to Fig. 2-2 and using Kirchhoff's voltage law, the following equations are written:

$$v_s = v_i + Z_o i_i$$

$$v_r = v_i - Z_o i_i$$

These values are substituted into Eq. (2-7) with the result

$$a_i = \frac{v_s}{2\sqrt{Z_o}}$$

$$b_i = \frac{v_r}{2\sqrt{Z_o}} \qquad (2\text{-}8)$$

From this, the following definitions are made:

$|a_i|^2$: available power from source which has an impedance of Z_o.

$|b_i|^2$: power that flows from the ith port of a network when the port is terminated in Z_o.

$|a_i|^2 - |b_i|^2 = \mathrm{Re}\,(v_i i_i^*)$

: power delivered to network through ith port, if positive; power received through ith port, if negative.

Accordingly, the S-parameters of the matrix are defined as follows:

$$S_{ii} = \left.\frac{b_i}{a_i}\right| \quad a_j = o,\ j = 1, 2, \ldots, n, \text{ but } \neq i.$$

$$S_{ij} = \left.\frac{b_i}{a_j}\right| \quad a_k = 0,\ k = 1, 2, \ldots, n, \text{ but } \neq j. \tag{2-9}$$

S_{ii} and S_{ij} are voltage reflection and transmission coefficients. The squares of the magnitude of S_{ii} and S_{ij} are more useful quantities. They are defined as follows:

$|S_{ii}|^2 = \dfrac{|b_i|^2}{|a_i|^2}$: power reflection coefficient at ith port

$|S_{ij}|^2 = \dfrac{|b_i|^2}{|a_j|^2}$: transducer power gain from the jth port to the ith port.

It should be noted that all of the preceding discussions are based on the assumption that the normalization impedance is Z_o in every instance.

For the case of arbitrary source and termination impedances, new equations must be derived. These functions are derived through the use of signal flow graphs.

From the 1-port network of Fig. 2-3, calculation of the input reflection coefficient yields

$$S_{11} = \frac{Z - Z_o}{Z + Z_o} = \frac{Y_o - Y}{Y_o + Y} \tag{2-10}$$

where Y_o and Y are reciprocals of Z_o and Z.

For the definition of Eq. (2-10) the source impedance is assumed to be Z_o, so there are no mismatch reflections, and a_i is solely determined by v_s without considering b_i. However, for the case of an arbitrary source impedance Z_s, there are two kinds of incident waves: one generated by the source voltage and the other is the wave reflected at the source impedance. In Fig. 2-4, this relationship is shown for a 1-port network:

$$a_1 = a_s + S_s b_1 \tag{2-11}$$

where $$a_s = \frac{v_s\sqrt{Z_o}}{Z_s + Z_o}$$

and S_s is the source reflection coefficient defined by Eq. (2-10) when Z is replaced by Z_s. The signal flow diagram for the 1-port network is shown in Fig. 2-5 (a).

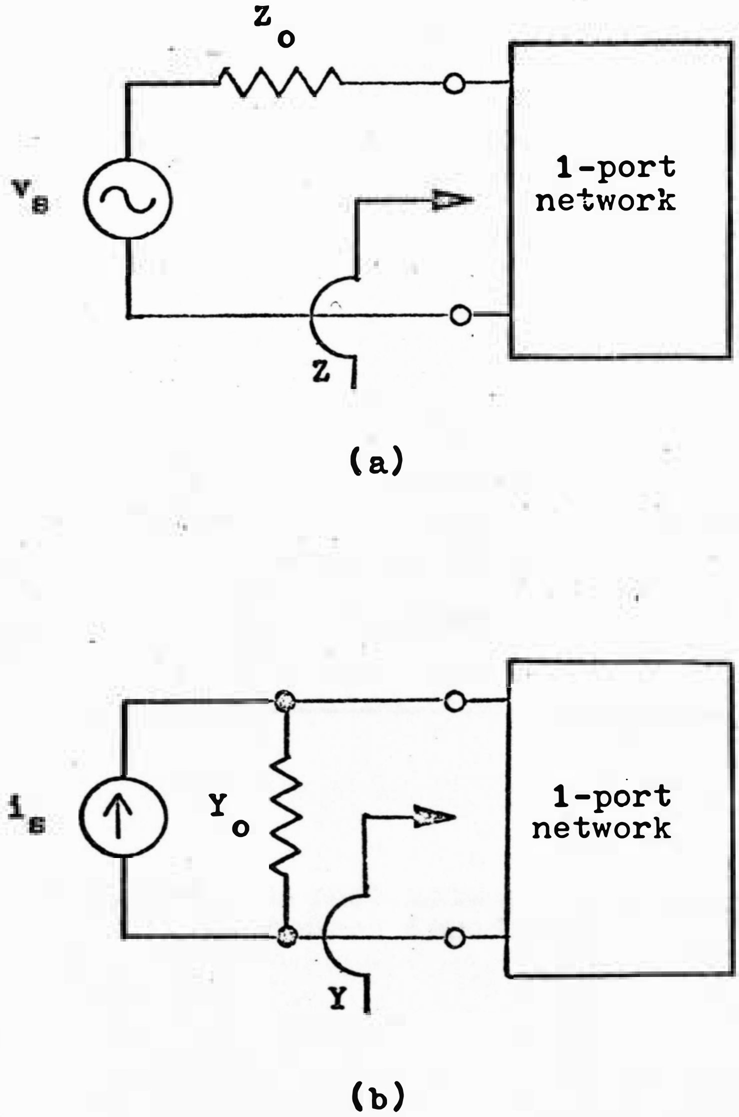

Fig. 2-3. (a) Impedance and (b) Admittance representations for 1-port network.

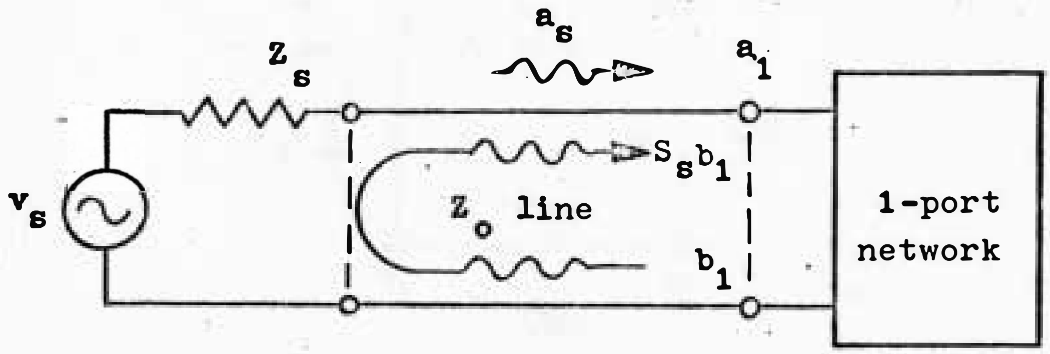

Fig. 2-4. 1-port network with arbitrary source impedance.

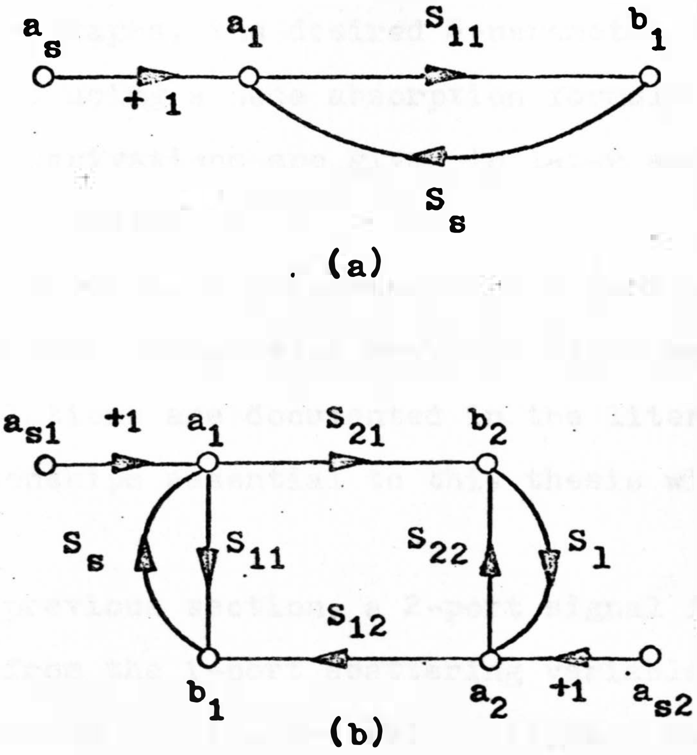

(a)

(b)

Fig. 2-5. Signal flow graphs: (a) 1-port; (b) 2-port.

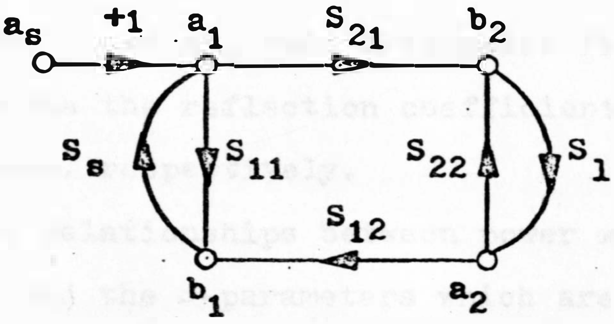

Fig. 2-6. 2-port signal flow graph without port 2 generator.

From the 1-port signal flow graph, the 2-port signal flow graph can be developed as illustrated in Fig. 2-5 (b). From the flow graphs, the desired S-parameter relationship can be derived using a node absorption formula or Mason's rule. These derivations are given in later sections.

B. Two-Port Formulation[8,10]

In this section, S-parameters for 2-port networks are studied employing signal flow graphs. Since well analyzed 2-port formulations are documented in the literature, only those relationships essential to this thesis will be presented.

In the previous section, a 2-port signal flow graph was derived from the 1-port scattering variable relationships. Referring to Fig. 2-5 (b) it is seen that the scattering relations of 2-port networks are clear.

In Fig. 2-5 (b), port 1 is assumed as the input port and port 2 as the output port. No signal generator is connected to port 2 and a_{s2} node disappears from the graph. S_s and S_1 denote the reflection coefficients at source and load impedances, respectively.

With the relationships between power wave variables, a's and b's, and the S-parameters which are shown in the flow graph of Fig. 2-6, the following set of equations is written:

$$b_1 = S_{11}a_1 + S_{12}a_2$$

$$b_2 = S_{21}a_1 + S_{22}a_2 \qquad (2\text{-}12)$$

$$a_1 = a_s + S_s b_1$$

$$a_2 = S_1 b_2 \qquad (2\text{-}13)$$

where $$a_s = \frac{v_s\sqrt{Z_o}}{Z_s + Z_o}$$

$$S_s = \frac{Z_s - Z_o}{Z_s + Z_o}$$

and $$S_1 = \frac{Z_1 - Z_o}{Z_1 + Z_o} \qquad (2\text{-}14)$$

S_s and S_1 are the source and load reflection coefficients, respectively. Obviously, S_s and S_1 will vanish when Z_s and Z_1 are equal to Z_o. This is the case where the source and load impedances are equated to the line characteristic impedance Z_o; no reflection occurs when the wave from the network arrives at the source or load impedance.

For the 2-port network, a_1 or a_2 can be equated to zero simply by adjusting v_s or v_1 to zero. Under this condition, scattering parameters then can be obtained according to Eq. (2-9). For example, $S_{11} = \left.\frac{b_1}{a_1}\right| a_2 = 0.$ The actual measurement procedures are discussed in Chapter IV.

Now the 2-port transducer power gain which is one of the most important design parameters is to be considered. For arbitrary source and load impedances the transducer power gain is defined as follows:

$$G_T = \frac{\text{Power delivered to the load}}{\text{Power available from the source}}$$

$$= \frac{P_L}{P_{avS}} \qquad (2\text{-}15)$$

From the definition of $|a_1|^2$ and $|b_1|^2$, and from Eq. (2-13),

$$P_L = |b_2|^2 - |a_2|^2 = |b_2|^2(1 - |S_1|^2) \qquad (2\text{-}16)$$

Power available from the source P_{avS} can be expressed compactly using a_s. Since a_s can be defined as the power wave applied to input port from an arbitrary source with voltage and internal impedance v_s and Z_s, respectively. Then $|a_s|^2$ is the power available to the Z_o line and has a definite relationship with P_{avS} which is defined as maximum power available at a matched load for a given source. That is,

$$P_{avS} = \frac{|a_s|^2}{1 - |S_s|^2} \qquad (2\text{-}17)$$

The factor $(1 - |S_s|^2)$ is the power transmission coefficient at the discontinuity between Z_s and Z_o.

Transducer power gain is

$$G_T = \frac{|b_2|^2}{|a_s|^2}(1 - |S_s|^2)(1 - |S_1|^2) \qquad (2\text{-}18)$$

Applying Mason's rule to Fig. 2-6,

$$\frac{b_2}{a_s} = \frac{S_{21}}{(1 - S_{11}S_s)(1 - S_{22}S_1) - S_{21}S_{12}S_sS_1} \qquad (2\text{-}19)$$

Combining Eqs. (2-18) and (2-19),

$$G_T = \frac{|S_{21}|^2(1 - |S_s|^2)(1 - |S_1|^2)}{|(1 - S_{11}S_s)(1 - S_{22}S_1) - S_{21}S_{12}S_sS_1|^2} \qquad (2\text{-}20)$$

Eq. (2-20) is an expression of the transducer power gain for arbitrary source and load impedances in terms of 2-port S-parameters.

The input and output reflection coefficients for arbitrary source and load impedances are also important for impedance matching. In general the input or output impedance varies with the load or source impedance. Also, the input and output reflection coefficients deviate from S_{11} and S_{22} for arbitrary terminations other than Z_o.

First, for an arbitrary load reflection coefficient S_1, the input reflection coefficient S_{11}' can be derived using the flow graph in Fig. 2-5 (b) and the node absorption formula:

$$S_{11}' = S_{11} + \frac{S_{12}S_{21}S_{l}}{1 - S_{22}S_{l}} \qquad (2\text{-}21)$$

In the same manner, the output reflection coefficient is derived for the case of an arbitrary source reflection coefficient S_s. The resulting output reflection coefficient is denoted as S_{22}'.

$$S_{22}' = S_{22} + \frac{S_{12}S_{21}S_{s}}{1 - S_{11}S_{s}} \qquad (2\text{-}22)$$

In circuit theory, maximum power transfer is obtained by matching the complex impedance source with the complex conjugate of the load impedance. In using the S-parameter method, this matching is also represented as complex conjugate matching. For instance, for an output reflection coefficient S_{22}', the load reflection coefficient of $S_l = S_{22}'^*$ will match with S_{22}' resulting in maximum power transfer. Simultaneous matching conditions for S_s and S_l can be obtained setting S_s and S_l equal to $S_{11}'^*$ and $S_{22}'^*$, respectively, in Eqs. (2-21) and (2-22).

The stability of a 2-port network can also be considered by using Eqs. (2-21) and (2-22). The magnitude of the reflection coefficient is always less than unity when a transmission line is terminated with a passive element. For stability criterion the critical condition exists when

S_{11}' and S_{22}' equal unity. If the magnitude of either reflection coefficient is larger than unity, the network may oscillate. This oscillation is possible even for the case of a passive source impedance because there is sufficient reflected power to maintain oscillation.

If S_{11}' and S_{22}' are equated to unity in Eqs. (2-21) and (2-22), then S_l and S_s can be found in terms of 2-port S-parameters. The loci of S_l and S_s obtained in this manner trace out circles on the reflection coefficient plane, the Smith Chart. These circles, which represent the boundary between the stable and unstable regions of S_s and S_l, are defined as stability circles.

C. Unilateral Case

When the reverse gain of a 2-port network is zero, i.e. $S_{12} = 0$, power flows only in the forward direction independent of the impedance associated with the load and source. This is the unilateral case of a 2-port network. In an actual device, however, reverse gain always exists but is usually much smaller in magnitude than the forward gain, and can be ignored.

If the reverse gain, S_{12}, is assumed as zero, the total number of 2-port S-parameters is reduced from 4 to 3. For this condition, the path connecting a_2 and b_1 on the flow graph of Fig. 2-6 vanishes. Eqs. (2-21) and (2-22), for the unilateral case $S_{12} = 0$, reduce to

$$S_{11}' = S_{11} \tag{2-21)'}$$

and

$$S_{12}' = S_{22} \tag{2-22)'}$$

It should be noted that these parameters are independent of Z_s and Z_1. Thus a simultaneous conjugate match is always possible with passive Z_1 and Z_s, if the reflection coefficients S_{11} and S_{22} do not have a magnitude greater than unity. For the unilateral case maximum transducer power gain can be attained when the source and load reflection coefficients are

$$S_s = S_{11}^* \tag{2-23}$$

and

$$S_1 = S_{22}^*$$

Once S_s and S_1 are found from Eq. (2-23), the corresponding source and load impedances can be read directly from the Smith Chart or can be calculated using Eq. (2-14). These impedances are the complex conjugates of input and output impedances of the 2-port network.

Unilateral transducer gain can be derived from Eq. (2-20) by letting $S_{12} = 0$.

$$G_{TU} = \frac{|S_{21}|^2(1 - |S_s|^2)(1 - |S_1|^2)}{|(1 - S_{11}S_s)(1 - S_{22}S_1)|^2} \tag{2-20}$$

When the input and output impedances are conjugately matched to the source and load impedances, maximum unilateral gain G_U is obtained. From Eq. (2-20)'

$$G_U = \frac{|S_{21}|^2}{(1 - |S_{11}|^2)(1 - |S_{22}|^2)} \qquad (2\text{-}24)$$

It should be noted that G_U is invariant regardless of source and load impedances.

Let us define the unilateral figure of merit U as

$$U = \frac{|S_{11}S_{22}S_{12}S_{21}|}{(1 - |S_{11}|^2)(1 - |S_{22}|^2)} \qquad (2\text{-}25)$$

It can be shown from Eqs. (2-20), (2-24), and (2-25) that

$$\frac{1}{(1 + U)^2} < \frac{G_T}{G_{TU}} < \frac{1}{(1 - U)^2} \qquad (2\text{-}26)$$

In order to justify the unilateral design, the figure of merit may be evaluated to check the error in power gain calculation (error from using Eqs. (2-20)' and (2-24), rather than the exact Eq. (2-20)). Depending upon the purpose of a circuit, maximum permissible U can be determined from the design accuracy required.

It should be noted that the magnitudes of S_{11} and S_{22} are assumed to be smaller than unity for all the preceding equations.

D. Three-Port Formulation[17]

In this section, the relationships between 3-port and

2-port parameters will be discussed. The most common active device network is a 2-port network. However, many active devices have more than 3 terminals. In order to represent a device that has more than 3 terminals, 2-port parameters are not sufficient for characterizing the device for all possible arbitrary configurations.

Even in 3-terminal devices such as transistors, a 3-port representation is sometimes convenient even though there is redundancy. A 3-port model of a 3-terminal device is exactly the case in which the indefinite admittance matrix representation is more general and versatile than the general definite admittance matrix representation. This is especially true for the cases of port interconnections and arbitrary terminations at the ports. The application to 3-terminal transistors is fully appreciated in Bodway's paper.

A 3-port signal flow graph is shown in Fig. 2-7 (a). Port 1 and port 2 are the input and output ports, respectively, and port 3 is terminated with an arbitrary impedance whose equivalent reflection coefficient is S_3. A 2-port model can be obtained using the node absorption formula to eliminate the nodes of port 3. The resulting 2-port S-parameters obtained in this manner are as follows:

$$S_{11(3)} = S_{11} + \frac{S_{31}S_{13}S_3}{1 - S_{33}S_3}$$

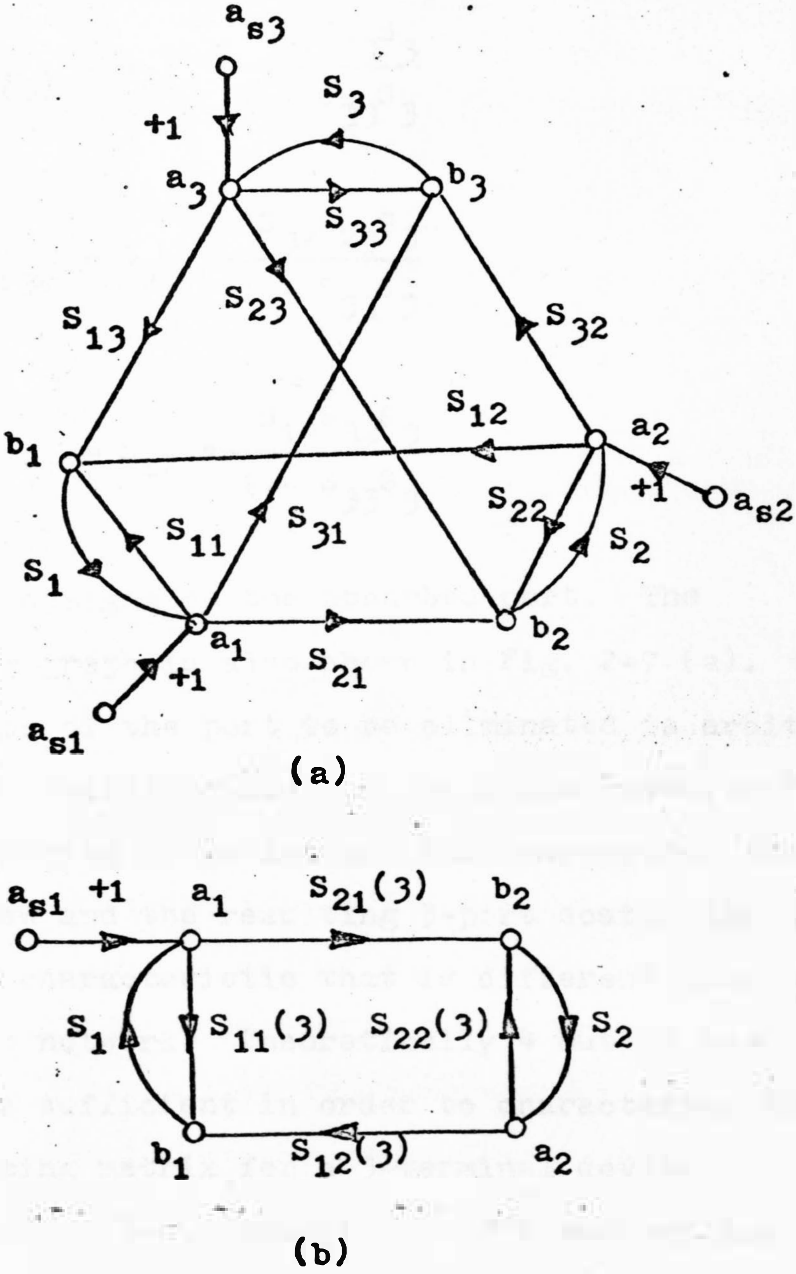

Fig. 2-7. (a) 3-port signal flow graph; (b) Derived 2-port absorbing port 3 nodes. ($a_{s2} = a_{s3} = 0$)

Is this part of the title?

$$S_{21(3)} = S_{21} + \frac{S_{31}S_{23}S_3}{1 - S_{33}S_3}$$

$$S_{22(3)} = S_{22} + \frac{S_{32}S_{23}S_3}{1 - S_{33}S_3}$$

$$S_{12(3)} = S_{12} + \frac{S_{13}S_{32}S_3}{1 - S_{33}S_3} \qquad (2\text{-}27)$$

Subscript (3) designates the absorbed port. The resulting flow graph is also shown in Fig. 2-7 (a). Note that the choice of the port to be eliminated is arbitrary.

For a 3-terminal device such as illustrated in Fig. 2-8, the scattering variables are not independent from Kirchhoff's Law and the resulting 3-port scattering parameters have a characteristic that is different from that of general 3-port network. Theoretically 4 out of the 9 components are sufficient in order to characterize the (3x3) 3-port scattering matrix for a 3-terminal device.

Refer to Fig. 2-8, from Kirchhoff's current law at the reference or ground node

$$i_1 + i_2 + i_3 = 0$$

Also, no current will flow if the potentials applied to every terminal pair are made equal, i.e.

$$i_1 = i_2 = i_3 = 0, \text{ if } v_1 = v_2 = v_3$$

The above two equations can be expressed in scattering variables

$$a_1 + a_2 + a_3 = b_1 + b_2 + b_3$$

and $$a_1 - b_1 = a_2 - b_2 = a_3 - b_3 = 0, \text{ if } a_1 = a_2 = a_3 \tag{2-28}$$

The conditions as set forth in the preceding equations are summarized as follows:

$$\sum_{i=1}^{i=3} S_{ij} = \sum_{j=1}^{j=3} S_{ij} = 1 \tag{2-29}$$

Eq. (2-29) dictates the dependency of the individual S-parameters. It can be seen that 4 independent S-parameters determine the remaining S-parameters according to Eq. (2-29). Although in practice all of the 9 parameters are measured for precision, the number of measurements can be reduced to 4 and the rest can be obtained from Eq. (2-29).

If the upper limits of Eq. (2-29) are extended from 3 to n the equation will then be good for all n-terminal n-port networks.

Before concluding this chapter it is worthwhile to discuss another possible 3-port representation for a 3-terminal

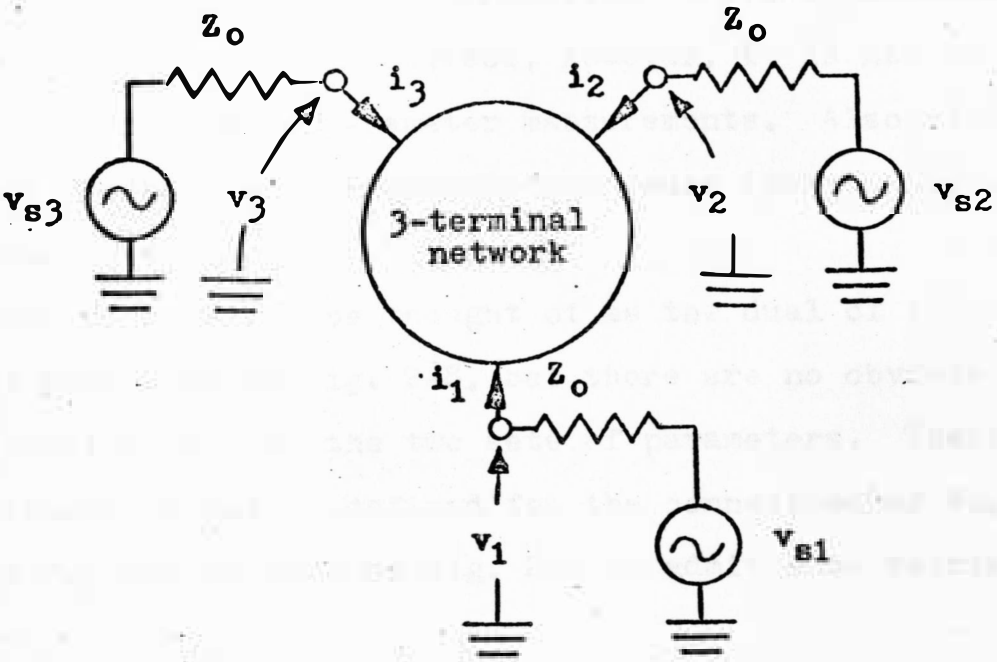

Fig. 2-8. 3-port representation of 3-terminal device with common reference.

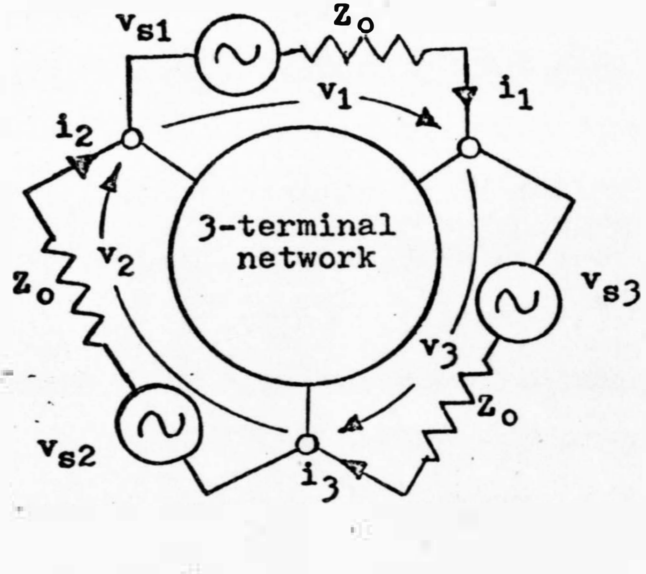

Fig. 2-9. 3-port representation of 3-terminal device without common reference.

device. Fig. 2-9 shows the connection. This connection is very common in actual devices; however, it is not so practical when making parameter measurements. Also, the inherent feedback of the circuit may cause instability when measurements are made.

This circuit can be thought of as the dual of the circuit discussed in Fig. 2-8, but there are no obvious relationships between the two sets of parameters. There is no impedance matrix defined for the connection of Fig. 2-8 and for the network of Fig. 2-9 no admittance matrix is defined.

CHAPTER III

APPLICATION TO HIGH-FREQUENCY SEMICONDUCTOR DEVICES

In the preceding chapter, the concept of scattering relations was introduced along with definitions of 2-port and 3-port parameters. In this chapter high-frequency semiconductor devices are discussed from the viewpoint of relating the S-parameters to existing equivalent circuits.

A. General Review of High-Frequency Semiconductor Devices

1. Bipolar Transistors. At high frequencies the performance of a bipolar transistor is limited by diffusion capacitance, junction transition capacitance, and base-spreading resistance. The hybrid Pi equivalent[18,19] circuit of Fig. 3-1 is one equivalent circuit that models the approximate high-frequency performance of a bipolar transistor. However, the equivalent circuit is not valid at frequencies where the transition time of minority carriers across the base region cannot be neglected. For this case, some of the parameters in Fig. 3-1 are frequency dependent.

At a single frequency, the parameters of a transistor vary with the operating point. In general, diffusion capacitance is proportional to the forward junction current and junction transition capacitance is inversely proportional to the absolute value of square or cube root of the junction

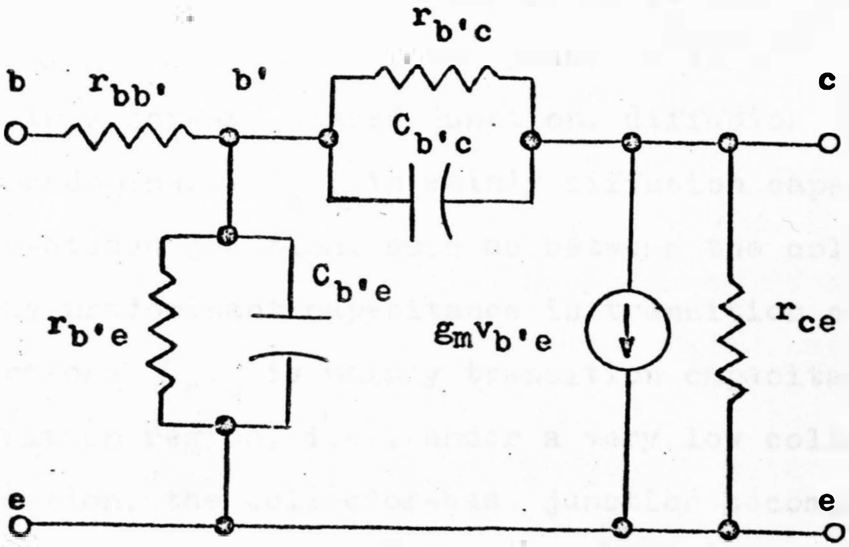

Fig. 3-1. Junction transistor equivalent circuit for common-emitter configuration.

potential difference. Whether the square or cube root applies depends on the impurity profile, i.e., for a homogenously-doped p-n junction, the power is 1/2, and for a linearly-graded junction, the power is 1/3.[18]

Since, in a forward-biased junction, diffusion capacitance is predominant, $C_{b'e}$ is mainly diffusion capacitance. At a reverse-biased junction, such as between the collector and base, the predominant capacitance is transition capacitance. Therefore, $C_{b'c}$ is mainly transition capacitance. In the saturation region, i.e., under a very low collector voltage condition, the collector-base junction becomes forward-biased; in this case, diffusion capacitance and a low dynamic resistance would replace $C_{b'c}$ and $r_{b'c}$ of the active region model.

At frequencies within the VHF band, S-parameters of a device may exhibit the characteristics of the equivalent circuit in Fig. 3-1, since the time delay due to minority carrier transit time in the frequency range is not significant for a graded-bade junction transistor. For a typical silicon npn transistor, 2N3478, it is reported that transit time is about 112 ps.[8] Using this transit time, a calculation for phase shift at 200 MHz yields about 10 degrees. This will appear directly in S_{21}, but not explicitly in other parameters since only S_{21} is directly related with the minority carrier transit time.

At high frequencies, the input impedance of a bipolar device consists of $r_{bb'}$, $r_{b'e}$, and $C_{b'e}$, if we neglect the feedback elements, $r_{b'c}$ and $C_{b'c}$. S_{11} is then determined by this impedance, and will follow a constant resistant circle on the Smith Chart, if frequencies are high enough to reduce the capacitive impedance of $C_{b'e}$ much below that of $r_{b'e}$. A plot of S_{22} follows a constant conductance circle and the conductance is the parallel conductance of $r_{b'c}$ and r_{ce}. For this plot it is assumed that impedance between b' and e is negligible.

S_{21} and S_{12} will be discussed in Chapter V, along with discussions of parameter variations due to bias voltages.

2. MOSFET.[20] One of the main limitations of high-frequency bipolar devices depends upon the relatively low minority carrier velocity in base region. From this point of view, the radically different structure of the field effect transistor, in which current movement depends on majority carriers controlled by electric field, can be expected to show better high-frequency performance. However, this was not true for early junction FETs in which the large ineffective areas of the gate provided large internal feedback capacitance and large channel capacitance, resulting in very low cut-off frequency. Furthermore, highly-developed bipolar transistor technologies began to produce GHz range devices of good performance, and in the light of this fact,

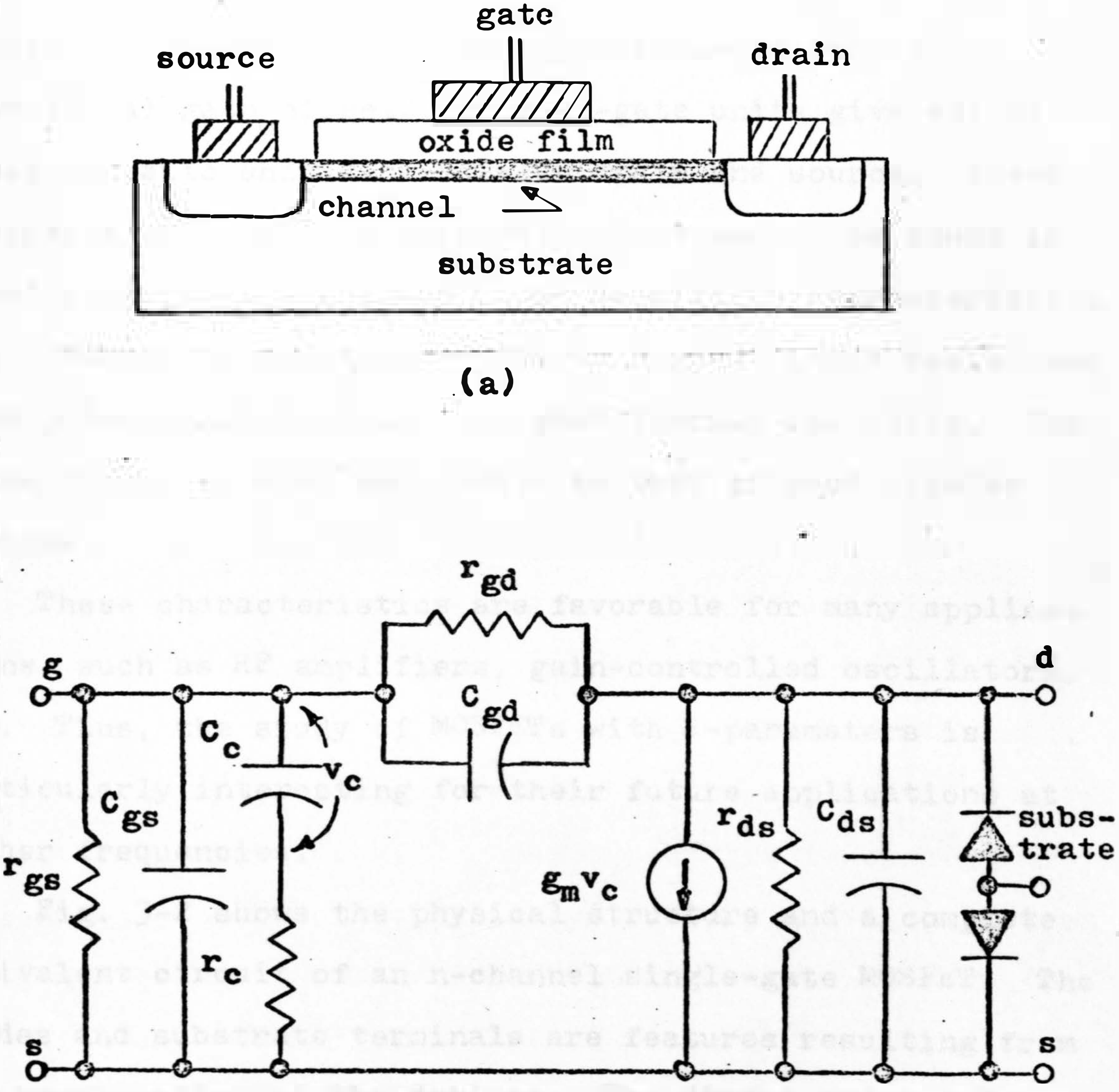

(a)

(b)

Fig. 3-2. (a) Structure of depletion mode MOSFET; (b) Equivalent circuit.

it is natural that the early FETs failed to receive attention as high-frequency devices.

Recent improvements in MOSFET technology present a good prospect for these devices in high-frequency applications. The reverse feedback capacitance is reduced by geometrical gate offset, and dual-gate units give effective electro-static shielding between drain and source. These devices also have many properties that cannot be found in bipolar devices: excellent cross modulation characteristics, small AGC power consumption due to high DC input resistance, high power amplification, and good thermal stability. The noise figure is also comparable to that of good bipolar devices.

These characteristics are favorable for many applications, such as RF amplifiers, gain-controlled oscillators, etc. Thus, the study of MOSFETs with S-parameters is particularly interesting for their future applications at higher frequencies.

Fig. 3-2 shows the physical structure and a complete equivalent circuit of an n-channel single-gate MOSFET. The diodes and substrate terminals are features resulting from the construction of the devices. The diodes are p-n junctions formed between the heavily-doped source and drain, and the lightly-doped substrate. To some degree, the substrate may also form a p-n junction with the channel, and can be used as a second gate, but due to difficulty in controlling the transconductance the terminal is usually grounded for operation in the common-source connection.

The principal difference between the equivalent circuit of bipolar transistors and MOSFETs is the addition of series combination, r_c and C_c, that connect the gate and source. This combination represents the distributed nature of the channel and the gate. g_m is controlled by the voltage across C_c so the reduction in gain at high frequencies is related to the time constant r_cC_c.

r_{gs} and r_{gd} represent the leakage paths associated with the oxide layer of the gate and source, and the gate and drain, respectively. r_{ds} is given by the slope of the common source output characteristics and varies widely with V_{GS}.

The capacitances C_{gd}, C_{gs}, and C_{ds} include intrinsic and extrinsic capacitances between corresponding electrodes. The intrinsic portion of C_{gd} decreases with increasing drain voltage due to the effective widening of separation between drain and gate by carrier depletion region.

One more consideration has to be given to the equivalent circuit in Fig. 3-2 (b). For an offset gate MOSFET, a resistance appears in series with the drain terminal because of the bulk resistance of the unmodulated region. The output impedance at high frequencies then exhibit a second order effect.[21]

At frequencies above 400 MHz, deviations from the simple low frequency theory are reported by Kolk and Johnson.[20] According to their report, significant differences were observed in input and forward transfer admittance above 400 MHz, and at low frequencies in the case of reverse transfer admittance. They also mention that some of the deviations may be accounted for by small but significant inductances in the transistor assembly and measurement equipment; however, the experimental data indicate that further refinement of the equivalent circuit is necessary at these frequencies. Further discussion of this will be given in Chapter V; the remainder of this section will be devoted to dual-gate MOSFETs.

As was discussed early in this section, one of the effective ways to reduce feedback capacitance is by adding another gate between drain and gate of a single-gate MOSFET. Actually this becomes a cascode amplifier if gate 2 is RF grounded, by creating a common-source and common-gate pair. Fig. 3-3 shows a schematic diagram for the cascode connection. The input and output impedance values in this connection are about equal to those of common-source and common-gate connections, respectively. This amplifier gain is also about the same as that of single-common-source stage. But reverse gain or feedback becomes much smaller than that for a single common-source or common-gate stage.

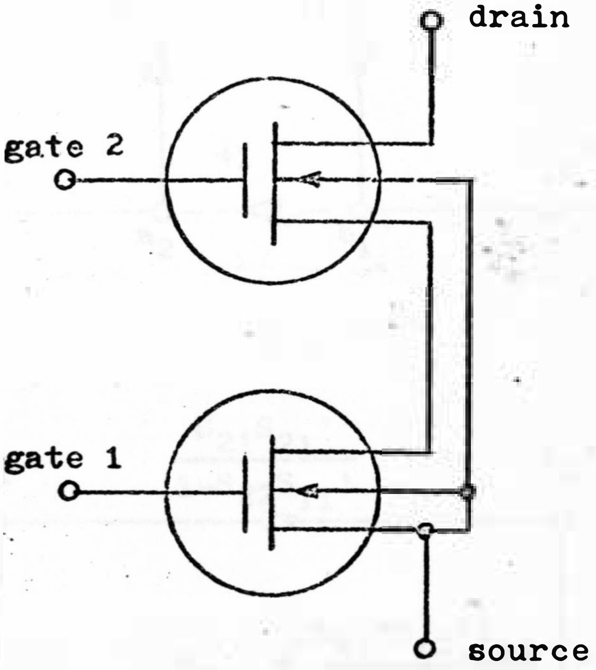

Fig. 3-3. Equivalent circuit of dual-gate MOSFET.

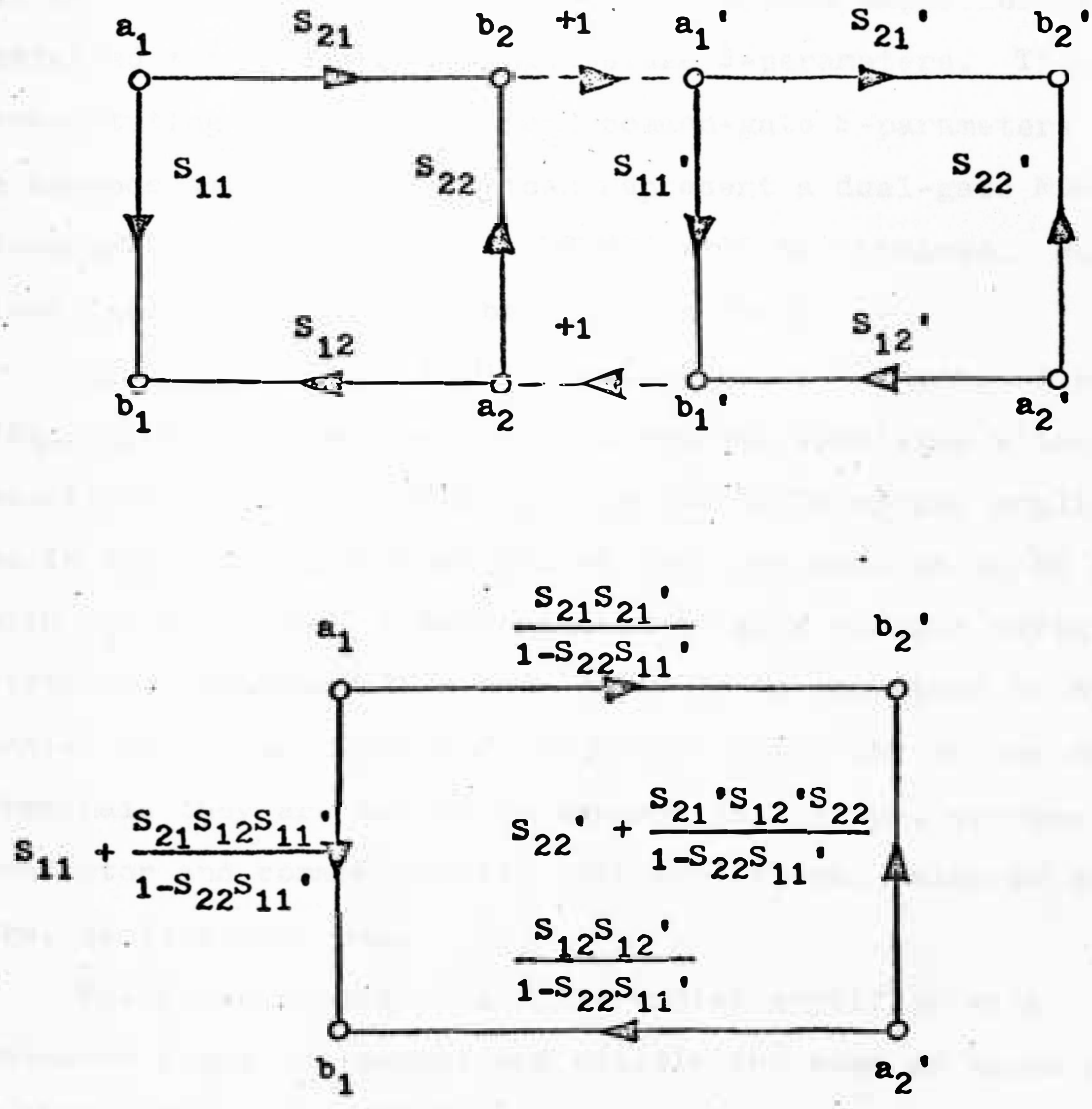

Fig. 3-4. Cascaded two-port for dual-gate MOSFET study.

To understand the behavior of a dual-gate MOSFEY using S-parameters, it is convenient to derive a 2-port expression for a cascaded amplifier. Referring to Fig. 3-4, it is seen that S-parameters for a cascaded amplifier are obtained from 2 sets of single-stage S-parameters. Then, substituting common-source and common-gate S-parameters for a cascode amplifier, which can represent a dual-gate MOSFET, S-parameters of a dual-gate MOSFET will be obtained. Numerical justifications will be given in Chapter V.

3. Differential Amplifier-Integrated Circuit. A configuration that can provide good thermal stability without sacrificing low frequency gain is the differential amplifier. As in Fig. 3-5, identical transistors are made on an IC chip, with Q_1, Q_2, and Q_3 interconnected to give minimum wiring distance. However, this type of IC is not confined to differential amplifier applications; by utilizing the proper access terminals they are usable as cascode amplifiers, common-collector and common-emitter pair amplifiers, balanced mixers, oscillators, etc.

The S-parameters of a differential amplifier with balanced input and output are exactly the same as those of a single transistor if the normalization impedance is doubled. For the circuit in Fig. 3-6, the impedance due to Q_3 does not appear in the amplifier action so that Q_1 and Q_2 are in a series connection, and their impedance parame-

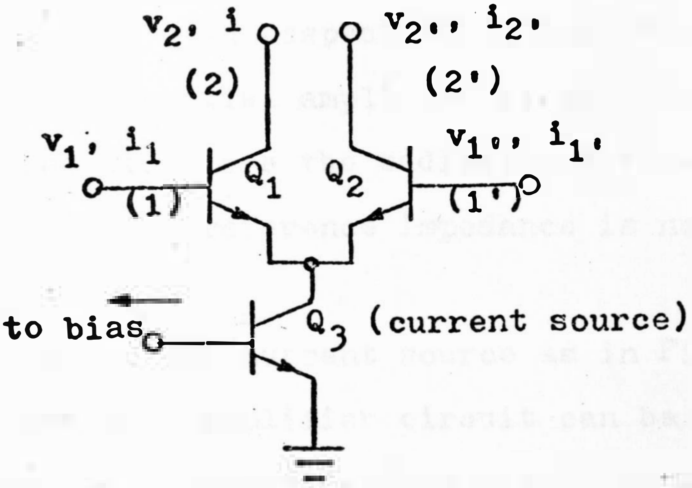

Fig. 3-5. IC differential amplifier (RCA-CA 3049).

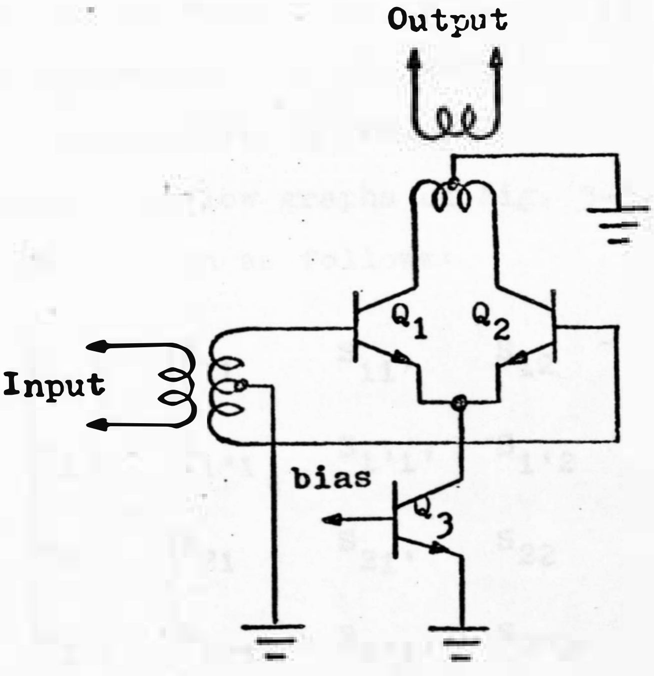

Fig. 3-6. Balanced input and output for ideal differential operation.

ters add. For example, the S-parameters for a particular transistor are measured with respect to 50 ohms then the S-parameters of a differential amplifier circuit consisting of 2 identical transistors are the addition of those of the single transistor and the reference impedance is now 100 ohms.

When Q_3 is used as the current source as in Fig. 3-5, this type of differential amplifier circuit can be a 5-terminal network and may be characterized by 4-port parameters. Assuming symmetry of the parameters due to identical characteristics of Q_1 and Q_2, the number of parameters required to characterize this IC circuit is 8. If it is assumed that the output impedance of Q_3 is very large, the number of independent parameters is reduced to 4.

By using the flow graphs of Fig. 3-5, the 4-port relations can be written as follows:

$$\begin{bmatrix} b_1 \\ b_{1'} \\ b_2 \\ b_{2'} \end{bmatrix} = \begin{bmatrix} S_{11} & S_{11'} & S_{12} & S_{12'} \\ S_{1'1} & S_{1'1'} & S_{1'2} & S_{1'2'} \\ S_{21} & S_{21'} & S_{22} & S_{22'} \\ S_{2'1} & S_{2'1'} & S_{2'2} & S_{2'2'} \end{bmatrix} \begin{bmatrix} a_1 \\ a_{1'} \\ a_2 \\ a_{2'} \end{bmatrix} \tag{3-1}$$

If Q_1 and Q_2 are identical then

$$S_{ij} = S_{i'j'}$$

and $$S_{ij'} = S_{i'j} \tag{3-2}$$

Also, the sum of each column or row is unity for very high output impedance of Q_3. This was discussed in Chapter II where an n-port network with a common reference was considered.

In a practical case it is convenient to measure 8 parameters for a complete set from Eqs. (3-1) and (3-2). Four parameters can be measured for a good approximation in the case where the output impedance of Q_3 is very high.

Once the scattering matrix of Eq. (3-1) is known then S-parameters for every possible configuration can be derived. For instance, S-parameters for a differential mode can be obtained where new scattering variables are defined.

From Fig. 3-5 and the relationships of impedance and scattering variables in Chapter II, differential and common mode variables are represented as

$$v_1 \pm v_{1'} = \sqrt{Z_o}\left[(a_1 \pm a_{1'}) + (b_1 \pm b_{1'})\right]$$
$$i_1 \pm i_{1'} = \frac{1}{\sqrt{Z_o}}\left[(a_1 \pm a_{1'}) - (b_1 \pm b_{1'})\right] \tag{3-3}$$

For port 2 and port 2' the above equations can be extended if the subscripts 1 and 1' are changed to 2 and 2', respectively. A simple linear transformation of Eq. (3-1) finally yields

$$\bar{B}_{dc} = \bar{C}\,\bar{S}\,\bar{C}^{-1}\,\bar{A}_{dc} \qquad (3\text{-}4)$$

where

$$\bar{A}_{dc} = \begin{bmatrix} a_1 - a_{1'} \\ a_1 + a_{1'} \\ a_2 - a_{2'} \\ a_2 + a_{2'} \end{bmatrix} \quad \bar{B}_{dc} = \begin{bmatrix} b_1 - b_{1'} \\ b_1 + b_{1'} \\ b_2 - b_{2'} \\ b_2 + b_{2'} \end{bmatrix} \quad \bar{C} = \begin{bmatrix} 1 & -1 & 0 & 0 \\ 1 & 1 & 0 & 0 \\ 0 & 0 & 1 & -1 \\ 0 & 0 & 1 & 1 \end{bmatrix}$$

and $\bar{S}$ is a scattering matrix defined by Eq. (3-1).

If Q_1 and Q_2 are assumed to be identical then no common mode variables will appear for the differential mode of operation with balanced input and output. In other words, for identical Q_1 and Q_2, $a_1+a_{1'}$, $a_2+a_{2'}$, $b_1+b_{1'}$, and $b_2+b_{2'}$ terms will vanish substituting the conditions of $v_1 = -v_{1'}$, $v_2 = -v_{2'}$, $i_1 = -i_{1'}$, and $i_2 = -i_{2'}$ into Eq. (3-3). Then 2 sets of differential mode terms are left in $\bar{A}_{dc}$ and $\bar{B}_{dc}$, resulting in a 2-port relation. In this case the scattering matrix $\bar{C}\,\bar{S}\,\bar{C}^{-1}$ has 4 significant components relating the differential mode terms of $\bar{A}_{dc}$ and $\bar{B}_{dc}$. Referring to Eq. (3-3), it is seen that 4 parameters represent the differential mode S-parameters that are normalized with $2Z_o$. (Refer to Eq. (2-7) and note that port current represented by Eq. (3-3) is 2 times the actual port current.) The resulting 4 differential mode S-parameters obtained from the scattering matrix of Eq. (3-4) are given below.

$$\begin{aligned}
S_{11d} &= \tfrac{1}{2}(S_{11} + S_{1'1'} - S_{11'} - S_{1'1}) \\
S_{22d} &= \tfrac{1}{2}(S_{22} + S_{2'2'} - S_{22'} - S_{2'2}) \\
S_{21d} &= \tfrac{1}{2}(S_{21} + S_{2'1'} - S_{21'} - S_{2'1}) \\
S_{12d} &= \tfrac{1}{2}(S_{12} + S_{1'2'} - S_{12'} - S_{1'2})
\end{aligned} \tag{3-5}$$

The normalization impedance of the differential mode S-parameters in Eq. (3-5) is $2Z_o$ while 4-port parameters are measured with respect to a normalization impedance of Z_o. Then Eq. (3-5) is combined with Eq. (3-2) to give the S-parameters of the differential amplifier with identical Q_1 and Q_2 of Fig. 3-5.

Eq. (3-5) provides the means whereby the S-parameters of the constituent transistors in a differential amplifier can be measured. For instance, the common-emitter input reflection coefficient of Q_1 and Q_2 in Fig. 3-5 is $S_{11}-S_{11'}$ and can be obtained by 4-port measurement.

B. S-Parameters as Indirect Means of Measurement for Other Parameters

At frequencies above 100 MHz, direct measurement[22] of h-, y-, or z-parameters, ordinarily used in active circuit design at low frequencies, is very inconvenient because of the difficulty in establishing the required short or open circuit condition. Also, a short or open circuit frequently causes the device to oscillate.

Short circuit admittance or y-parameters are the most popular high-frequency parameters. It is possible to measure them up to microwave frequencies with the slotted line technique. But there are two major inconveniences when compared with the S-parameter measurement technique. First, for wide-band measurement, the slotted line should be tuned every time the frequency is varied. This tuning requires too much time and labor. Second, as discussed before, the short or open condition of a device easily can result in an oscillatory state. This causes unstable measurement.

Because of these difficulties, it is expedient to derive y-parameters or any other immittance parameters from the more precise and easily obtainable S-parameters which are measured with a more stable wide-band measurement system. Conversion tables are provided in Appendix I.

Other equivalent circuit parameters, such as hybrid Pi, normal Pi,[19] or others, can also be derived from the measured S-parameters as long as the equivalent circuits are valid at the frequency of interest. However, it should be noted that there is no reason to insist on equivalent circuits at much higher frequencies where the lumped element representation fails.

At relatively low frequencies, i.e. 200 MHz, the equivalent circuits are still useful for understanding a transistor. As was shown earlier in this chapter, the equivalent circuit of the MOSFET can be thought of as a derived form of the normal Pi circuit of Fig. 3-7. The normal Pi elements can be derived directly from the y-parameters without introducing conversion errors. This provides a convenient way to approach the equivalent circuit from measured parameters. Also, referring to Fig. 3-7 and the scattering admittance conversion table in Appendix I, it is possible to use approximate formulas for VHF band transistors. The approximate equations are given for the elements of the normal Pi circuit.

$$A = y_1 + \frac{S_{12}(S_{21} - 2)}{M}$$

$$B = \frac{2S_{12}}{M}$$

$$C = \frac{-2S_{21}}{M}$$

$$D = y_2 + \frac{S_{12}(S_{21} - 2)}{M} \qquad (3\text{-}6)$$

where $y_1 = \frac{1 - S_{11}}{1 + S_{11}}$

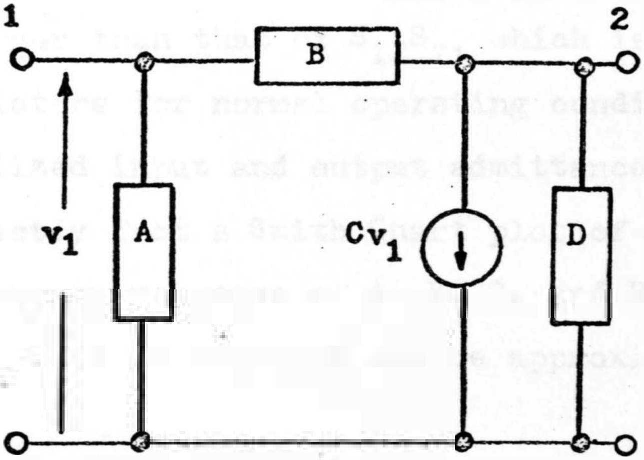

$A = y_{11} + y_{12}$

$B = -y_{12}$

$C = y_{21} - y_{12}$

$D = y_{22} + y_{12}$

Fig. 3-7. Normal Pi model.

$$y_2 = \frac{1 - S_{22}}{1 + S_{22}}$$

and $$M = (1 + S_{11})(1 + S_{22})$$

A, B, C, and D are admittances normalized with $1/Z_o$. Eqs. (3-6) are derived with the assumption that the magnitude of M is much larger than that of $S_{12}S_{21}$ which is always true in VHF transistors for normal operating conditions. y_1 and y_2 are normalized input and output admittances that can be obtained directly from a Smith Chart plot of S_{11} and S_{22}. From the frequency response of A, B, C, and D, the MOSFET equivalent circuit of Fig. 3-2 can be approximated by trial and error.

The hybrid Pi circuit of Fig. 3-1 can also be derived mathematically for a bipolar transistor through a double conversion, i.e., first to y-parameters and then to hybrid Pi parameters. However, since the equivalent circuit is not an exact representation of the device performance, the reliability is inferior to the direct measurement method. An approximate method is more useful and is given in Appendix II.

C. Mixer S-Parameters

In Chapter II, the possibility of S-parameters as amplifier design parameters was fully described in the discussion of 2-port formulation. The practical design procedures appear in Weinert,[7] Anderson,[8] Froehner,[9] and Bodway.[10] However, no attempt has been made in the literature to characterize a mixer circuit with S-parameters. It will be shown that S-parameters can also be used in designing a mixer circuit.

Conventionally, short circuit admittance parameters have been employed in mixer circuit design. However, at frequencies where y-parameters cannot be easily obtained it is desirable to define mixer parameters in terms of S-parameters. Once the S-parameters are known, designing a mixer is similar to amplifier design.

It can be noted in Fig. 3-8 that there are three major frequencies associated with a mixer stage. Only 2 of these are pertinent: the RF input signal and IF output signal. When an ideal IF filter is provided all frequencies are attenuated except the IF signal. For the balanced modulator circuit as in Fig. 3-9, elimination of local oscillator signal from an RF input end can easily be achieved. Then a linear relationship between the RF and IF signal amplitudes can be measured as in the normal 2-port S-parameter case.

From Fig. 3-8, 3 important S-parameters for z mixer design can be defined as follows:

$$S_{11}(RF) = \left.\frac{b_1(RF)}{a_1(RF)}\right| \quad a_2(RF) = 0$$

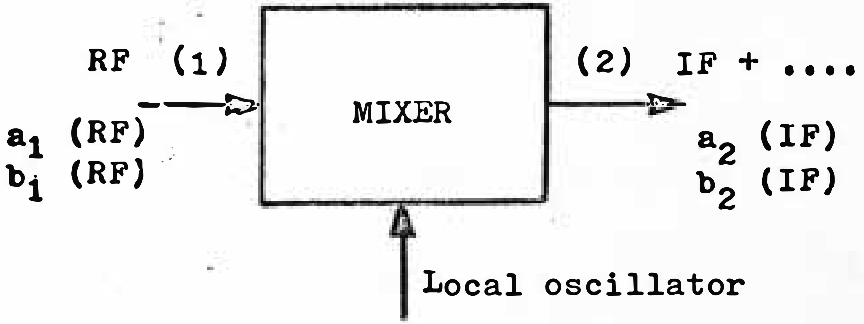

Fig. 3-8. Mixer model.

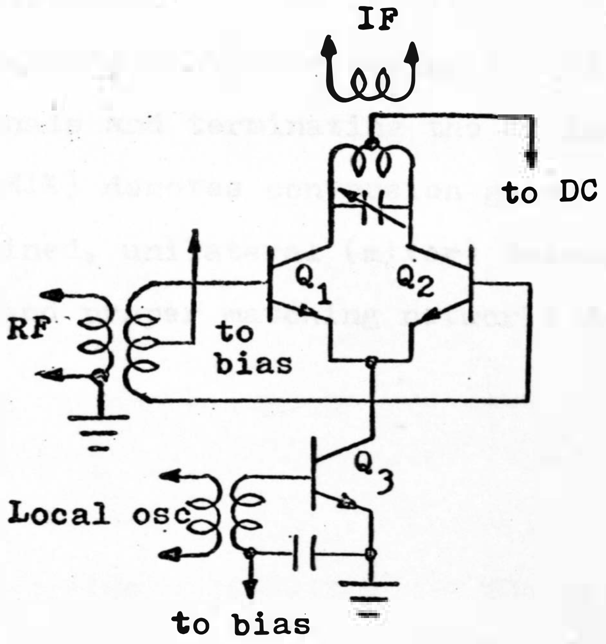

Fig. 3-9. An example of a balanced mixer.

$$S_{22}(IF) = \left. \frac{b_2(IF)}{a_2(IF)} \right|_{a_1(IF) = 0}$$

$$S_{21}(MIX) = \left. \frac{b_2(IF)}{a_1(RF)} \right|_{a_2(IF),\ a_2(RF) = 0} \tag{3-7}$$

These parameters are a function of the local oscillator input level as well as the DC operating point. If the IF input impedance is Z_o, i.e. 50 ohms, $S_{11}(RF)$ is the input reflection coefficient for the RF signal. $S_{22}(IF)$ is the output reflection coefficient for the IF signal. $S_{22}(IF)$ can be measured approximately after removing the RF and local oscillator signals and terminating the RF input terminals with Z_o. $S_{21}(MIX)$ denotes conversion gain. Once the parameters are obtained, unilateral (mixer) transducer gain can be calculated and proper matching networks designed to give maximum gain.

CHAPTER IV

MEASUREMENT OF S-PARAMETERS AT VHF FREQUENCIES

In Chapter II it was suggested that S-parameters can be obtained from the ratio of b's to a's according to Eq. (2-9). This is for the case where a signal source of internal impedance Z_o is connected to one port and the remaining ports are terminated in Z_o. Under this condition the a's are all zero except at the port where the signal source is connected. Actual measurement procedures for obtaining S-parameters will be treated in this chapter.

A. Measurement Set-Up for 2-Port S-Parameters

A block diagram for making 2-port S-parameter measurements is shown in Fig. 4-1. Referring to the block diagram it can be seen that the over-all accuracy of a given measurement is determined by many factors such as VSWR (due to bias networks, directional couplers, transistor jig or any discontinuity in the signal path), loss in defective connectors, errors in vector voltmeter (VVM), etc. The VVM is the most important component of the measurement system. In order to get reliable results it is necessary to use a high-quality instrument.

The specifications for the equipment and the necessary accessories corresponding to the blocks in Fig. 4-1 are as

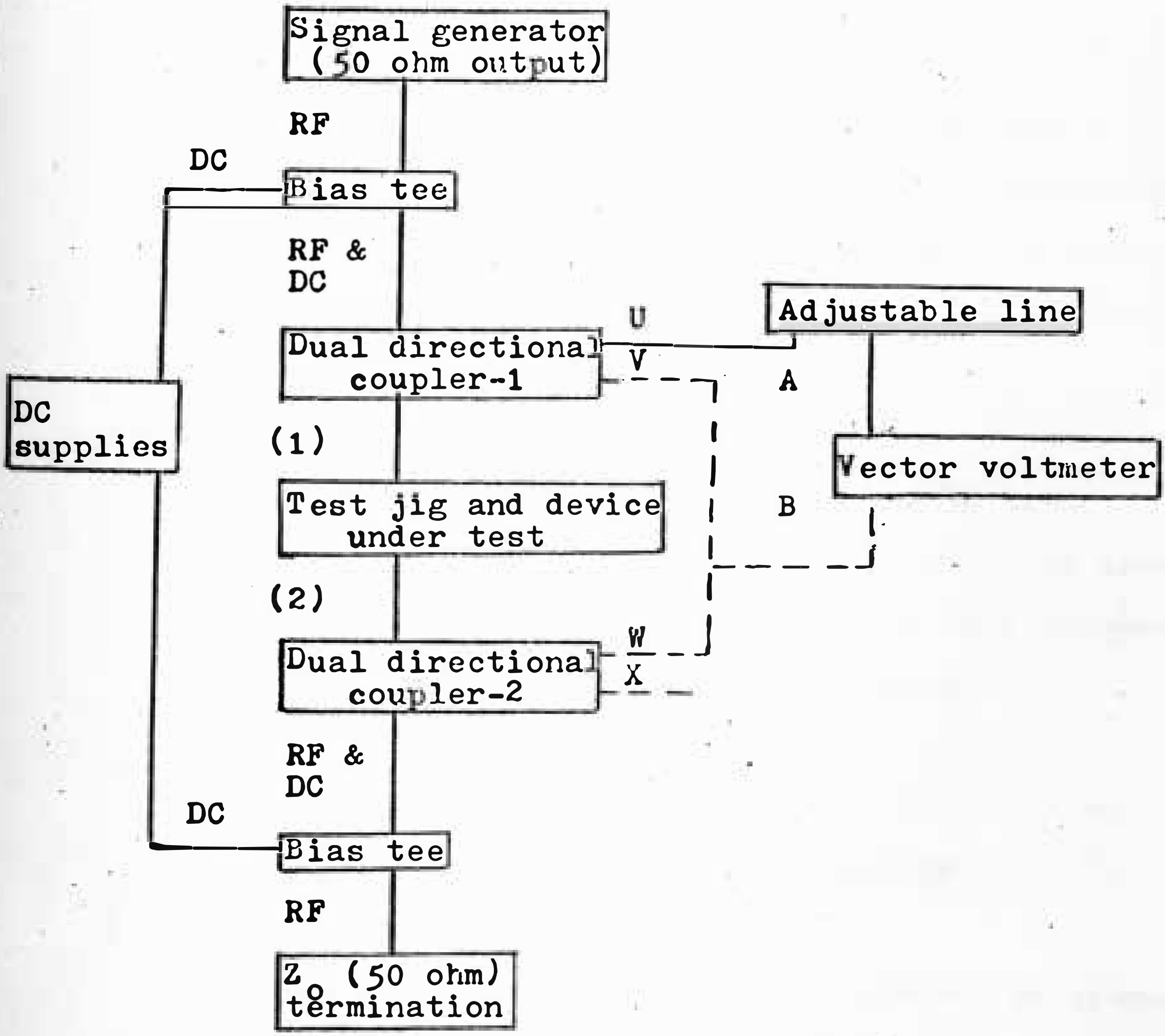

Fig. 4-1. Block diagram for 2-port S-parameter measurements.

follows:

1. Signal Generator: GR 1201-A

   Variable frequency signal generator with a 50 ohm coaxial output. The signal output is attenuable continuously from several volts down to zero volts. Frequency ranges of 40-250 MHz and 250-920 MHz are available in this type.

2. Bias Tee: MICRO LAB/FXR HW-02N

   To mix or separate RF signals and DC bias currents, bias tees must be used. The monitor tees, MICRO LAB/FXR HW-02N, are employed for this purpose. Characteristics for HW-02N are as follows:

   a. Maximum VSWR = 1.3
   b. Impedance = 50 ohms
   c. Maximum insertion loss = 0.2 dB

3. Dual Directional Coupler: HP 774D

   For sampling the incident, reflected, or transmitted wave, dual directional couplers are used. HP 774D Couplers, which are of strip line structure, are especially good for VHF applications. The close tracking of the auxiliary arms makes these couplers useful for wide-band measurement. S-parameters are determined by the ratios of the outputs of two arms so coupling variations with frequency are eliminated. The characteristics of the HP 774D by the manufacturer are as follows:

a. Frequency range = 215-450 MHz

b. Minimum directivity = 40 dB

c. Coupling attenuation = 20 dB

d. Maximum primary line SWR = 1.15

4. Vector Voltmeter: HP 8405A

The HP 8405A Vector Voltmeter measures the magnitude and the phase difference between two voltage vectors from 1 to 1000 MHz. It uses a sampling method. The a's and b's are measured with the VVM, and the reflection coefficients are the ratios of b_i to a_i.

Bridge tees and isolators, which do not appear in the block diagram of Fig. 4-1, are employed when readings are taken. Specifications of the HP 8405A VVM are as follows:

a. Frequency range = 1-1000 MHz

b. Voltage ratio accuracy = ± 2%

c. Phase accuracy = at single frequency $\pm 1.5^{\circ}$

d. Voltage range (rms) = 300 uV - 1.0 V for A channel and 100 uV - 1.0 V for B channel at frequency of 10-500 MHz.

5. Test Jig or Transistor Mounting

The test jig is a device which accomodates the transistor during test. There are two types

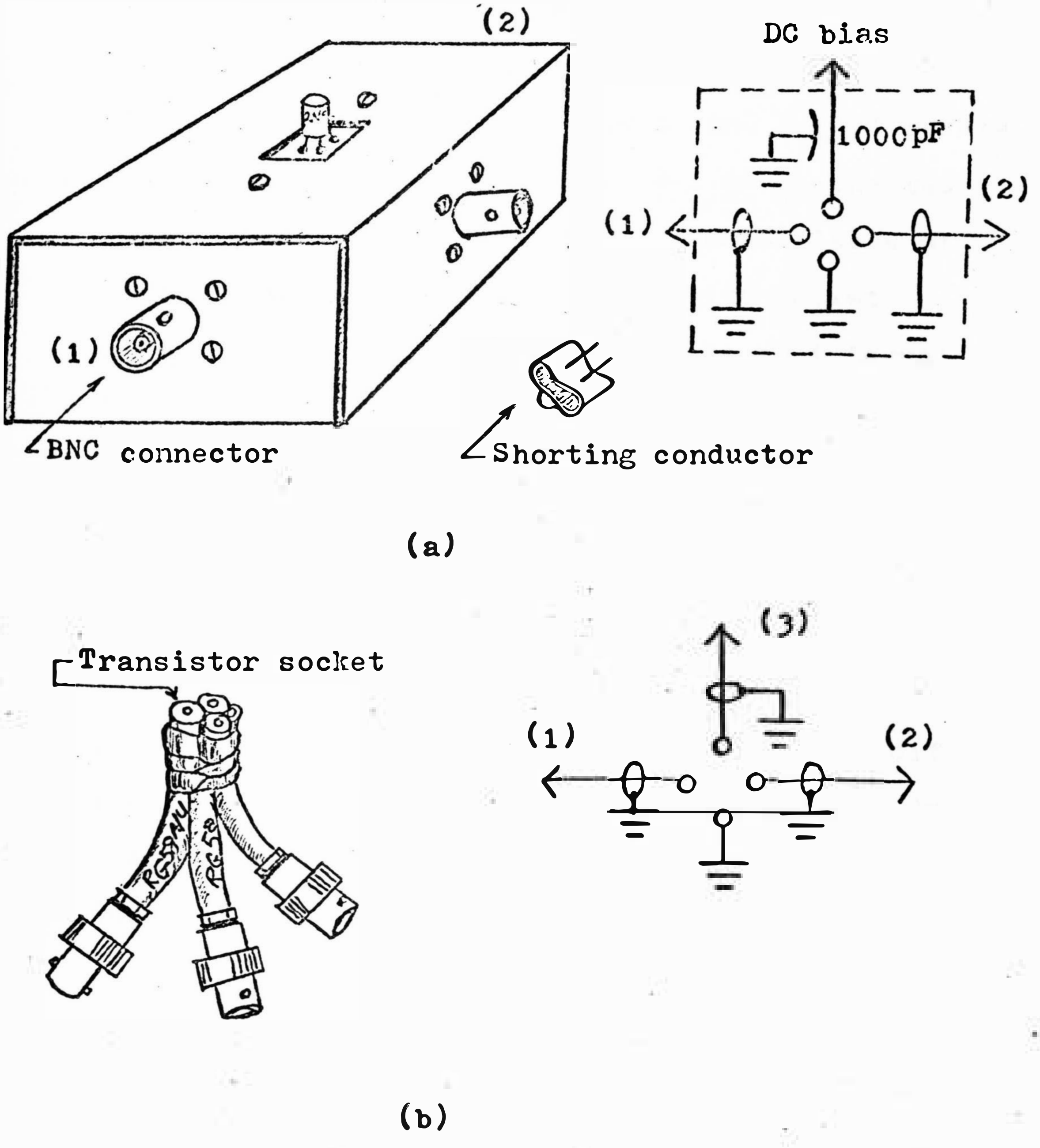

Fig. 4-2. Test jigs for (a) 2-port and (b) 3-port measurements.

of test jigs: strip-line and coaxial.

For this experiment, several test jigs were attempted so that 2-port, 3-port, and 4-port parameters could be measured. Fig. 4-2 shows the test jigs used. Coaxial jigs where several pieces of flexible dielectric line, RG A/U with socket pins built inside the lines that are an integral part of the inner conductors, have been used.

The lines are cut to identical lengths so the paths for the reflected and transmitted waves are equal. By doing this the ports are interchangeable thereby reducing set-up time. The path differences observed for each branch of the jigs can be minimized by trial and error. The residual path differences caused a phase shift of less than 3° at frequencies between 150 and 250 MHz.

6. Adjustable Line: GR 874-LA

Since the phase differences between incident and scattered center are to be measured, it is necessary for the waves to have equal electrical lengths. An adjustable coaxial line with an impedance of 50 ohms was used for this purpose.

7. 50 Ohm Coaxial Terminations: HP Model 908 A

For VHF frequencies precise terminations over a wide range of measurement frequencies are necessary so there are no undesired reflections at the termination points during measurement. At relatively low frequencies the terminations can be constructed with carbon film or solid resistors as shown in Fig. 4-3. Biasing terminals are also shown in the figure.

8. DC Supplies

It is desirable to use very stable and finely adjustable DC supplies. A high resistance may be connected in series with the bias supply to give smoother control of bias current during bipolar device testing.

B. Reference Plane

It has been shown that when a traveling wave encounters a discontinuity on a transmission line, twp scattered waves traveling in opposite directions are generated. S-parameters can be obtained by comparing the amplitudes and phase angles of the scattered waves with those of the original wave.

However, measurements cannot be made directly at the scattering center (port terminals). This is because of the physical size of the directional couplers and connecting leads (50-ohm line between measurement system and device to be tested). As a result, the scattered waves travel finite

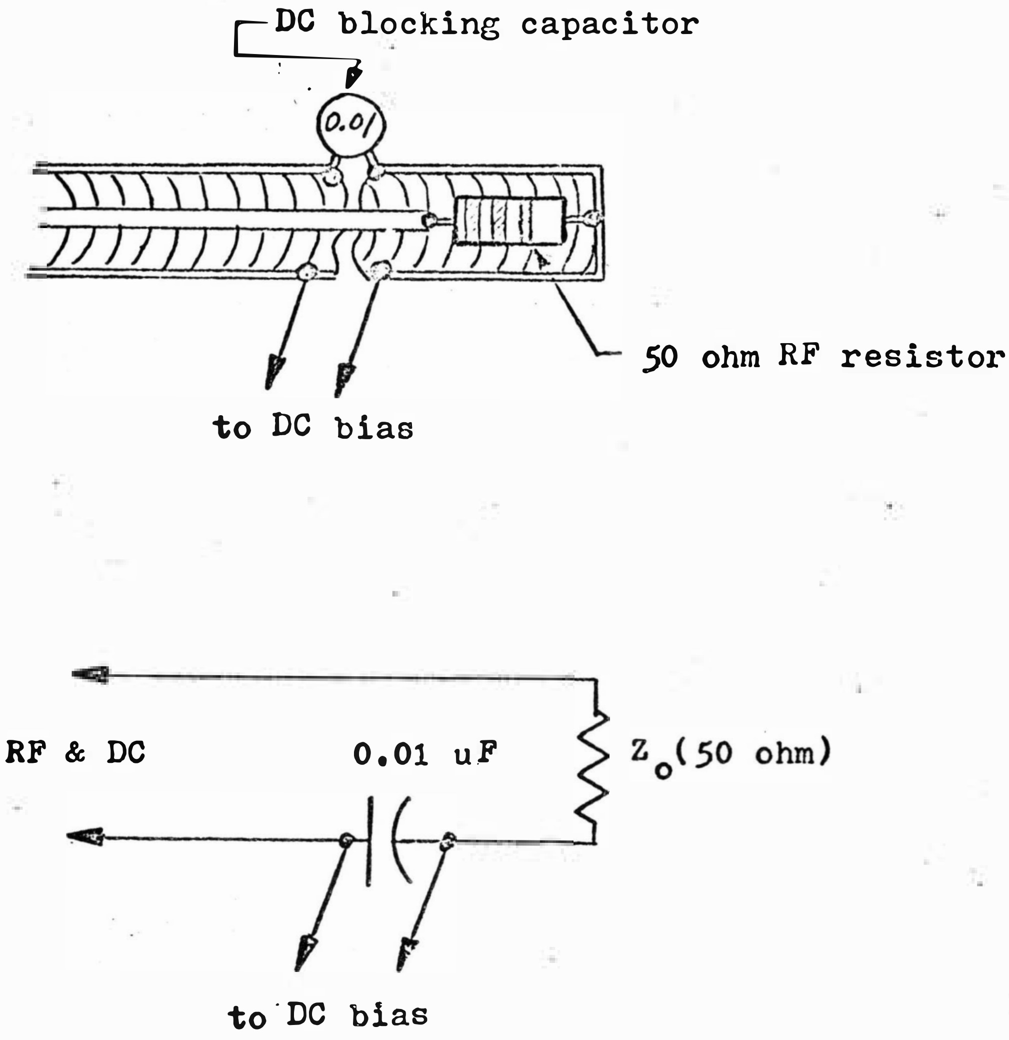

Fig. 4-3. Termination with DC block.

distances along lossless lines before they are measured. To obtain the relationships between the scattered and original waves at the scattering center, phase compensation is made by adjusting the path length of the original (incident) wave.

Traveling distances for the waves are shown in Fig. 4-4 for a 2-port measurement. L_i, L_r, and L_t are the electrical path lengths (excluding that of the device to be tested) of incident, reflected, and transmitted waves measured from an arbitrary input point. L_r and L_t are equal if the test jig is symmetrical and both directional couplers are identical. L_i can be adjusted by changing the length of the adjustable line. When the length L_i is made equal to L_r and L_t, the amplitude and phase relationships for the incident and reflected waves at the measurement point and the original scattering point are identical. Further, the relationships are independent of frequency.

The scattering plane P in Fig. 4-4 is often called the "reference plane."[6] The reference plane can be located by employing short or open termination in place of the device to be tested. The phase difference between incident and reflected waves for short and open ends are 180° and 0°, respectively; however, the fringing effect at an open end may not allow precise positioning of the reference plane. The short termination method is more commonly employed for

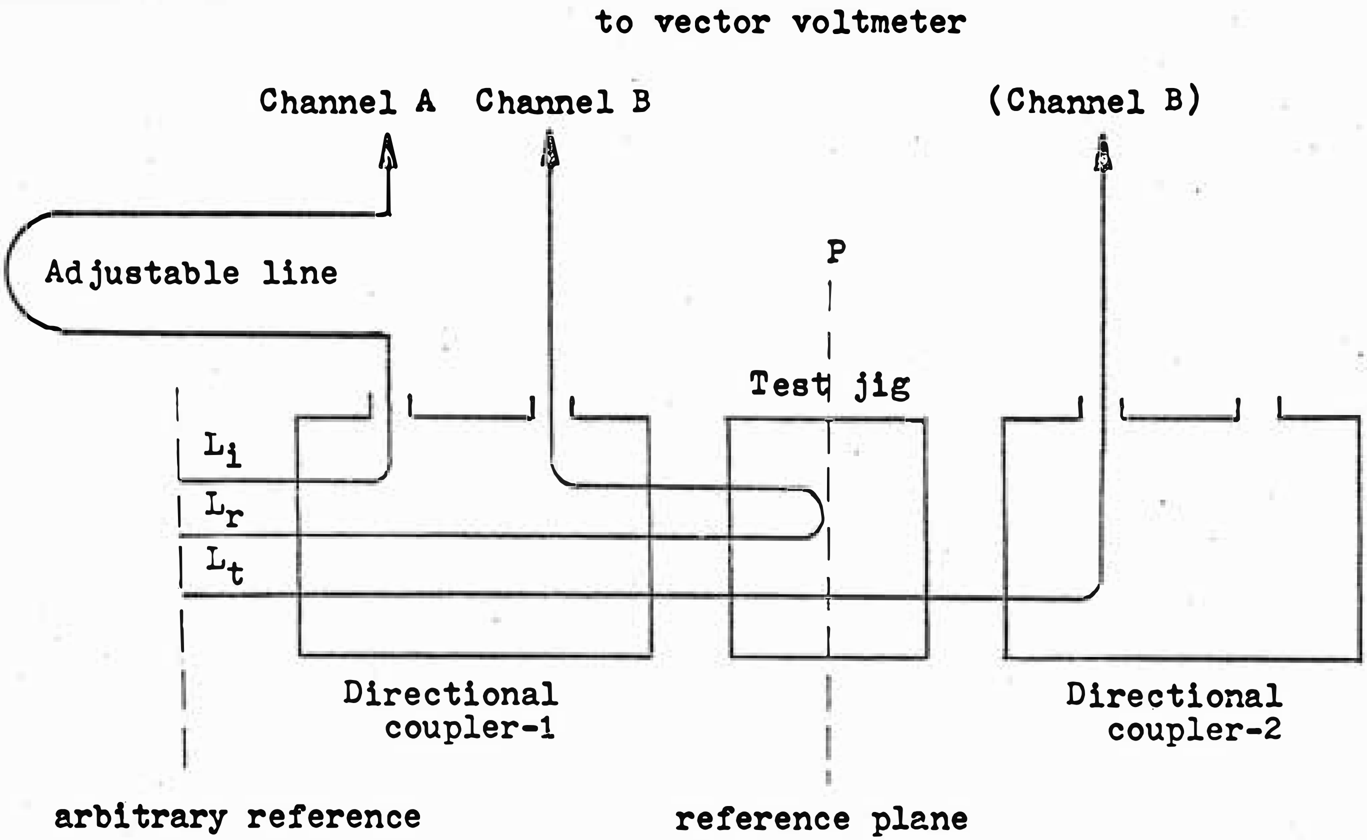

Fig. 4-4. Block diagram showing reference plane calibration.

that practical reason. A "through-section"[12] can also be used to adjust the path lengths but is not necessary in a test set-up where L_r and L_t are equal.

C. Measurement Procedures

1. Preliminary check of equipment before mounting test jig (channel A probe connected to V in Fig. 4-1).

After every connector is firmly locked, the amplitude difference between channel A and channel B is read without test jig in position. The amplitude ratios of channel A and channel B outputs in this manner should be very close to unity with open or short termination in place of the test jig, and approach zero with a 50-ohm termination. Typical observed values are 0.99 for open or short termination and 0.01 for 50-ohm termination at 150 MHz. These amplitude errors can be attributed to the directional couplers and VVM.

2. Set-up of reference plane.

The test jig is mounted in position and the shorting conductor is plugged into the socket. The adjustable line should be changed until the phase meter of the VVM reads 180 degrees. The test jig is then reversed by connecting the input to the opposite end. The phase differences observed in this manner are due to the difference between the input and output path lengths. This difference has to be minimized by careful construction of the test jig. The adjustable line should be readjusted so that the same reference plane is attained when the input and output ports are interchanged during calibration.

3. DC supplies consideration.

After the reference plane is set up, the transistor to be tested is plugged in. Then proper DC voltages are provided to the transistor through the bias tees.

4. Signal generator.

The signal generator is first set at the desired frequency with a minimum output level. Then the output is slowly increased until the reading of channel A voltage reaches full scale on the -50 dB or 1 mV range. Assuming that the coupling factor of the directional coupler, HP 774D, is 25 dB maximum, the magnitude of the input signal is less than 20 mV.

5. S-parameters measurement (2-port parameters0.

Refer to Fig. 4-1. Initially channel B is connected to the V arm of directional coupler 1 in order to measure reflection coefficients S_{11} and S_{22}. Port number 1 or 2 must be defined in terms of the terminals of the device being tested. For example, in bipolar transistor measurements it may be convenient to define the base and the collector terminals as port 1 and port 2, respectively.

If port 1 of the device being tested is connected to directional coupler 1, S_{11} can now be measured. If the channel A voltage is set at full scale, then the voltage of channel B and the phase angle between channel A and channel B represents the magnitude and phase of the input reflection coefficient, S_{11}. Measurement of the output reflection coefficient, S_{22}, is exactly the same as that of S_{11} except that the input and output ends of test jig are interchanged. The DC supply must also be changed.

The forward gain S_{21} is obtained by plugging the channel B probe into arm W of directional coupler 2. The ratio of channel A and channel B voltage amplitudes and phase angles between them are the polar expression of S_{21}. S_{12}, the reverse gain, is measured in the same way as S_{21}, but input and output ports are interchanged.

If the base and the collector of a bipolar device (or the gate and drain of a MOSFET) are properly assigned port 1 and port 2, respectively, then S_{12} is usually very small for those devices in common-emitter (or common-source) configuration. These small values can be read accurately using the log step scale of VVM. Also, in order to read a small S_{12}, injection of large signal is necessary. A minimum of 100 mV applied at the output port was required for satisfactory reading.

6. Three-port parameters and differential-amplifier type IC measurement.

The same set-up for 2-port parameter measurement was used, only replacing test jigs. In 3-port measurements, auxiliary termination with proper DC bias is connected to the remaining port.

7. Error approximation.

By varying the frequency of the signal generator over the frequency range where measurements are to be made, the maximum deviation of amplitude and phase errors can be approximated. The maximum deviation in the frequency range from 150 MHz to 250 MHz was ±1% in amplitude and ± 2 degrees in phase. It should also be noted, however, that amplitude errors are measured at full scale where reading accuracy is a maximum.

The fringing effect error is also significant particularly for the reflection coefficients phase angles when ports are terminated in a high impedance. When the shorting conductor is removed from the socket of the test jig, the phase deviation from 0^o is measured without changing the adjustable line. This measures the fringing effect error. (Refer to Appendix III-B.) A maximum of 5 degrees positive phase error was observed at frequencies between 150 and 250 MHz.

CHAPTER V

EXPERIMENTAL DATA AND DISCUSSION OF RESULTS

S-parameters of several VHF semiconductor devices are obtained with the measurement set-up discussed in Chapter IV. This chapter will be devoted to the presentation of the experimental results based on the discussions of Chapter III.

A. Bipolar Transistor - Common-Emitter 2-Port Parameters

The VHF range is a relatively low frequency category for these devices. At VHF frequencies, the time delay due to minority carrier transit time is negligible and the hybrid Pi equivalent circuit of Fig. 3-1 can be employed in explaining experimental data.

Two sets of curves, $S\text{-}I_C$ and $S\text{-}V_{CE}$ in common-emitter configurations, are measured in order to study the nonlinear behavior. The resulting curves are shown in Figs. 5-1 and 5-2. The frequency was fixed at 150 MHz for these data.

1. S-Parameters versus Collector Current Curves.

1-1. $S_{11}\text{-}I_C$ (Fig. 5-1 (a)). The results are plotted on a Smith Chart (Fig. 5-3) which gives the input impedance with a 50-ohm terminated output. The reciprocal of this impedance is approximately y_{11}, since 50-ohm output termination impedance is relatively small when compared with the output impedance of the device. Internal feedback is also very small at 150 MHz.

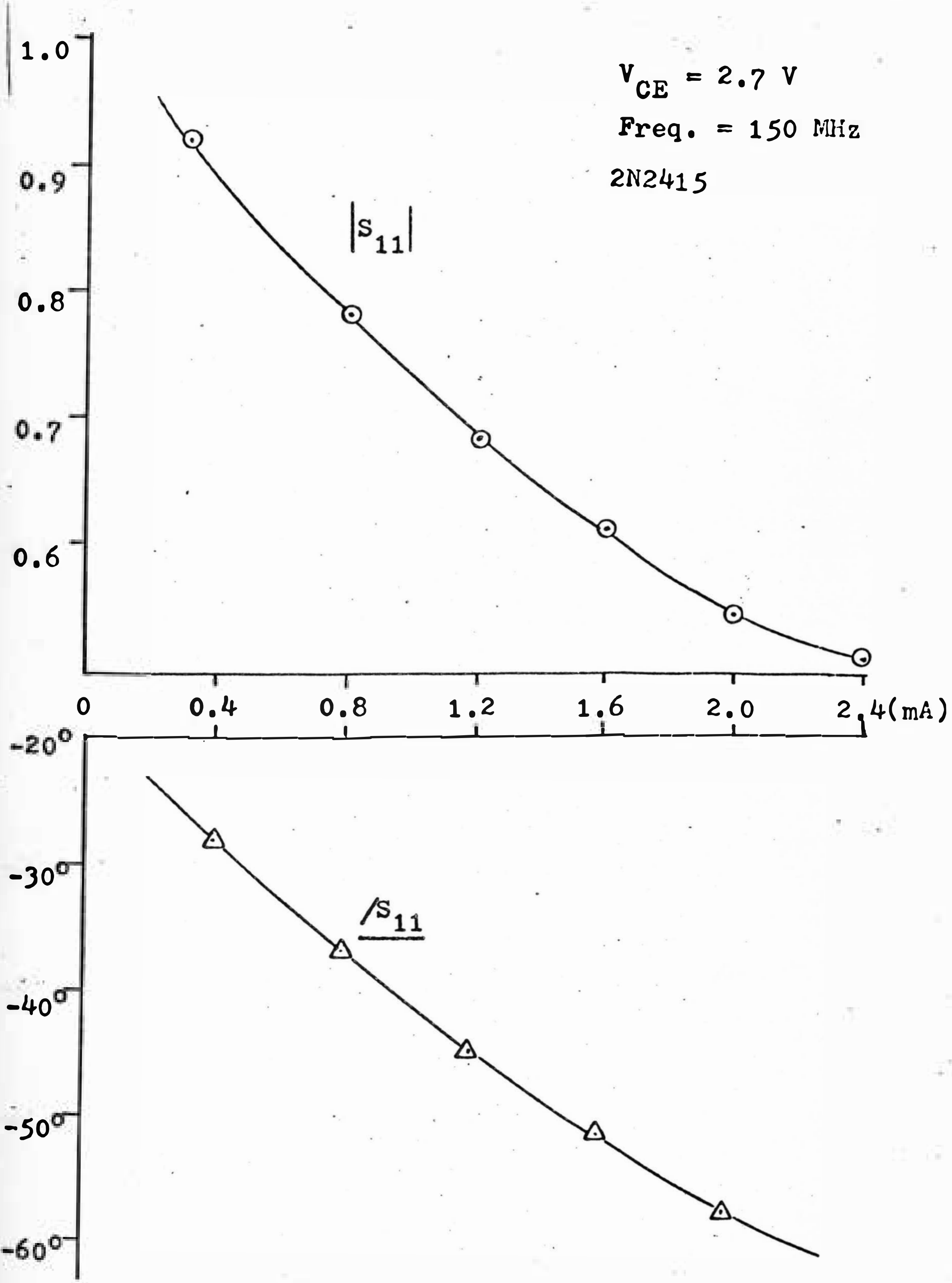

Fig. 5-1(a). Common-emitter S_{11}-I_C curve.

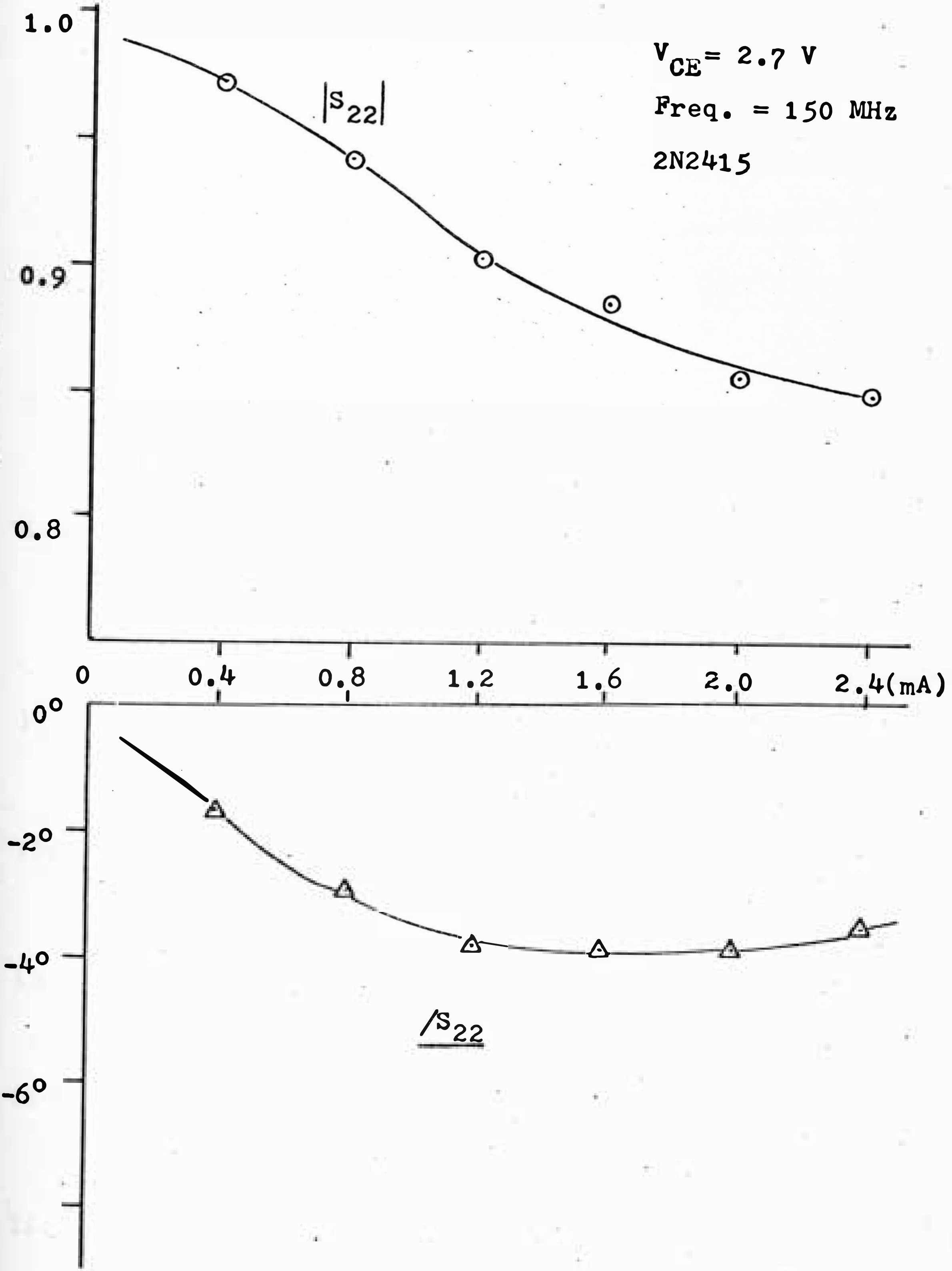

Fig. 5-1(b). Common-emitter S_{22}-I_C curve.

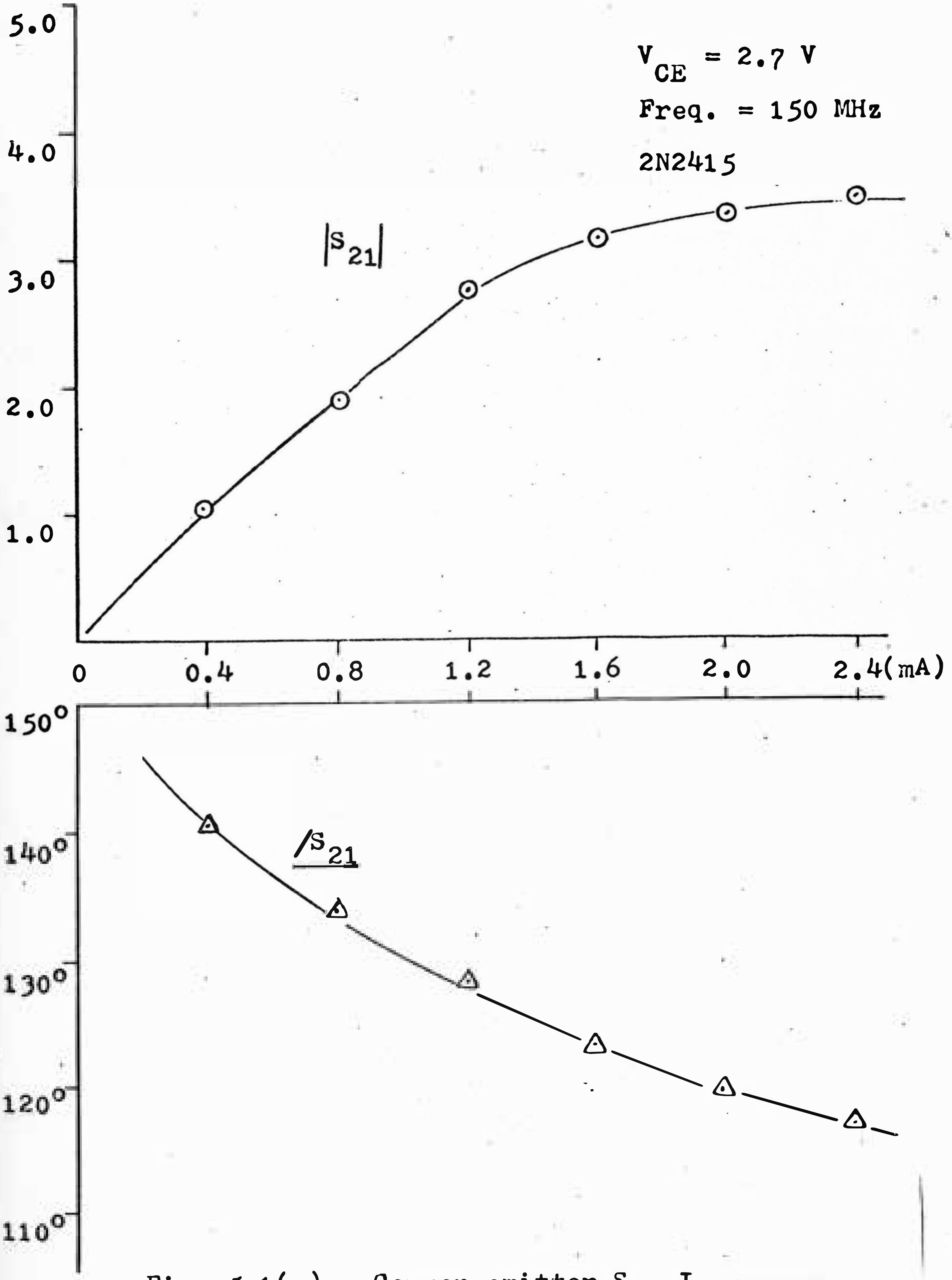

Fig. 5-1(c). Common-emitter S_{21}-I_C curve.

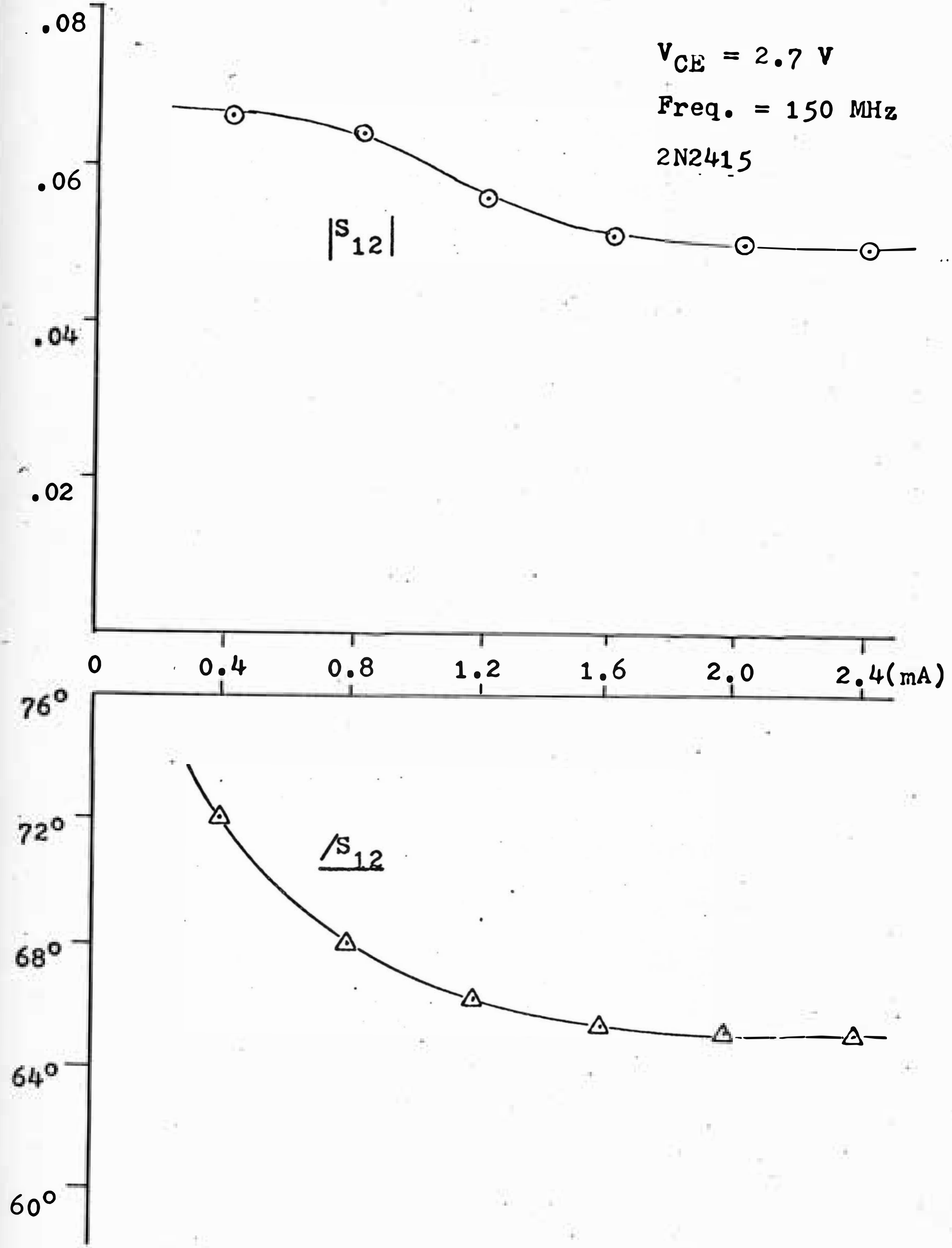

Fig. 5-1(d). Common-emitter S_{12}-I_C curve.

The Smith Chart shows that the locus of S_{11} with increasing I_C lies on a constant resistant circle. This implies the effect of the base spreading resistance, $r_{bb'}$ of Fig. 3-1. As was discussed in Chapter III, $r_{bb'}$ is constant regardless of the DC operating point. The value of $r_{bb'}$ from the Smith Chart of Fig. 5-1 is constant at about 50 ohms.

1-2. S_{22}-I_C (Fig. 5-1 (b)). S_{22} is generally not as sensitive to I_C variations as S_{11}; however, the magnitude of S_{22} decreases gradually with increasing I_C, while the angle, $\underline{/S_{22}}$ is almost constant.

These variations can be explained by a decreasing dynamic resistance, r_{ce}. The variation of $\underline{/S_{22}}$ in the region of I_C less than 1 mA is mainly due to the variations in the capacitance $C_{b'c}$. This capacitance is a function of the collector-base junction voltage.

1-3. S_{21}-I_C (Fig. 5-1 (c)). This curve is analogous to g_m-I_C curves (or more closely y_{21}-I_C curves). The result can be checked in Appendix I. S_{21} can be approximated assuming $S_{12} = 0$ by

$$S_{21} = -\tfrac{1}{2}y_{21}(1 + S_{11})(1 + S_{22}) \qquad (5\text{-}1)$$

where y_{21} is normalized forward transfer admittance.

From Eq. (5-1) it can be seen that S_{21} is in proportion to I_C (or g_m where $g_m = \Lambda I_C$) for small collector currents (i.e. less than 1 mA). Note that the impedance between the e and b' nodes of the hybrid Pi circuit is much larger than $r_{bb'}$ and y_{21} is approximately proportional to g_m for this collector current. The variations due to the product, $(1 + S_{11})(1 + S_{22})$ of Eq. (5-1), do not appear explicitly in the magnitude data of S_{21}.

$|S_{21}|$ deviates from a straight line with increasing I_C because the impedance between b' and e decreases inversely with I_C. The terms y_{21} and $(1 + S_{11})$ decrease as the results in Fig. 5-1 (c) show.

If the measurement frequency is sufficiently high the impedance between b' and e is mainly due to $C_{b'e}$, i.e., $\omega r_{b'e} C_{b'e} \gg 1$. Therefore, at high frequencies y_{21} can be approximated in terms of g_m, $C_{b'e}$, and $r_{bb'}$ where the feedback elements $C_{b'c}$ and $r_{b'c}$ are neglected.

$$y_{21}/Z_o = \frac{g_m/j\omega C_{b'e}}{r_{bb'} + 1/j\omega C_{b'e}} \qquad (5\text{-}2)$$

The denominator $(r_{bb'} + 1/j\omega C_{b'e})$ is approximately equal to the input impedance of the device at this frequency. The input impedance can then be expressed in terms of the S-parameter relationships

$$(r_{bb'} + 1/j\omega C_{b'e})/Z_o = (1 + S_{11})/(1 - S_{11}) \qquad (5\text{-}3)$$

where S_{11} is the common-emitter input reflection coefficient.

When these results are substituted into Eq. (5-1), the phase angle of S_{21} takes a simple form:

$$\underline{/S_{21}} = 90^{\circ} + \underline{/1 - S_{11}} + \underline{/1 + S_{22}} \qquad (5\text{-}4)$$

For collector currents greater than 1 mA, Eq. (5-4) agrees with the data given in Fig. 5-1. For example, the phase angle from Eq. (5-4) using measured values for S_{11} and S_{22} at $I_C = 2$ mA is about 122° and the measured phase angle of S_{21} is 118°. This result can be used to check the validity of the bipolar hybrid Pi circuit, i.e., another application of Eq. (5-4) is the estimation of minority carrier transit time. Since Eq. (5-4) is derived with the assumption of real g_m, the phase shift due to minority carrier transit time is not considered. The phase difference between measured S_{21} and calculated S_{21} then implies this phase shift, which is, for the above data, 4°. In the light of the assumptions for Eq. (5-4), this angle, 4°, is negligible. At higher frequencies these angles will be more significant.

1-4. S_{22}-I_C (Fig. 5-1 (d)). The same argument for Eq. (5-1) can be applied for S_{12} by replacing y_{21} and S_{21} in the equation with y_{12} and S_{12}, respectively. For negligible $|S_{12}S_{21}|$

$$S_{12} = -\tfrac{1}{2}y_{12}(1 + S_{11})(1 + S_{22}) \qquad (5\text{-}5)$$

where y_{12} is normalized reverse transfer admittance.

Y_{12} is now given in terms of hybrid Pi parameters.

$$y_{12}/Z_o = - \frac{Y_{b'c}}{Y_{b'e}} \cdot \frac{1}{r_{bb'} + 1/Y_{b'e}} \qquad (5\text{-}6)$$

where $Y_{b'c} = 1/r_{b'c} + j\omega C_{b'c}$

$Y_{b'e} = 1/r_{b'e} + j\omega C_{b'e}$

but $(r_{bb'} + 1/Y_{b'e})$ is approximately the input impedance, for $Y_{b'c}$ is assumed to be negligible. Then the scattering parameter relationship is as follows:

$$(r_{bb'} + 1/Y_{b'e})/Z_o = (1 + S_{11})/(1 - S_{11}) \qquad (5\text{-}7)$$

By substituting Eq. (5-6) and Eq. (5-7) into Eq. (5-5), S_{12} is finally expressed in the following form:

$$S_{12} = \frac{Y_{b'c}}{Y_{b'e}}(1 - S_{11})(1 + S_{22}) \qquad (5\text{-}8)$$

Since the $Y_{b'c}$ and $(1 + S_{22})$ terms in Eq. (5-8) are not sensitive to collector current, $(1 - S_{11})$ and $Y_{b'e}$ terms are the main source of S_{12} variation. However, the magnitude of S_{12} in Fig. 5-1 (d) is approximately constant over wide variations of I_C, implying that the magnitudes of $(1 - S_{11})$ and $Y_{b'e}$ increase with increasing I_C.

Where the measurement frequency is sufficiently high, i.e. $\omega r_{b'e}C_{b'e} \gg 1$, $Y_{b'e}$ is approximately $j\omega C_{b'e}$. Then the phase relations for Eq. (5-8) can be written as

$$\underline{/S_{12}} = \underline{/Y_{b'c}} - 90^{\circ} + \underline{/1 - S_{11}} + \underline{/1 + S_{22}} \qquad (5\text{-}9)$$

but $\underline{/Y_{b'c}}$ does not vary with I_C and can be assumed constant. Eqs. (5-9) and (5-4) show that the curves for $\underline{/S_{12}}$ and $\underline{/S_{21}}$ are parallel with a constant angular difference of $180^{\circ} - \underline{/Y_{b'c}}$. This constant angle in Fig. 5-1 is about 65° indicating $\underline{/Y_{b'c}}$ is about 115°.

2. S-Parameters versus Collector Voltage Curves.

Severe parameter changes can be observed in the saturation region. This is where the collector voltage fails to provide sufficient reverse bias at the collector junction for encouraging the drift movement of minority carriers. To understand parameter behavior at low collector voltage, a transistor can be thought of as consisting of two diodes. At low collector voltages the base bias voltage may be higher than the collector voltage and the two diodes are effectively forward-biased. Input impedance then becomes much smaller in this case as compared with the input impedance when sufficient collector voltage is applied.

2-1. $S_{11} - V_{CE}$ (Fig. 5-2 (a)). S_{11}-V_{CE} curve shows the behavior just discussed. Where V_{CE} is smaller than 1 V, the magnitude and phase curves drop down very quickly according to the forward-biased diode characteris-

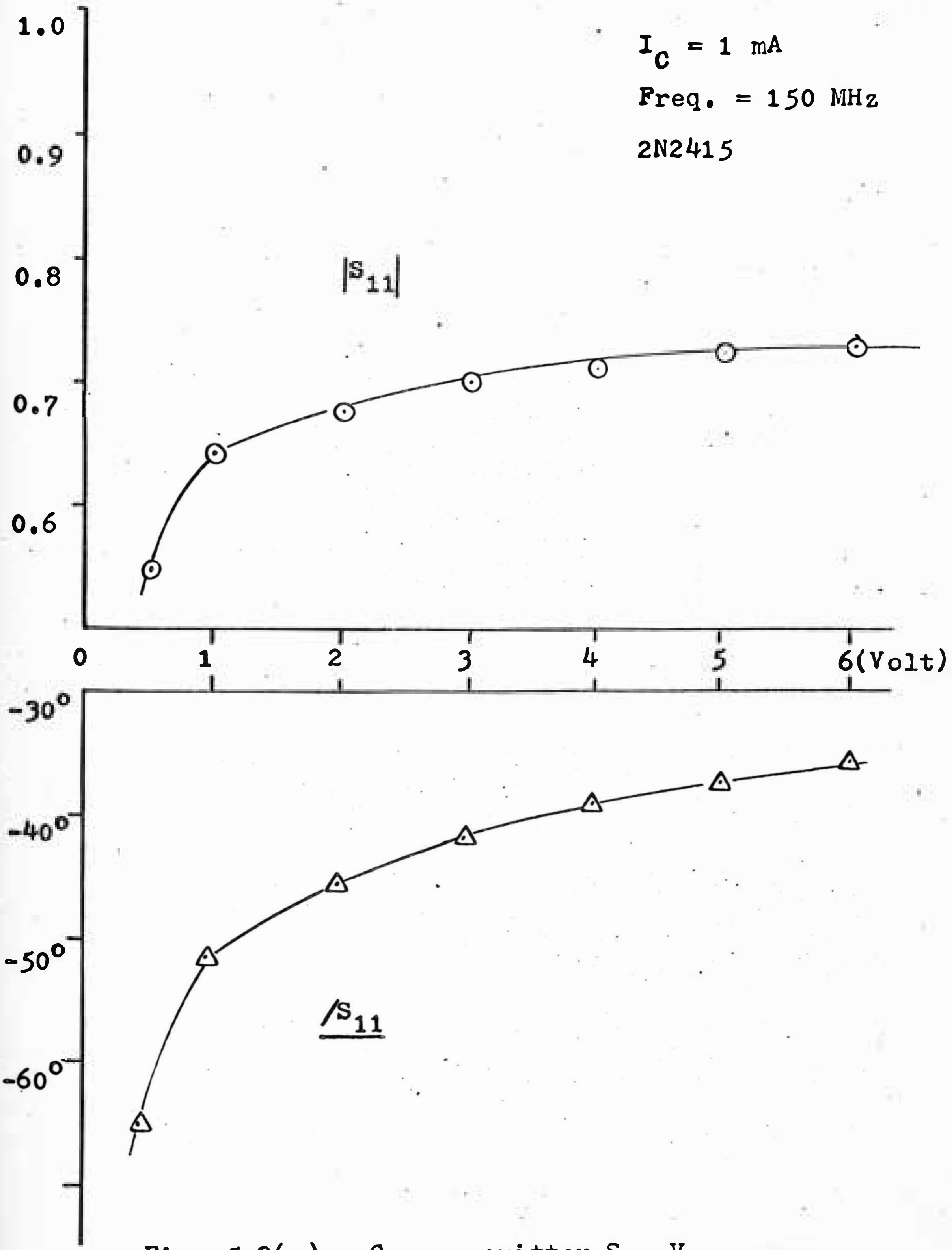

Fig. 5-2(a). Common-emitter S_{11}-V_{CE} curve.

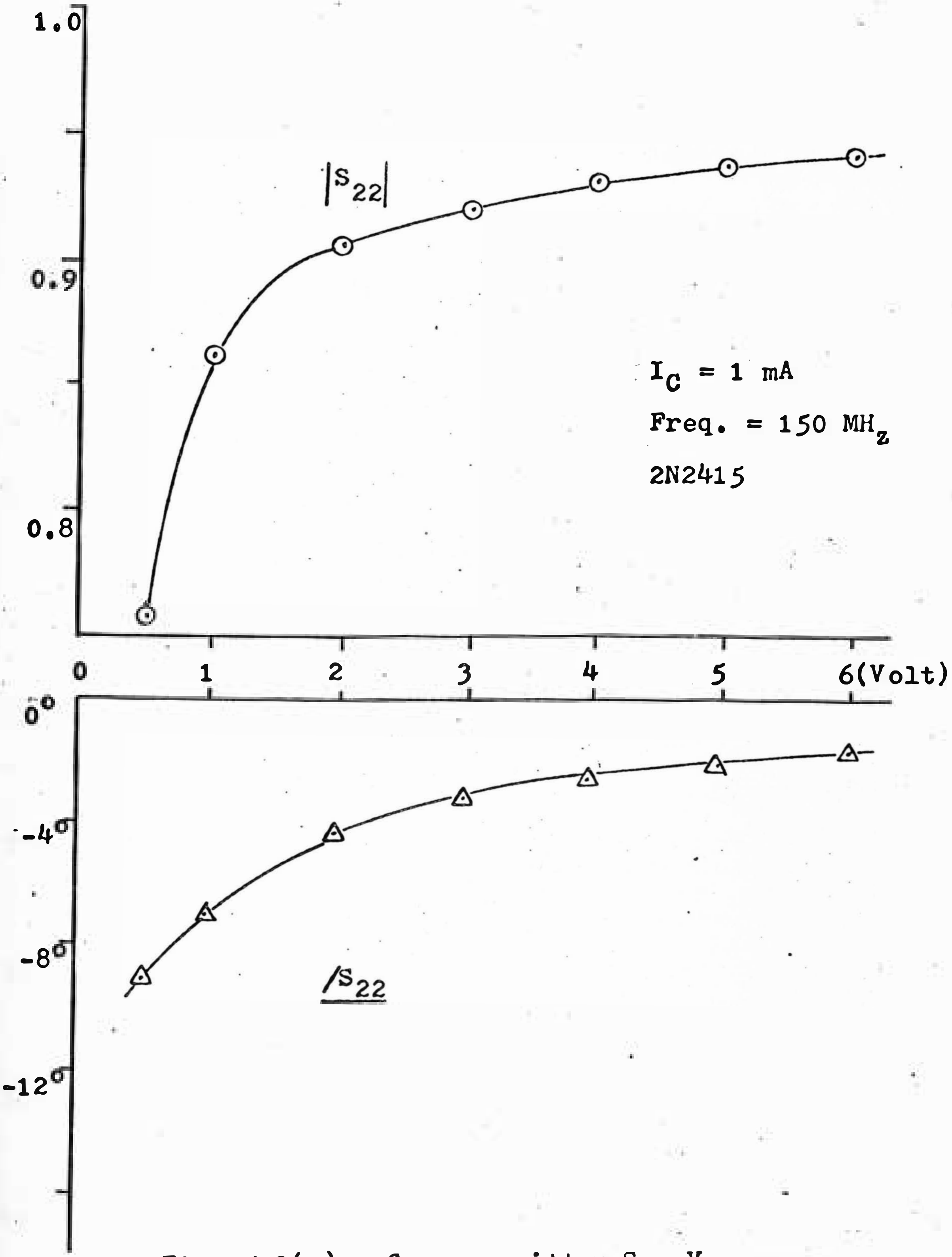

Fig. 5-2(b). Common-emitter S_{22}-V_{CE} curve.

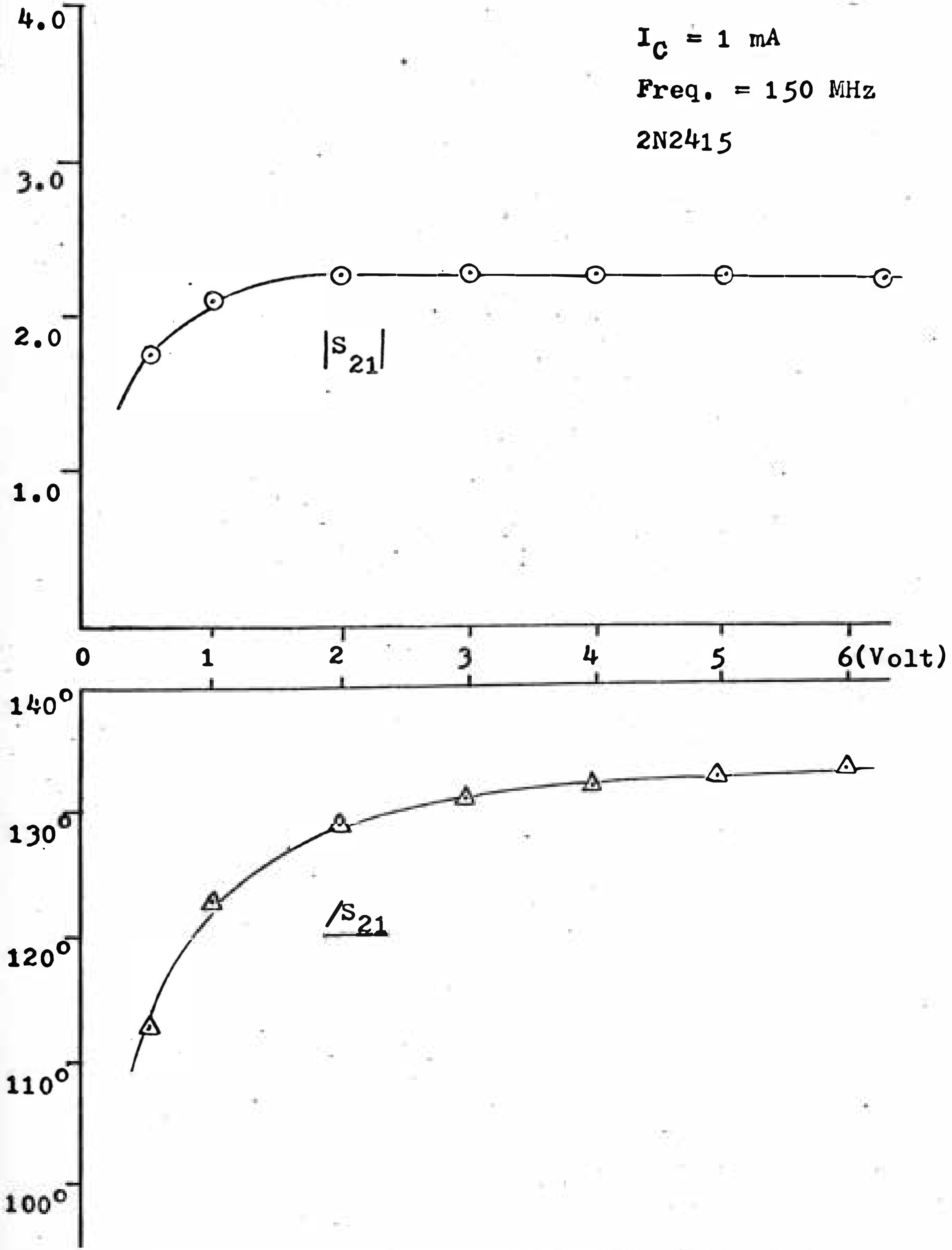

Fig. 5-2(c). Common-emitter S_{21}-V_{CE} curve.

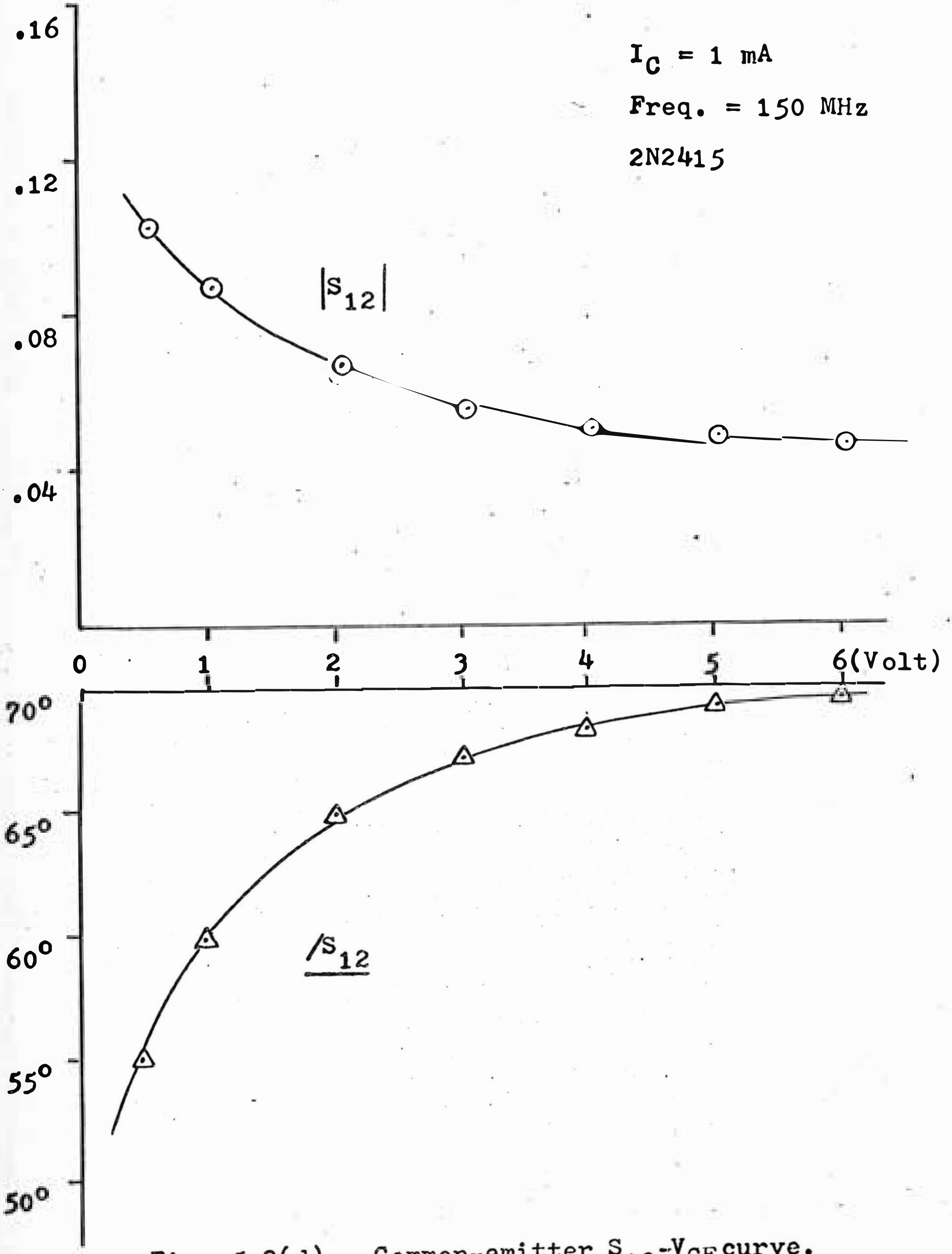

Fig. 5-2(d). Common-emitter S_{12}-V_{CE} curve.

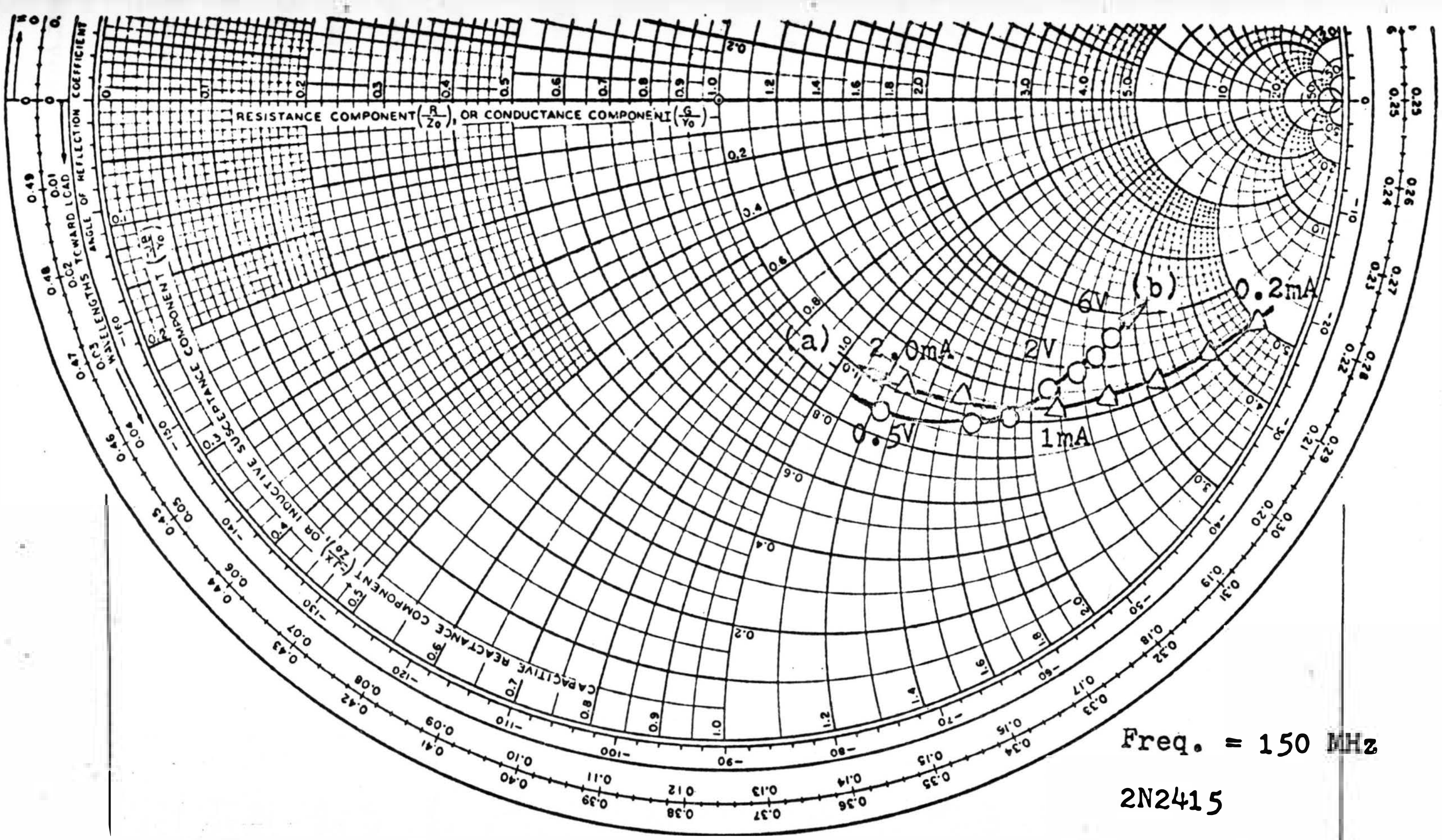

Fig. 5-3. Smith Chart plot of common-emitter S_{11} curves: (a) S_{11}-I_C (V_{CE} = 2.7 V); (b) S_{11}-V_{CE} (I_C = 1 mA).

But the curves become much flatter once sufficient collector voltages are supplied; input impedance now mainly depends on the base-to-emitter diode. (See Fig. 5-3.)

2-2. S_{22}-V_{CE} (Fig. 5-2 (b)). In the saturation region the same explanation is valid for the S_{22}-V_{CE} curve; the output impedance corresponding to S_{22} shows the forward-biased diode characteristic until sufficient reverse bias is provided between the base-collector junction. S_{22} varies with increasing V_{CE} mainly due to the decrease of $C_{b'c}$ and the increase of dynamic resistance r_{ce}.

2-3. S_{21}-V_{CE} (Fig. 5-2 (c)). By recalling Eq. (5-1) the behavior of S_{21} is more clearly understood. Since I_C is held constant, y_{21} can also be assumed a constant. The phase variation then is approximately the sum of the variations of $\underline{/1 + S_{11}}$ and $\underline{/1 + S_{22}}$. The data shown in Fig. 5-2 (c) agree very well with this type variation.

It can also be noted that S_{21} is almost constant once V_{CE} passes from the saturation region. This point can be easily understood by referring to the hybrid equivalent circuit. Under normal operating conditions most of the hybrid Pi parameters are unaffected by changes in collector voltage. $C_{b'c}$ is collector voltage dependent, but is not significant in the S_{21} calculations.

2-4. S_{12}-V_{CE} (Fig. 5-2 (d)). Lastly, S_{12}-V_{CE} curves are shown. The decrease of $|S_{12}|$ with increase of V_{CE}

implies an effective decrease in the feedback admittance, $Y_{b'c}$. See Eq. (5-8).

By now, interpretation of the experimental results for a bipolar device has been made. At higher frequencies, such as in microwave frequency range, the transit time of minority carriers would have to be taken into account. Investigation of this point of view is beyond the scope of this thesis and is not discussed.

B. MOSFETs (Single-Gate and Dual-Gate) - Common-Source 2-Port Parameters

Measurements on MOSFET transistors are made in the same manner as for bipolar transistor measurements. During dual-gate MOSFET measurements, additional bias for gate 2 is provided through an RF-grounded terminal. Grounding of this terminal eliminates parasitic effects. The case and substrate are also in common with the source terminal for common-source operation. The test jig is shown in Fig. 4-2(a).

Reading $|S_{11}|$ and $|S_{22}|$ requires great care since these values are generally close to unity for low-frequency (i.e. 150 MHz) common-source measurements. Sophisticated calibration is required for these measurements.

A heat sink may have to be prepared to prevent thermal runaway or excessive excursions of the operating point whenever the transistor is operated at large DC input levels. Severe changes in the forward transmission coefficient are observed for large DC inputs. Readjustment of the bias voltages to compensate for the decrease of drain current can result in a wide variation of parameter values.

1. Single-gate MOSFET - Common-source S-V_{DS} Curves.

1-1. S_{11}-V_{DS} (Fig. 5-4 (a)). A family of curves is obtained for various drain voltages. From typical values of the hybrid Pi parameters, for a high-frequency MOSFET (Fig. 3-2 (b)), it can be seen that S_{11} will largely depend on C_c and r_c, the gate-channel capacitance and the channel-source bulk resistance. But the behavior of r_c is different from that of $r_{bb'}$ of bipolar devices; r_c as well as C_c vary with the gate bias voltage V_{GS}.

The input impedance of a MOSFET can be approximated by r_c and C_c as a series impedance and shunt capacitance C_{gs}, r_{gs}, C_{gd}, and r_{gd} are neglected. Now the input impedance Z_i can be represented in terms of r_c, C_c, and C_{gs}.

$$Z_i = \frac{r_c + 1/j\omega C_c}{(C_c + C_{gs})/C_c + j\omega r_c C_{gs}} \tag{5-10}$$

For typical MOSFET data,[20] C_{gs} is much smaller than C_c and $\omega r_c C_{gs}$ term is negligible at 200 MHz. Then

$$Z_i = \frac{C_c}{C_c + C_{gs}} r_c + \frac{1}{j\omega(C_c + C_{gs})} \tag{5-11}$$

Eq. (5-11) indicates that the contribution of C_{gs} to the r_c and C_c series impedance causes only a small amount of

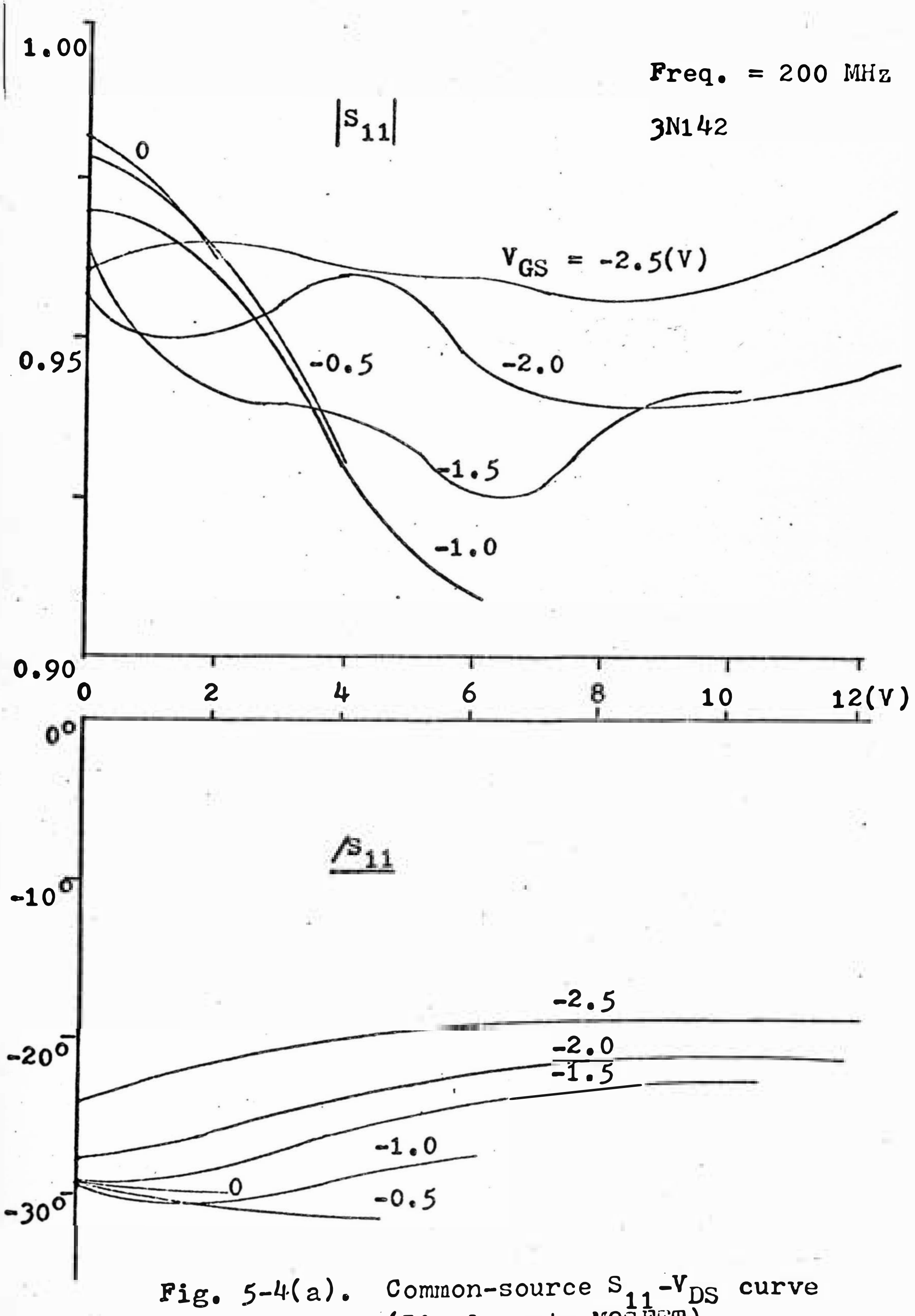

Fig. 5-4(a). Common-source S_{11}-V_{DS} curve (Single-gate MOSFET).

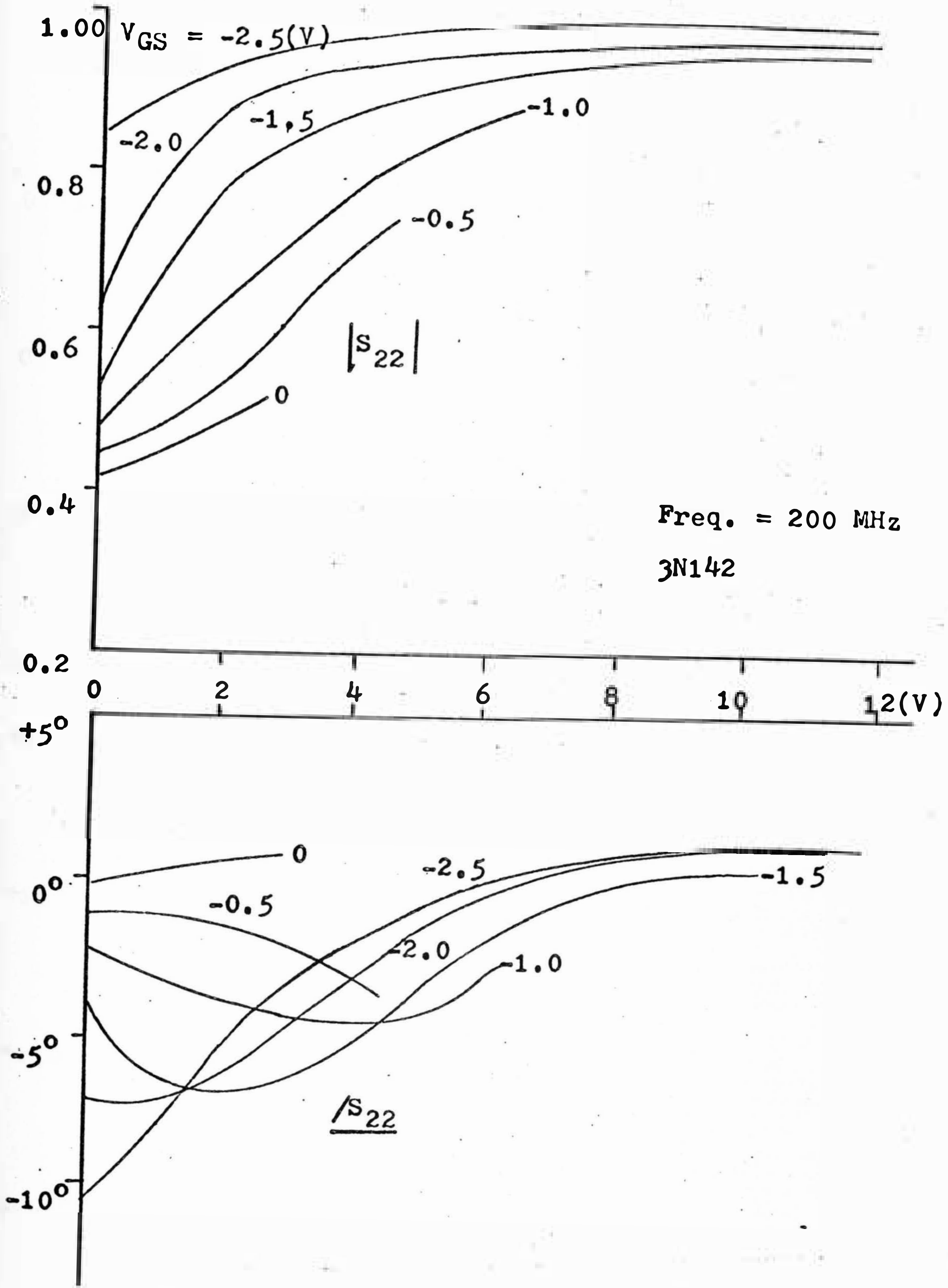

Fig. 5-4(b). Common-source S_{22}-V_{DS} curve (Single-gate MOSFET).

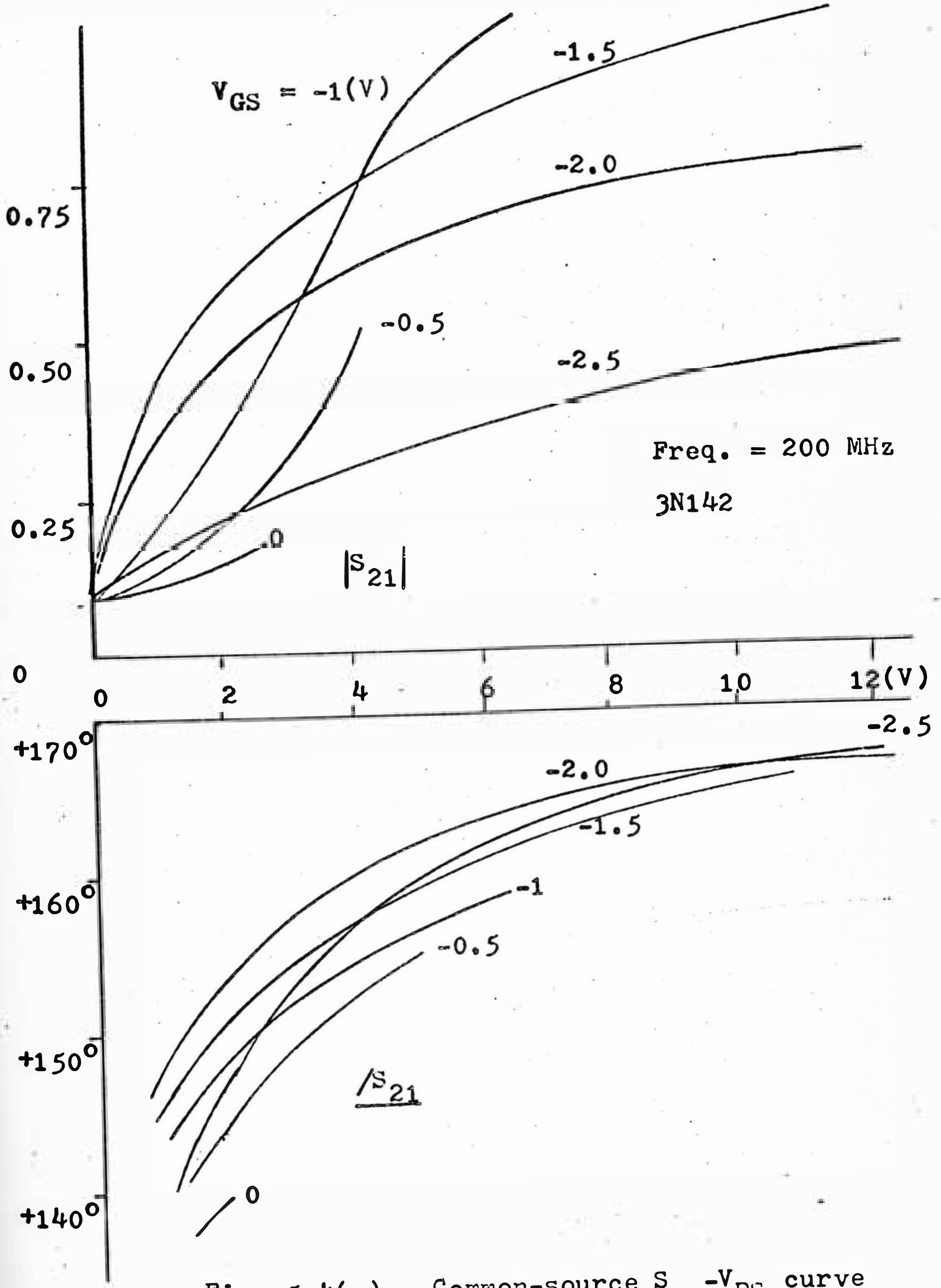

Fig. 5-4(c). Common-source S_{21}-V_{DS} curve (Single-gate MOSFET).

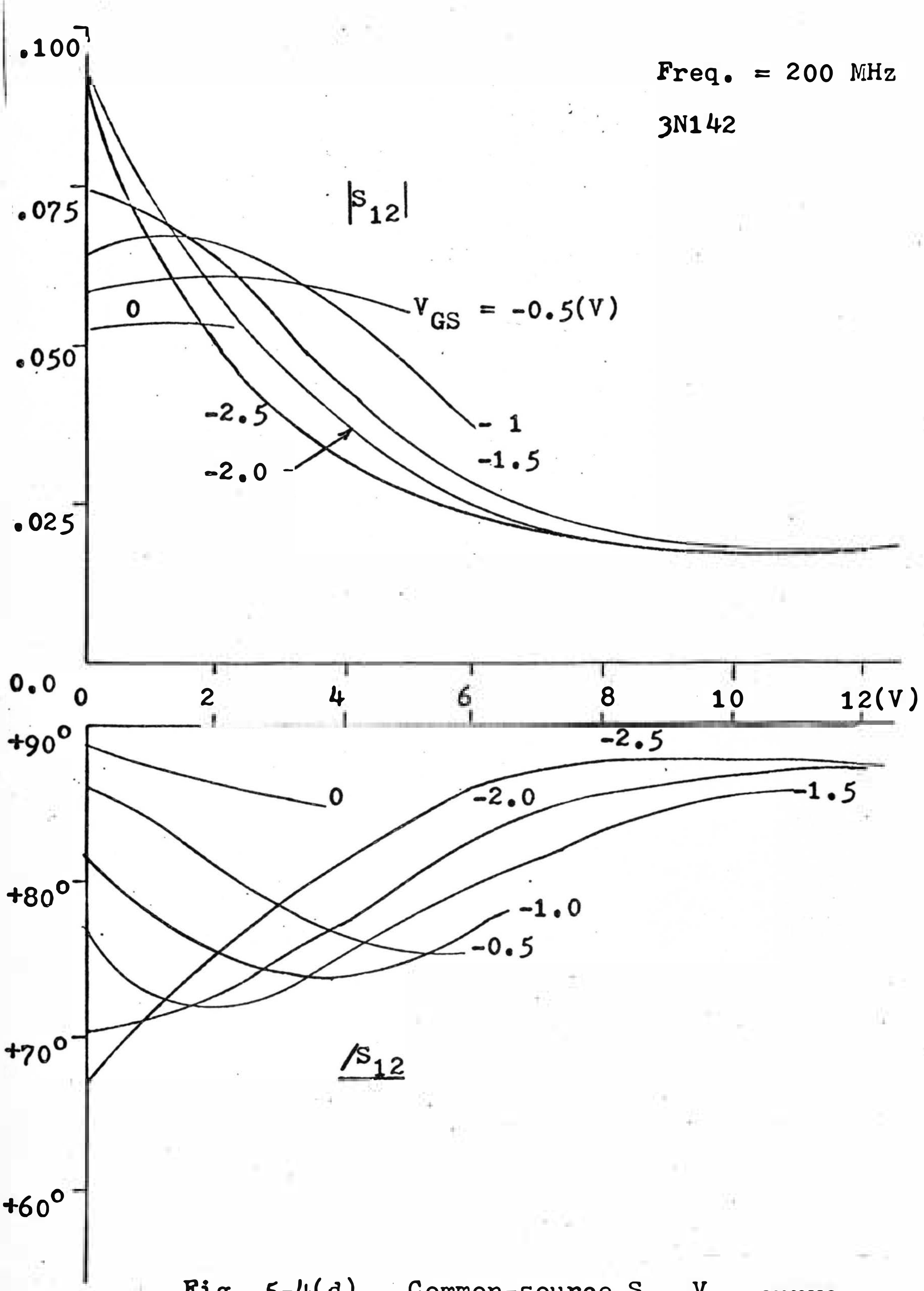

Fig. 5-4(d). Common-source S_{12}-V_{DS} curve (Single-gate MOSFET).

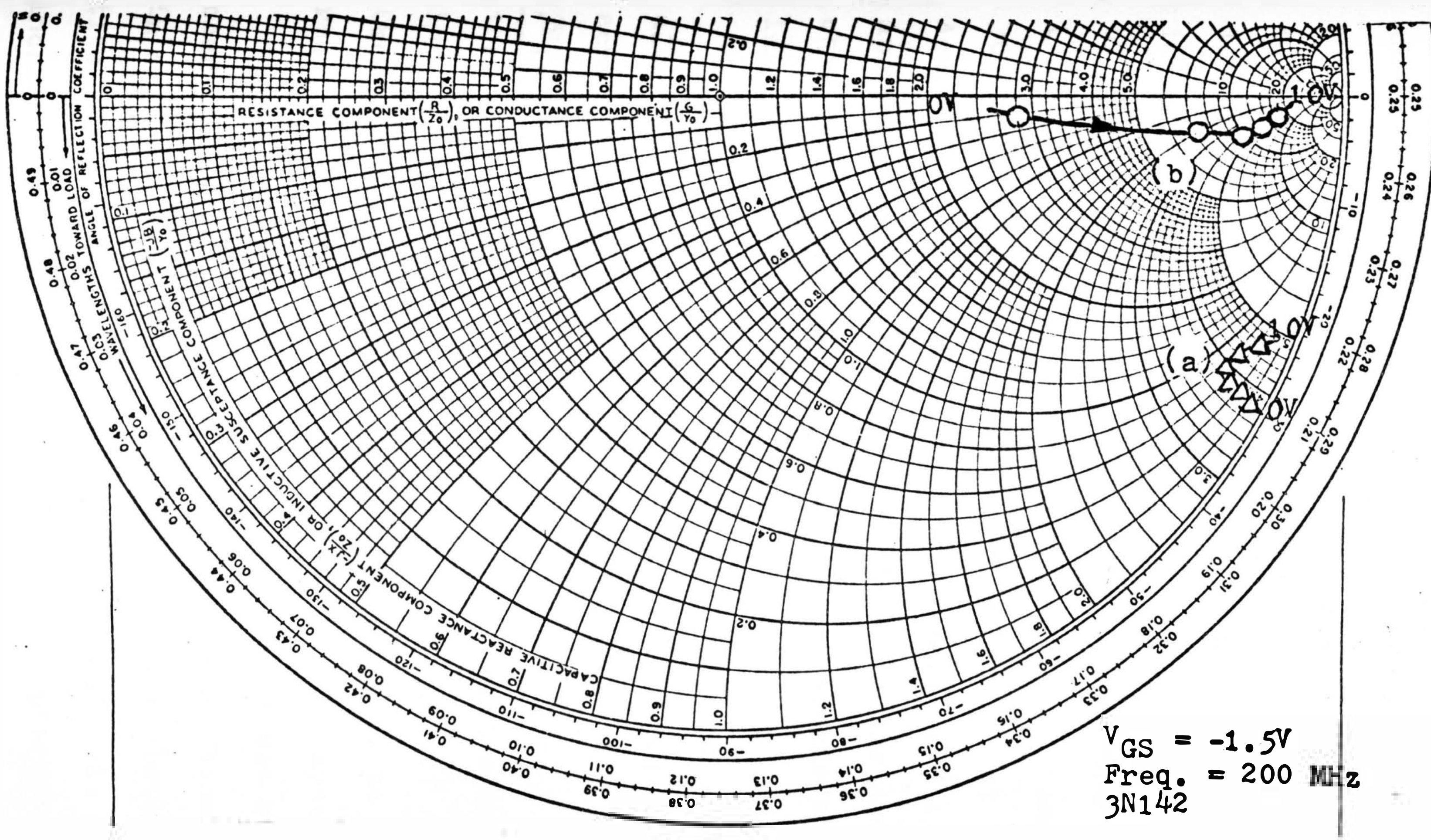

V_{GS} = -1.5V
Freq. = 200 MHz
3N142

Fig. 5-5. Smith Chart plot of common-source S-parameters: (a) S_{11}-V_{DS}; (b) S_{22}-V_{DS} (Single-gate MOSFET).

decrease in the magnitude. In other words input impedance still can be approximated by a series impedance consisting of r_c' and C_c' where r_c' and C_c' are defined by the equivalent resistance and capacitance of Z_i in Eq. (5-11). This impedance can be obtained directly from a Smith Chart plot of S_{11}. (Refer to Fig. 5-5.) The variations of r_c' and $1/\omega C_c'$ observed in this manner are in the range of 10 to 30 ohms and 200 to 250 ohms, respectively, at 200 MHz. Assuming $C_c = 5C_{gs}$, the variations of r_c and $1/\omega C_c$ are approximately in the range of 12 to 36 ohms and 240 to 300 ohms, respectively. The exact value depends on the operating point.

When V_{DS} is increased the gate-channel voltage will also slightly increase because of the DC potential drop across the channel-source DC resistance. The increase of $\angle S_{11}$ in Fig. 5-4 (a) implies this effect; once V_{DS} reaches the pinch-off region, the DC drop will not change, resulting in constant $\angle S_{11}$. Anomalous inversion of $\angle S_{11}$ curves (bend downward) at low drain voltages seems to be the result of another nonlinearity of the MOS capacitor.

1-2. S_{22}-V_{DS} (Fig. 5-4 (b)). A set of drain characteristics can be used to explain the behavior of S_{22}. In the triode region the dynamic output resistance is relatively small, resulting in low $|S_{22}|$. But this resistance increases and reaches saturation in the pinch-off region.

resulting in an $|S_{22}|$ that is close to unity.

In conjunction with the dynamic resistance variation, the drain-source capacitance decreases. The capacitance changes because of an effective increase in the width of the drain-source depletion region.[21] The positive phase angles of S_{22} in the figure are partly due to phase error of the measurement system (fringing effect error) and transistor lead lengths.

1-3. S_{21}-V_{DS} (Fig. 5-4 (c)). S_{21} data are considered under two conditions: S_{21} versus V_{DS} and S_{21} versus V_{GS}. S_{21}-V_{GS} relationship can be read directly from the figure for an arbitrary V_{DS}. On the other hand, $|S_{21}|$ -V_{DS} curves look like that of g_m-V_{DS} relationship except at very small V_{DS}.

This can be explained using Eq. (5-1), in which S_{12} is assumed negligible, i.e. $|S_{12}S_{21}| \ll |(1 + S_{11})(1 + S_{22})|$. Eq. (5-1) can be applied to this MOSFET.

y_{21} can now be derived from the hybrid Pi equivalent circuit in Fig. 3-2 (b).

Assuming $r_c \ll 1/\omega C_c$ and $r_{gd} \gg 1/\omega C_{gd}$

$$y_{21}/Z_o = g_m + j\omega C_{gd} \qquad (5\text{-}12)$$

When Eq. (5-12) is substituted into Eq. (5-1), S_{21} can be expressed as

$$S_{21} = -\tfrac{1}{2}(g_m + j\omega C_{gd})(1 + S_{11})(1 + S_{22})Z_o \qquad (5\text{-}13)$$

g_m and C_{gd} in Eq. (5-13) are obviously functions of V_{DS}. For an arbitrary V_{GS}, g_m increases with increasing V_{DS}(triode region) and it becomes constant when sufficient V_{DS} is applied (pinch-off region). The C_{gd}-V_{DS} curve is the opposite of g_m-V_{DS} relationship; C_{gd} decreases rapidly and approaches a minimum value, the extrinsic drain-gate capacitance.[20] g_m and C_{gd} also vary with V_{GS}. With increasing V_{GS}, both g_m and C_{gd} increase.

First, the S_{21}-V_{DS} relationship can clearly be understood using Eq. (5-13). At $V_{DS} = 0$, g_m is also 0 and S_{21} is determined by C_{gd}. For this case, it can be shown that y_{21} is equal to y_{12} and S_{21} is equal to S_{12}.

With increasing V_{DS}, g_m dominates C_{gd}. For sufficiently high V_{DS}, C_{gd} is negligible and S_{21} can be approximated by

$$S_{21} = -\tfrac{1}{2}g_m(1 + S_{11})(1 + S_{22}) \qquad (5\text{-}14)$$

Since g_m is a constant in the pinch-off region, $|S_{21}|$ will approximate a constant in view of the variations of the $(1 + S_{11})(1 + S_{22})$ product. Phases can also be checked by Eq. (5-14). At $V_{DS} = 10$ V, an angular difference of about 10° is found between the measured $\angle S_{21}$ and the calculated $\angle S_{21}$. The assumptions for Eq. (5-14), $g_m \gg \omega C_{gd}$ are justified.

For explaining the $|S_{21}|$ absolute maximum of the $|S_{21}|$ -V_{GS} relationship, Eq. (5-14) is useful. In the equation, S_{21} is a function of g_m and $(1 + S_{22})$, if the $(1 + S_{11})$ term is assumed constant. g_m and $(1 + S_{22})$ are distinctly functions of V_{GS}; one increases rapidly while the other decreases rapidly with increasing V_{GS}. Thus, the product will have an absolute maximum and so will S_{21} if the variation of $(1 + S_{11})$ term in Eq. (5-14) is not so significant with respect to V_{GS}.

1-4. S_{12}-V_{DS} (Fig. 5-4 (d)). Eq. (5-5) again is employed to explain these curves. If r_{gd} is ignored, y_{12} can be approximated in terms of C_{gd} such that

$$-y_{12}/Z_o = j\omega C_{gd} \qquad (5\text{-}15)$$

and combining Eq. (5-5) with Eq. (5-15),

$$S_{12} = \tfrac{1}{2} j\omega C_{gd}(1 + S_{11})(1 + S_{22}) \qquad (5\text{-}16)$$

For a very low bias voltage such as $V_{GS} = -2.5$ V, the variations of $(1 + S_{11})(1 + S_{22})$ are not significant and $|S_{21}|$ will be directly proportional to the feedback capacitance C_{gd}. S_{12}-V_{DS} curve for $V_{GS} = -2.5$ V is very close to the C_{gd}-V_{DS} curve.[20]

With increasing V_{GS}, the S_{12} curve deviates due to $(1 + S_{22})$ term and also due to the nonlinearity of C_{gd}. Effectively, C_{gd} can be increased by reducing the depletion layer at the drain-gate region with an increased V_{GS}. Note that the S_{12}-V_{DS} curves converge at $V_{DS} > 10$ to a minimum value indicating the effect of the extrinsic feedback capacitance.

2. Frequency Characteristics of Single-Gate MOSFET. Common-source S-parameters are measured and presented in Fig. 5-6. A normal Pi calculation is performed according to Eq. (3-6) and the results are plotted in Fig. 5-7.

It is seen that the rapid increase of the real part of A can be regarded as a second order effect of the R-C series circuit[21] combination of r_c' and C_c'. A 25 ohm resistor and 5 pF capacitor for the R-C series circuit gives excellent agreement over the frequency range.

The apparent inductive reactance of S_{22} is due to fringing effects. If an angular error of 5° (see Appendix Fig. A-III-4) is subtracted from $\underline{/S_{22}}$ then the true value of S_{22} is resistive and capacitive.

The frequency response of D does not show the exact behavior indicated by the simplified equivalent circuit of Fig. 3-2 (b). Some modifications, such as the addition of a drain-channel resistance, may be made for a more precise representation.[20]

The imaginary part of B represents the capacitive susceptance of C_{gd}, whose value is 0.15 pF. This value agrees with the 0.2 pF as given in the manufacturer's data (RCA MOS-160).[23]

The real part of B shows a negative conductance which cannot be explained by the equivalent circuit. It may be

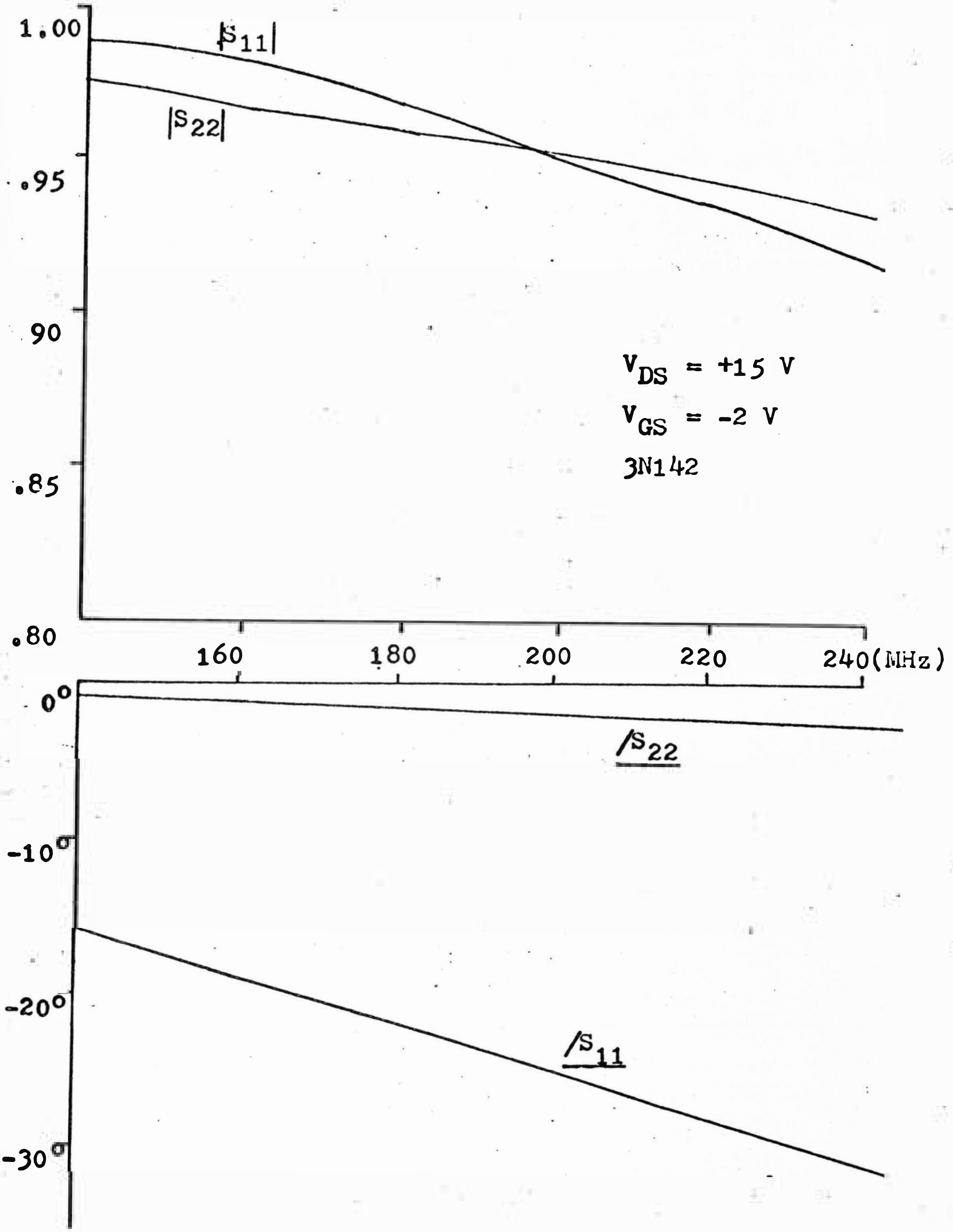

Fig. 5-6(a). Frequency response of common-source S-parameters (Single-gate MOSFET).

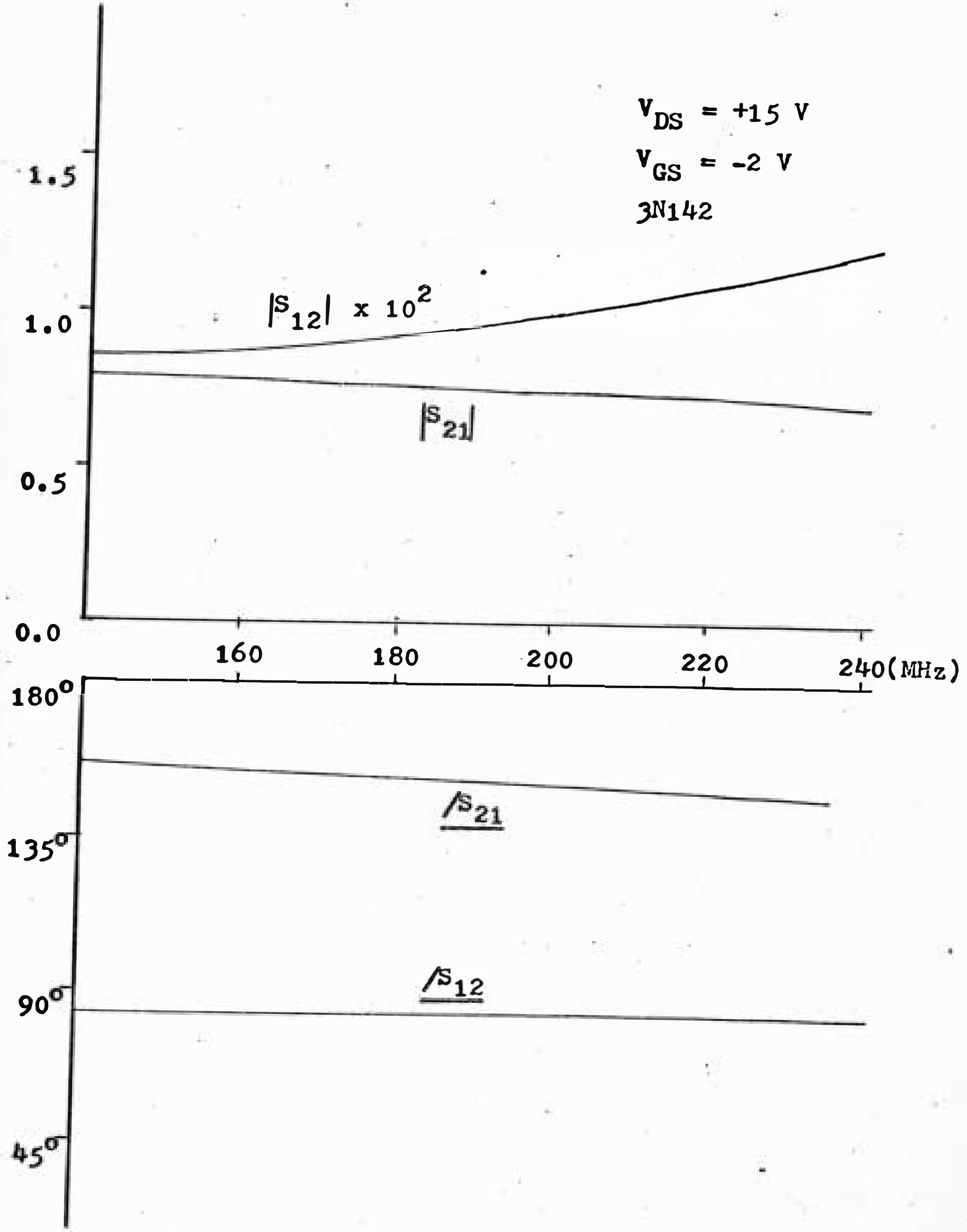

Fig. 5-6(b) Frequency response of common-source S-parameters (Single-gate MOSFET).

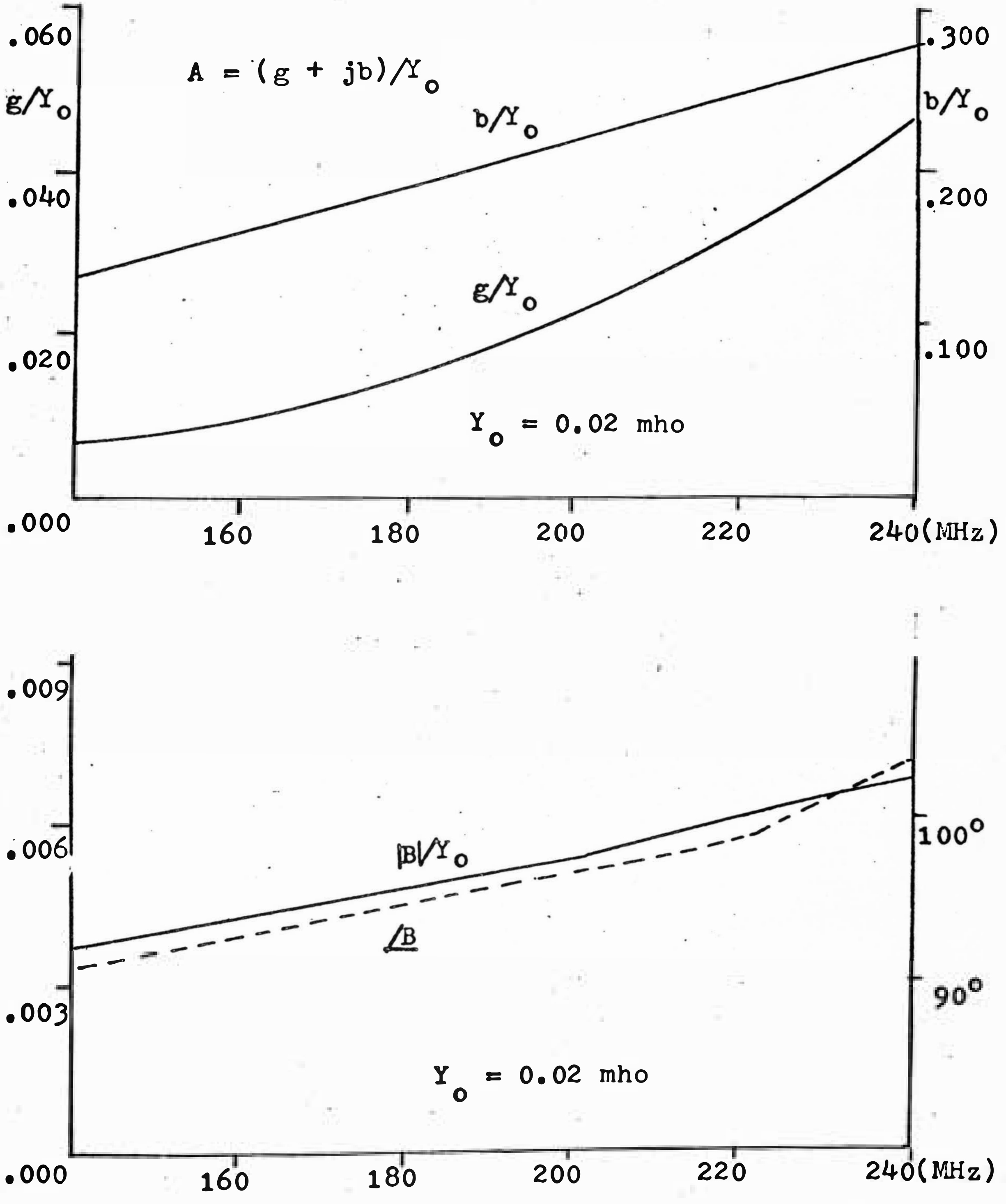

Fig. 5-7(a). Normal Pi versus frequency curves (Single-gate MOSFET 3N142).

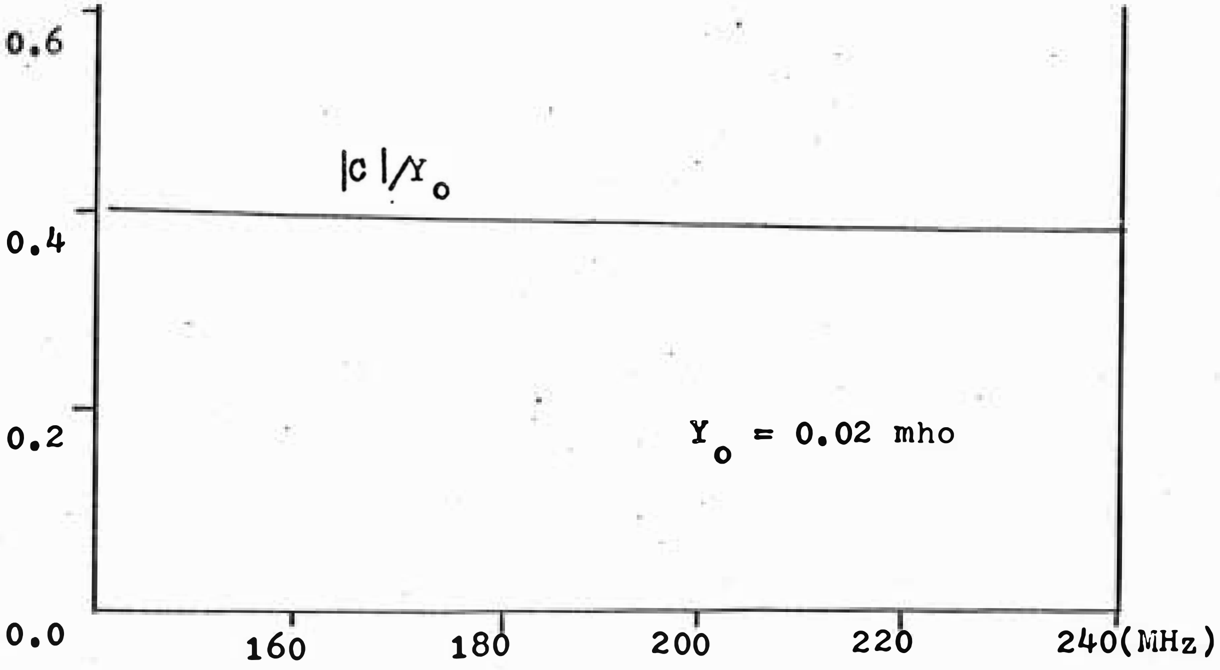

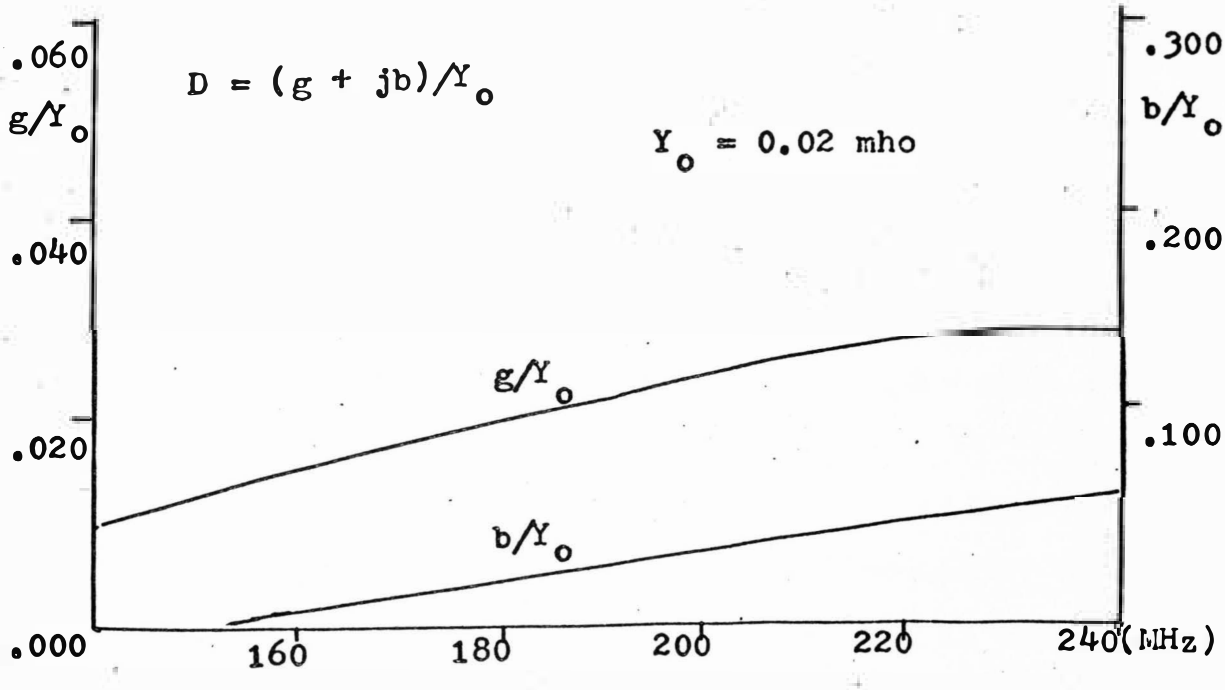

Fig. 5-7(b). Normal Pi versus frequency curves (Single-gate MOSFET 3N142).

regarded as the result of improper reference plane (i.e. longer L_i than required) or phase shift due to the distributed nature of the impedance in the channel region. The data show that the phenomenon is too distinct to be explained by measurement error, and a phase lead is also unlikely from a distributed R-C circuit viewpoint. Similar results are reported for y-parameters.[20]

The phase variation of C is more gradual than expected, but it is not so distinct as in S_{12}. It should be noted that the magnitude of C is practically constant over the measurement frequency; the value of C in Fig. 5-7 is approximately 8,000 umhos, which agrees with the g_m given by the manufacturer.[23]

3. Dual-Gate MOSFET - Common-Source S-V_{DS} Curves. As was discussed earlier in Chapter III, a dual-gate MOSFET may be analyzed as a cascode amplifier consisting of 2 single-gate MOSFETs. (Refer to Fig. 3-4.) Dual-gate MOSFET S-parameters, with gate 2 grounded, can be studied from common-source and common-gate S-parameters of a single-gate MOSFET.

Typical values of the S-parameters of a single-gate device are obtained from Fig. 5-4 and Appendix IV. The DC operating point of each single-gate MOSFET is made to agree with the drain current and drain voltage of the dual-gate MOSFET that is studied.

Common Source (200 MHz, $V_{GS} = +2.0$ V, and $V_{DS} = 6$V)

$S_{11} = 0.94 \angle -24^\circ$
$S_{22} = 0.92 \angle -0.4^\circ$
$S_{21} = 0.65 \angle +154^\circ$
$S_{12} = 0.025 \angle +82^\circ$

Common Gate (200 MHz, $V_{SG} = +2.0$ V, and $V_{DG} = 6$ V)

$S_{11}' = 0.45 \angle -30^\circ$
$S_{22}' = 0.96 \angle -1^\circ$
$S_{21}' = 0.30 \angle -15^\circ$
$S_{12}' = 0.05 \angle +85^\circ$

By substituting above measured values into the reflection coefficient formulas it can be shown that the input and output reflection coefficients of a dual-gate device can be approximated by S_{11} and S_{22}'. The forward and reverse transmission coefficients are calculated as $0.30 \angle +120^\circ$ and $0.0013 \angle +148^\circ$, respectively.

From the calculated values, one can expect that a dual-gate device will show almost the same characteristics as a common-source stage except for the large decrease in internal drain-gate feedback.

By referring to Fig. 5-8, the S-V_{DS} curves, the above approximation method can be fully justified. The only exception is that the magnitude of the reverse transmission

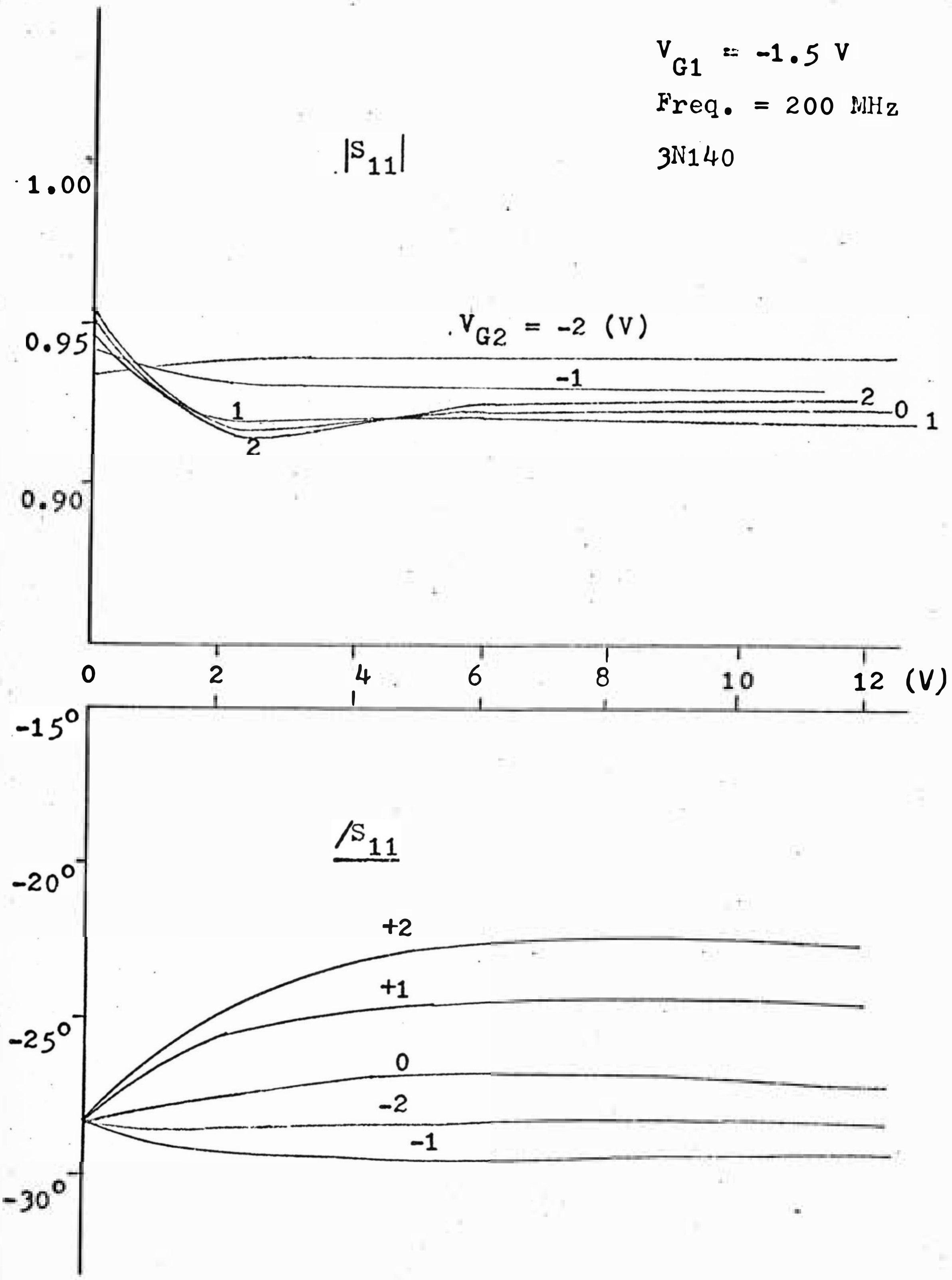

Fig. 5-8(a). Common-source S_{11}-V_{DS} curve (Dual-gate MOSFET).

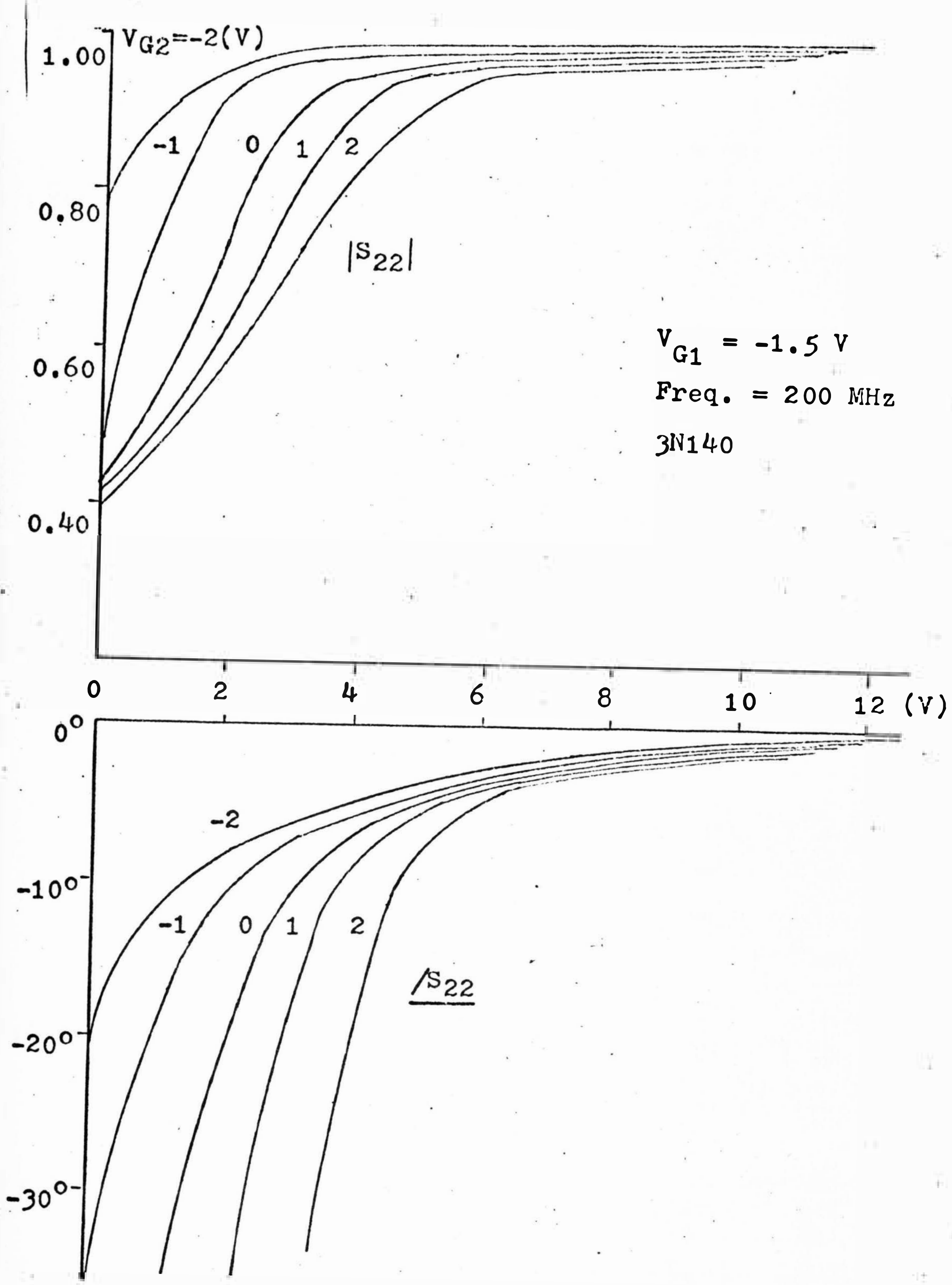

Fig. 5-8(b). Common-source S_{22}-V_{DS} curve (Dual-gate MOSFET).

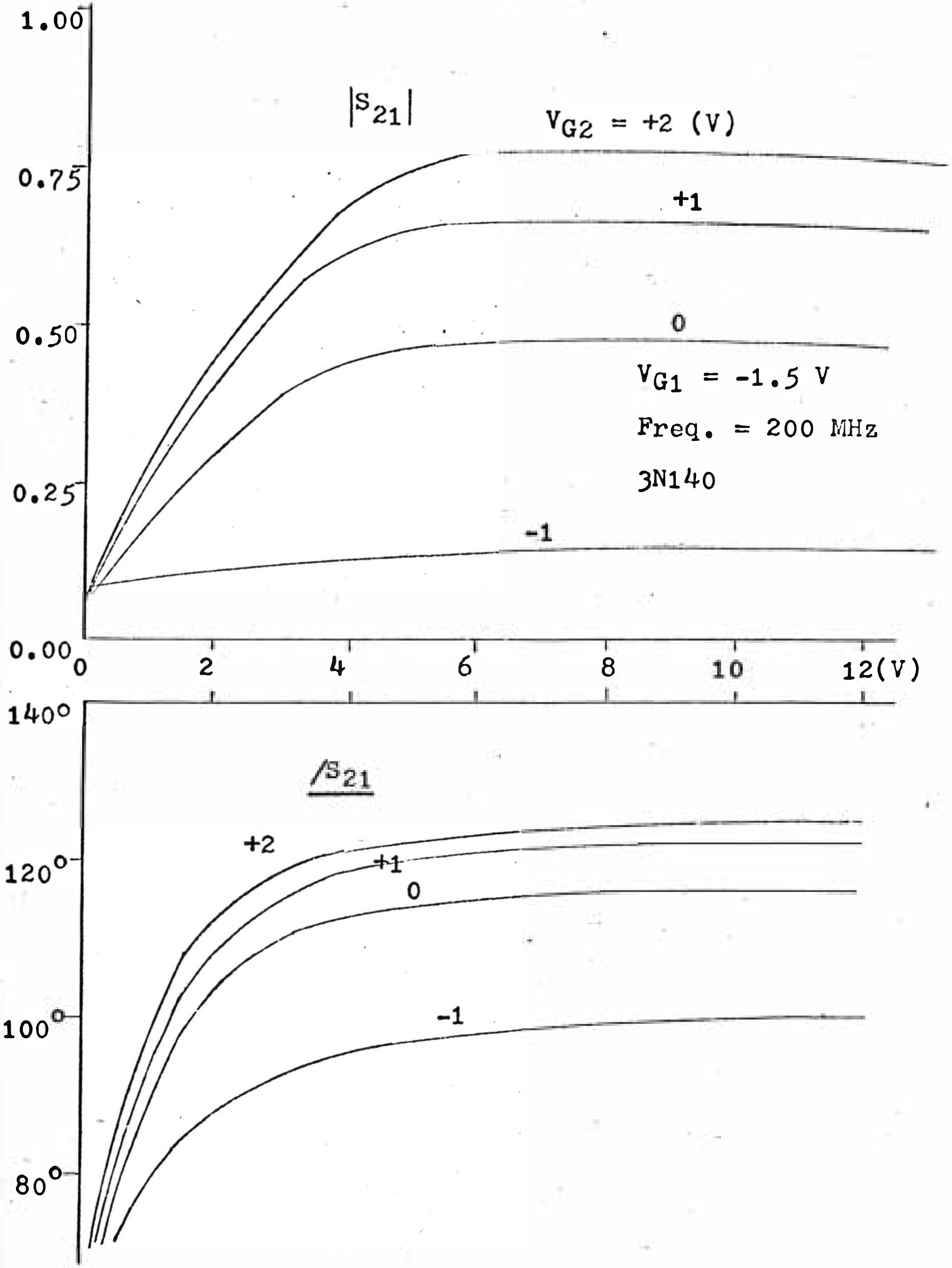

Fig. 5-8(c). Common-source S_{21}-V_{DS} curve (Dual-gate MOSFET).

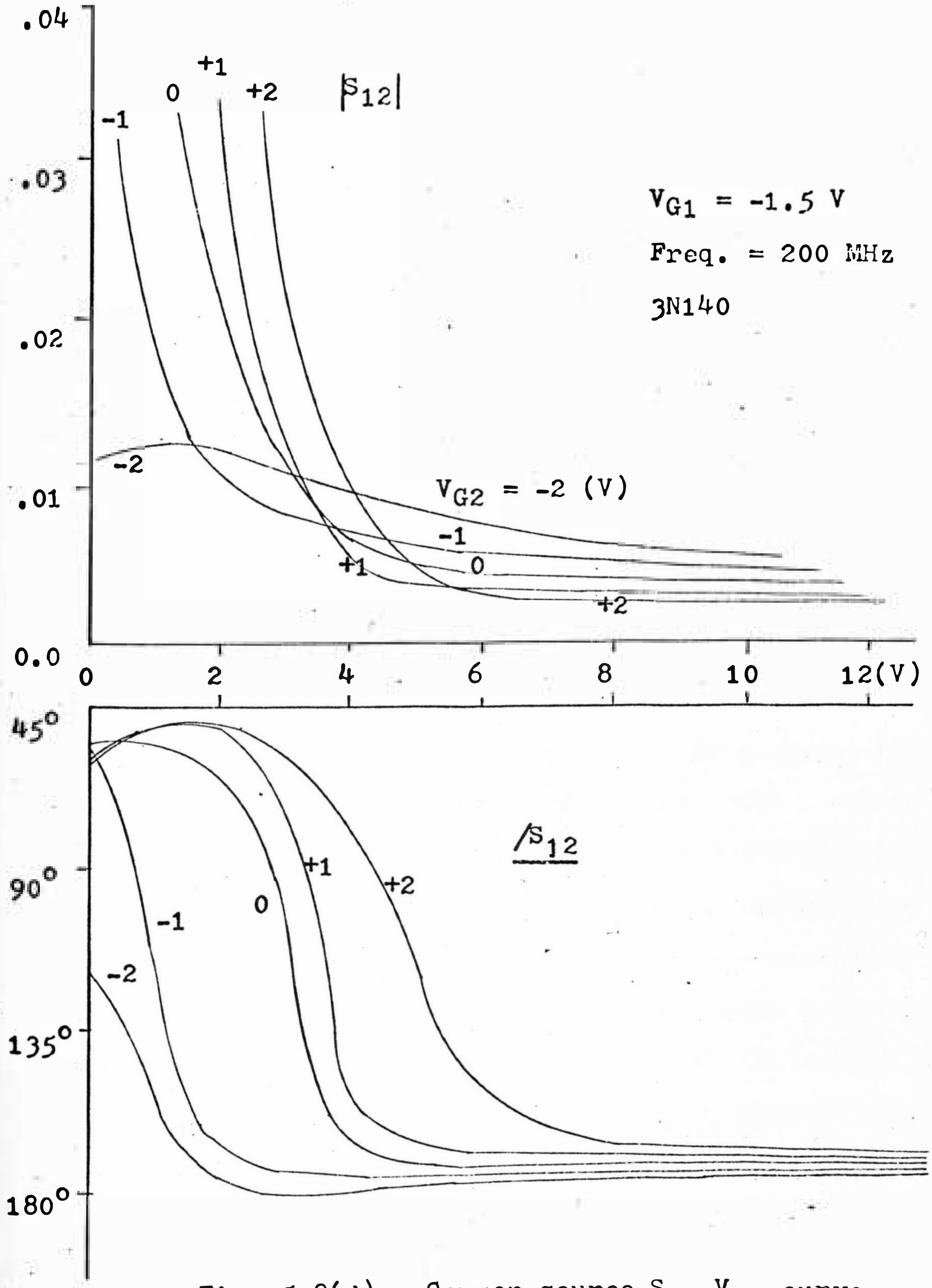

Fig. 5-8(d). Common-source S_{12}-V_{DS} curve (Dual-gate MOSFET).

coefficient S_{12} is a little larger than the values calculated from single-gate S-parameters. If substantial increase of internal feedback due to the geometry of a dual-gate MOSFET is considered, every behavior of a dual-gate device can be understood in terms of single-gate S-parameters.

4. Frequency Characteristics of Dual-Gate MOSFET. Significant differences can be found in S_{12} and S_{21} when the curves of Fig. 5-9 are compared with those of the single-gate device in Fig. 5-6. The phase angle of S_{12} is rather irregular and the slope of $\angle S_{21}$ is steeper than that of a single-gate device. The irregular variations of $\angle S_{12}$ are also confirmed at the higher frequencies. (Refer to Appendix V.) It is, however, impressive that the magnitude of S_{12} increases very uniformly in spite of a phase drift.

5. Interchangeability of Gate 1 and Gate 2. From the original purpose of gate 2 in a dual-gate MOSFET, it makes sense to use gate 2 as the AGC gate with RF ground, and gate 1 as the control gate for signal input. However, the roles of the gates may be interchanged such that gate 1 is used as the control gate. S-parameters for each connection are then certainly different. For example, $|S_{12}|$ is much larger when gate 2 is used as the control gate, and the phase angle is around $+90^{\circ}$ for that case.

Usually, for stable amplifier purposes, it is better

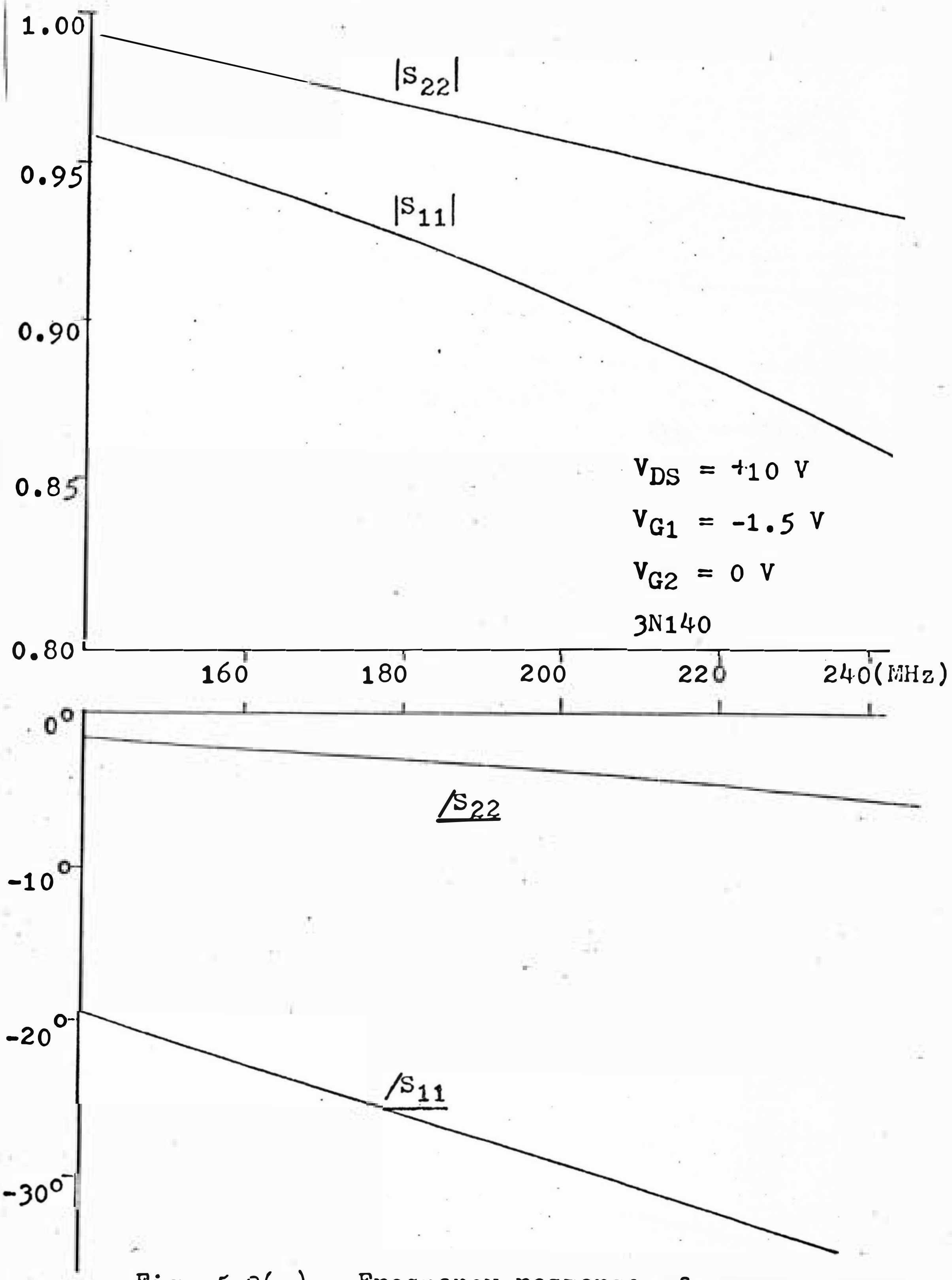

Fig. 5-9(a). Frequency response of common-source S-parameters (Dual-gate MOSFET).

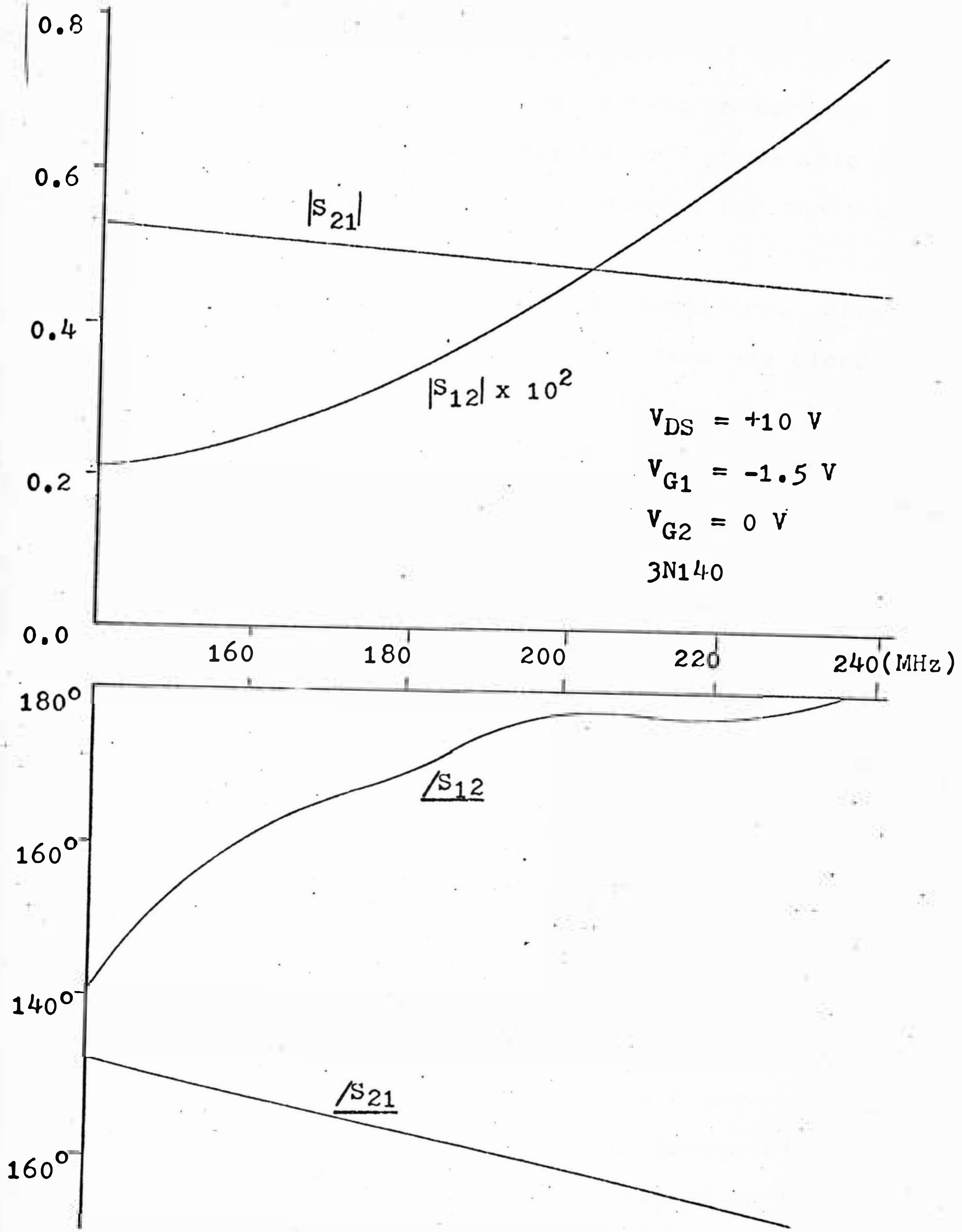

Fig. 5-9(b). Frequency response of common-source S-parameters (Dual-gate MOSFET).

to use gate 2 rather than gate 1 for AGC, but for oscillator applications specific phase angles of S-parameters may be required and the use of gate 1 may be more preferable for this purpose. In Appendix VII S-parameters for the two different connections are given.

6. Consideration of MOSFET as an Amplifier. Since $|S_{11}|$ and $|S_{22}|$ for the common-source configuration are close to unity at frequencies below 200 MHz (Fig. 5-6), a unilateral figure of merit U cannot be neglected, particularly for single-gate MOSFETs. Typical values of U and G_U at 200 MHz are 0.645 and 54.5, respectively. The lower the frequency, the worse the figure U becomes. In this case mismatching methods[10,22] may be employed using Eq. (2-20)'.

For dual-gate MOSFETs, G_U and U are obtained and plotted in Appendix VI. The unilateral figure of merit in this case is between 0.10 and 0.13 for the frequency range.

It should be noted that U and G_U are also functions of the DC operating point so proper selection of the operating point is necessary for optimization.

So far, single- and dual-gate MOSFET S-parameters have been discussed. It has been shown that other 2-port parameters can also be calculated from measured S-parameters and that these values agree with the data presented in the literature. Dual-gate devices can be analyzed on the basis of measured single-gate S-parameters.

C. Three-Port Parameters

A set of 3-port parameters has been attained for a bipolar transistor. In order to determine 9 components of (3x3) matrix, 9 individual measurements (18 numbers, i.e. magnitudes and phase angles of 9 complex numbers) have been made. At $I_C = 1$ mA and $V_{CE} = 6$ V, the scattering matrix obtained at 200 MHz is as follows:

Table I

$$\begin{bmatrix} S_{ee} & S_{eb} & S_{ec} \\ S_{be} & S_{bb} & S_{bc} \\ S_{ce} & S_{cb} & S_{cc} \end{bmatrix} = \begin{bmatrix} \underline{0.39\angle{+94^\circ}} & \underline{1.05\angle{-27^\circ}} & \underline{0.107\angle{+59^\circ}} \\ \underline{0.58\angle{+51^\circ}} & \underline{0.72\angle{-52^\circ}} & \underline{0.075\angle{+70^\circ}} \\ \underline{1.00\angle{-50^\circ}} & \underline{1.00\angle{+127^\circ}} & \underline{0.86\angle{-19^\circ}} \end{bmatrix}$$

3-Port S-Parameters, GM 0290

where e, b, and c denote the emitter, base, and collector terminals.

According to Eq. (2-29), each row and column can be summed in order to check whether each sum is unity. However, in actual devices, some RF current may flow directly to ground through stray capacitances producing an additional current path and the sums of each row and column may deviate from unity. In other words, the device is no more a 3-terminal device due to stray capacitances between the device and ground. The data given above also show some deviations from 3-terminal device theory. Certainly, some measurement errors were present.

From the data, 2-port S-parameters of any configuration (or, more generally, any termination) can be derived using the formulas of Eq. (2-27). For instance, common-emitter 2-port parameters can be obtained by substituting $S_3 = -1$ (short termination) into the formulas. Here, the port indices 1, 2, and 3 are replaced with b, c, and e, respectively, for convenience.

Two sets of common-emitter S-parameters, one calculated from 3-port parameters and the other from direct 2-port measurements, are given as follows:

Table II

	Calculated from 3-port S-parameters	Results of direct 2-port measurement
S_{11}	$0.56\angle{-103^\circ}$	$0.65\angle{-85^\circ}$
S_{22}	$0.76\angle{-20^\circ}$	$0.81\angle{-10^\circ}$
S_{21}	$2.00\angle{+128^\circ}$	$1.87\angle{+115^\circ}$
S_{12}	$0.04\angle{+35^\circ}$	$0.08\angle{+57^\circ}$

Common-Emitter S-Parameters
GM 0290, 200 MHz, $V_{CE} = 6$ V, $I_C = 1$ mA

The two sets of parameters are not in close agreement, although the proximity of their values can be appreciated.

The use of different test jigs and the parasitic effects due to stray capacitances are considered as the main sources of error. For further application of 3-port parameters, refer to Bodway.[17]

D. Four-Port Parameters

For the IC of Fig. 3-5, complete 4-port S-parameters are obtained; however, only 8 parameters are measured in order to determine a full set because of the symmetry of Q_1 and Q_2. The 4-port parameters obtained for the RCA CA 3049 integrated circuit are as follows:

Table III

S-parameters	2 mA	4 mA	6 mA
$S_{11}(1'1')$	$0.185\angle -25.3^\circ$	$0.77\angle -26.5^\circ$	$0.71\angle -28.5^\circ$
$S_{1'1}(11')$	$0.184\angle +31^\circ$	$0.237\angle +21.4^\circ$	$0.26\angle +16.4^\circ$
$S_{22}(2'2')$	$0.90\angle -19^\circ$	$0.88\angle -19^\circ$	$0.86\angle -19.5^\circ$
$S_{2'2}(22')$	$0.035\angle +71^\circ$	$0.041\angle +51.5^\circ$	$0.043\angle +32^\circ$
$S_{21}(2'1')$	$1.10\angle +123.5^\circ$	$1.56\angle +115^\circ$	$1.95\angle +110.7^\circ$
$S_{2'1}(21')$	$1.03\angle -66^\circ$	$1.46\angle -72.5^\circ$	$1.70\angle -77.2^\circ$
$S_{12}(1'2')$	$0.040\angle +85.5^\circ$	$0.039\angle +86^\circ$	$0.038\angle +83.5^\circ$
$S_{1'2}(12')$	$0.014\angle +130^\circ$	$0.015\angle +123^\circ$	$0.014\angle +118^\circ$

4-Port S-Parameters
RCA CA 3049, 200 MHz, $V_C = +3$ V, $V_B = +1.5$ V

The 2-port common-emitter S-parameters of the constituent transistors Q_1 and Q_2 can be obtained using Eq. (3-5). The results are given in the following table.

Table IV

	I_C = 1 mA	2 mA	3 mA
S_{11}	$0.72\angle -38^\circ$	$0.60\angle -40^\circ$	$0.55\angle -45^\circ$
S_{22}	$0.89\angle -20.2^\circ$	$0.86\angle -20.1^\circ$	$0.84\angle -20.1^\circ$
S_{21}	$2.10\angle +118^\circ$	$2.98\angle +110^\circ$	$3.60\angle +102^\circ$
S_{12}	$0.034\angle +62^\circ$	$0.032\angle +61^\circ$	$0.030\angle +61^\circ$

CA 3049, Q_1 and Q_2 C-E S-parameters
200 MHz, V_{CE} = 2.2 V (approximated
by assuming V_{BE} = 0.7 V for
silicon transistors)

These results are insufficient data to discuss the general characteristics of IC transistors; however, a little bit of information can be obtained by making a comparison with the data on discrete transistors. Several discrete VHF bipolar transistors and IC transistors are compared in Table V. Two isolated transistors on an IC chip (CA 3018) are also separately measured and the data are added in the table.

Table V

	S_{11}	S_{22}	S_{21}	S_{12}
2N2415	$0.73\angle{-60^\circ}$	$0.90\angle{-3.0^\circ}$	$1.30\angle{+121^\circ}$	$0.06\angle{+59^\circ}$
2N2415	$0.63\angle{-54^\circ}$	$0.88\angle{-5.2^\circ}$	$2.25\angle{+123^\circ}$	$0.074\angle{+65^\circ}$
GM0290	$0.63\angle{-88^\circ}$	$0.79\angle{-13^\circ}$	$1.83\angle{+108^\circ}$	$0.12\angle{+52^\circ}$
GM0290	$0.60\angle{-74^\circ}$	$0.89\angle{-4^\circ}$	$1.83\angle{+135^\circ}$	$0.06\angle{+60^\circ}$
2N918	$0.68\angle{-32^\circ}$	$0.90\angle{-4.5^\circ}$	$1.73\angle{+123^\circ}$	$0.09\angle{+77^\circ}$
CA3018	$0.72\angle{-35^\circ}$	$0.89\angle{-20^\circ}$	$2.0\angle{+120^\circ}$	$0.05\angle{+58^\circ}$
CA3018	$0.71\angle{-36^\circ}$	$0.87\angle{-17^\circ}$	$1.95\angle{+122^\circ}$	$0.05\angle{+60^\circ}$
CA3049	$0.72\angle{-38^\circ}$	$0.89\angle{-20.2^\circ}$	$2.10\angle{+118^\circ}$	$0.034\angle{+62^\circ}$

200 MHz, $I_C = 1$ mA, $V_{CE} = 2.2$ V

Comparison of Several Bipolar Devices

(C-E S-parameters)

In Table V, the difference between IC transistors and discrete transistors can be found in $\angle S_{22}$; calculation (see Appendix II) shows that in IC transistors output capacitance (obtained from S_{22}) values are substantially larger than those of the feedback capacitance. The difference can be explained by collector-to-substrate capacitance in ICs which ranged up to 2 pF.[24]

CHAPTER VI

CONCLUSIONS

Scattering parameters of several VHF semiconductor devices have been obtained from a special measurement setup. High-frequency characteristics of the device have been analyzed by means of their measured scattering parameters. Hybrid Pi equivalent circuits of bipolar transistors and single-gate MOSFETs can be extended to VHF frequency range in interpreting most of S-parameter data. However, modifications are necessary in view of the fact that some parameters such as S_{21} in bipolar transistors (due to minority carrier transit time) and S_{12} of a MOSFET which started showing an anomalous frequency response.

The S-parameters of bipolar devices generally follow expected behavior as derived from the basic theory. The bipolar transistor hybrid Pi equivalent circuit can be approximated from common-emitter S-parameters (see Appendix II). The minority carrier transit time, which appears in S_{21} of common-emitter configuration, is not significant at 150 MHz. When sufficient reverse bias is applied across the base-collector region, the differences given by Eq. (5-4) will be a good approximation of the phase delay due to minority carrier transit time. This linear phase shift should be considered in g_m for the bipolar hybrid Pi circuits at higher frequencies.

There are formulas that given conversions from one set of parameters to another. Conversions between S-parameters and y-parameters are most convenient in the light of parameter values for the ordinary configurations for VHF devices. The normal Pi equivalent circuit obtained from y-parameters is useful for a single-gate MOSFET representation. From the circuit, most desired design parameters such as g_m, C_{gd}, C_c, r_c, etc. can be obtained.

The common-source S-parameters of a dual-gate MOSFET can be closely approximated by two sets of single-gate MOSFET S-parameters: one of a common-source, and the other of a common-gate. The significant difference between the actual data and estimated values for single-gate MOSFET S-parameters can be found in the magnitudes of reverse transmission coefficient: the measured S_{12} is much larger than values estimated from single-gate MOSFET S-parameters.

Differential amplifier type ICs are fully characterized by 4-port S-parameters. Constituent transistor S-parameters can be obtained using a simple formula. From calculated values of constituent transistor S-parameters, no significant differences between an IC transistor and a discrete transistor can be found. Only the phase angle of S_{22} of the IC transistor shows a relatively higher shunt capacitance than that of a discrete transistor of the same kind.

As amplifier design parameters, a set of MOSFET S-parameters in VHF frequency range suggests that unilateral design for maximum gain may not be used, because of the relatively large unilateral figure of merit. This is because the magnitudes of S_{11} and S_{22} of the common-source MOSFET S-parameters are usually very close to unity at frequencies below 200 MHz. It also suggests that these devices should be assumed as voltage amplifiers for design purposes at these frequencies as was true for vacuum tube designs.

Since the common-emitter or common-source output impedances are usually very large for a normal DC operating point, significant fringing effect error (short and open position difference of a reference plane) can be observed. At frequencies between 150 MHz and 250 MHz, a maximum of +10 degrees could be found for the 2-port test jig of Fig. 4-2 (a). So some of these angles should be subtracted from the corresponding $\underline{/S_{22}}$ in order to eliminate the error.

In conclusion, the following statement can be made regarding S-parameters. S-parameters for VHF semiconductor devices can be obtained with sufficient accuracy and the results can be justified using simple equivalent circuits. The next step is to apply S-parameters to high-frequency active circuit design.

The superiority of the S-parameter method is distinct:

first in the convenience of making measurements; second in the simple design methods which are based on power relationships. The ample and accurate data obtained from the S-parameter method then can be combined with computers, resulting in fast and precise high-frequency circuit designs.

REFERENCES

1. Campbell, G.A. and R.M. Foster, "Maximum Output Networks for Telephone Substation and Repeater Circuits," Trans. of AIEE, Vol. 39, 1920.

2. Montgomery, C., R.H. Dicke, and E.M. Purcell, Principles of Microwave Circuits, McGraw-Hill, Inc., 1948.

3. Oono, Y. and K. Yasuura, "Synthesis of Finite Passive 2n-Terminal Networks with Prescribed Scattering Matrices," Annales des Telecommunication, Vol. 9, 1954.

4. Youla, D.C., "On Scattering Matrices Normalized to Complex Port Numbers," Proc. I.R.E., Vol. 49, July, 1961.

5. Penfield, P. Jr., "Noise in Negative Resistance Amplifier," IRE Trans. - CT, Vol. CT-7, June, 1960.

6. Lange, J. "Microwave Transistor Characterization Including S-Parameters," S-Parameters - Circuit Analysis and Design, Hewlett-Packard, Application Note 95, September, 1968.

7. Weinert, "Scattering Parameters Speed Design of High-Frequency Transistor Circuits," Electronics, September, 1966.

8. Anderson, D., "S-Parameter Techniques for Faster, More Accurate Network Design," Hewlett-Packard Journal, February, 1967.

9. Froehner, W., "Quick Amplifier Design with Scattering Parameters," Electronics, October, 1967.

10. Bodway, G., "Two-Port Power Analysis Using Generalized Scattering Parameters," Microwave Journal, May, 1967.

11. Robichaud, Boisvert, and Robert, Signal Flow Graphs and Applications, Prentice-Hall, 1962.

12. Hewlett-Packard, Inc., "Transistor Parameter Measurement," Application Note 77-1, February, 1967.

13. Collin, R., Foundation for Microwave Engineering, McGraw-Hill, 1966.

14. Carlin and Giordano, Network Theory, Prentice-Hall, 1964.

15. Mason, S.J., "Feedback Theory: Some Properties of Signal Flow Graphs," Proc. I.R.E., September, 1953.

16. ___________, "Feedback Theory: Further Properties of Signal Flow Graphs," Proc. I.R.E., July, 1956.

17. Bodway, G., "Circuit Design and Characterization of Transistors by Means of Three-Port Scattering Parameters," Microwave Journal, Vol. II, No. 5, May, 1968.

18. Fitchen, F.C., Transistor Circuit Analysis and Design (2nd Ed.), Van Nostrand, 1966.

19. Cochrun, B., Transistor Circuit Engineering, The MacMillan Co., 1967.

20. Wallmark and Johnson, Field Effect Transistors, Prentice-Hall, 1966.

21. Walston and Miller, Transistor Circuit Design, McGraw-Hill, 1963.

22. Sevin, Field Effect Transistors, McGraw-Hill, 1965.

23. RCA Product Guide, "MOS Field Effect Transistor," MOS-160, December, 1967.

24. RCA Product Guide, "Linear Integrated Circuit," File No. 378, January, 1969.

APPENDICES

APPENDIX I

CONVERSION TABLE BETWEEN SCATTERING AND IMMITTANCE PARAMETERS

$$S_{11} = \frac{(z_{11} - 1)(z_{22} + 1) - z_{12}z_{21}}{(z_{11} + 1)(z_{22} + 1) - z_{12}z_{21}} \qquad z_{11} = \frac{(1 + S_{11})(1 - S_{22}) + S_{12}S_{21}}{(1 - S_{11})(1 - S_{22}) - S_{12}S_{21}}$$

$$S_{12} = \frac{2z_{12}}{(z_{11} + 1)(z_{22} + 1) - z_{12}z_{21}} \qquad z_{12} = \frac{2S_{12}}{(1 - S_{11})(1 - S_{22}) - S_{12}S_{21}}$$

$$S_{21} = \frac{2z_{21}}{(z_{11} + 1)(z_{22} + 1) - z_{12}z_{21}} \qquad z_{21} = \frac{2S_{21}}{(1 - S_{11})(1 - S_{22}) - S_{12}S_{21}}$$

$$S_{22} = \frac{(z_{11} + 1)(z_{22} - 1) - z_{12}z_{21}}{(z_{11} + 1)(z_{22} + 1) - z_{12}z_{21}} \qquad z_{22} = \frac{(1 + S_{22})(1 - S_{11}) + S_{12}S_{21}}{(1 - S_{11})(1 - S_{22}) - S_{12}S_{21}}$$

Note: h-, y-, and z-parameters listed above and in the succeeding pages are all normalized to Z_o. See end of this appendix.

$$S_{11} = \frac{(1 - y_{11})(1 + y_{22}) + y_{12}y_{21}}{(1 + y_{11})(1 + y_{22}) - y_{12}y_{21}} \qquad y_{11} = \frac{(1 + S_{22})(1 - S_{11}) + S_{12}S_{21}}{(1 + S_{11})(1 + S_{22}) - S_{12}S_{21}}$$

$$S_{12} = \frac{-2y_{12}}{(1 + y_{11})(1 + y_{22}) - y_{12}y_{21}} \qquad y_{12} = \frac{-2S_{12}}{(1 + S_{11})(1 + S_{22}) - S_{12}S_{21}}$$

$$S_{21} = \frac{-2y_{21}}{(1 + y_{11})(1 + y_{22}) - y_{12}y_{21}} \qquad y_{21} = \frac{-2S_{21}}{(1 + S_{11})(1 + S_{22}) - S_{12}S_{21}}$$

$$S_{22} = \frac{(1 + y_{11})(1 - y_{22}) + y_{12}y_{21}}{(1 + y_{11})(1 + y_{22}) - y_{12}y_{21}} \qquad y_{22} = \frac{(1 + S_{11})(1 - S_{22}) + S_{12}S_{21}}{(1 + S_{22})(1 + S_{11}) - S_{12}S_{21}}$$

****

$$S_{11} = \frac{(h_{11} - 1)(h_{22} + 1) - h_{12}h_{21}}{(h_{11} + 1)(h_{22} + 1) - h_{12}h_{21}} \qquad h_{11} = \frac{(1 + S_{11})(1 + S_{22}) - S_{12}S_{21}}{(1 - S_{11})(1 + S_{22}) + S_{12}S_{21}}$$

$$S_{12} = \frac{2h_{12}}{(h_{11} + 1)(h_{22} + 1) - h_{12}h_{21}} \qquad h_{12} = \frac{2S_{12}}{(1 - S_{11})(1 + S_{22}) + S_{12}S_{21}}$$

$$S_{21} = \frac{-2h_{21}}{(h_{11} + 1)(h_{22} + 1) - h_{12}h_{21}} \qquad h_{21} = \frac{-2S_{21}}{(1 - S_{11})(1 + S_{22}) + S_{12}S_{21}}$$

$$S_{22} = \frac{(1 + h_{11})(1 - h_{22}) + h_{12}h_{21}}{(h_{11} + 1)(h_{22} + 1) - h_{12}h_{21}} \qquad h_{22} = \frac{(1 - S_{22})(1 - S_{11}) - S_{12}S_{21}}{(1 - S_{11})(1 + S_{22}) + S_{12}S_{21}}$$

****

If H, Y, and Z are the actual parameters, conversion is obtained as follows:

$Z_{11} = z_{11}Z_o$ $\qquad$ $Y_{11} = y_{11}/Z_o$ $\qquad$ $H_{11} = h_{11}Z_o$

$Z_{12} = z_{12}Z_o$ $\qquad$ $Y_{12} = y_{12}/Z_o$ $\qquad$ $H_{12} = h_{12}$

$Z_{21} = z_{21}Z_o$ $\qquad$ $Y_{21} = y_{21}/Z_o$ $\qquad$ $H_{21} = h_{21}$

$Z_{22} = z_{22}Z_o$ $\qquad$ $Y_{22} = y_{22}/Z_o$ $\qquad$ $H_{22} = h_{22}/Z_o$

APPENDIX II

APPROXIMATION OF HYBRID PI ELEMENTS BY S-PARAMETER METHOD

1. $r_{bb'}$

From Smith Chart plot of S_{11}-I_C curve at sufficiently high frequency (i.e. $\omega C_{b'e} r_{b'e} \gg 1$) the resistance value of the constant resistance circle is approximately $r_{bb'}$. (Refer to Fig. 5-3.)

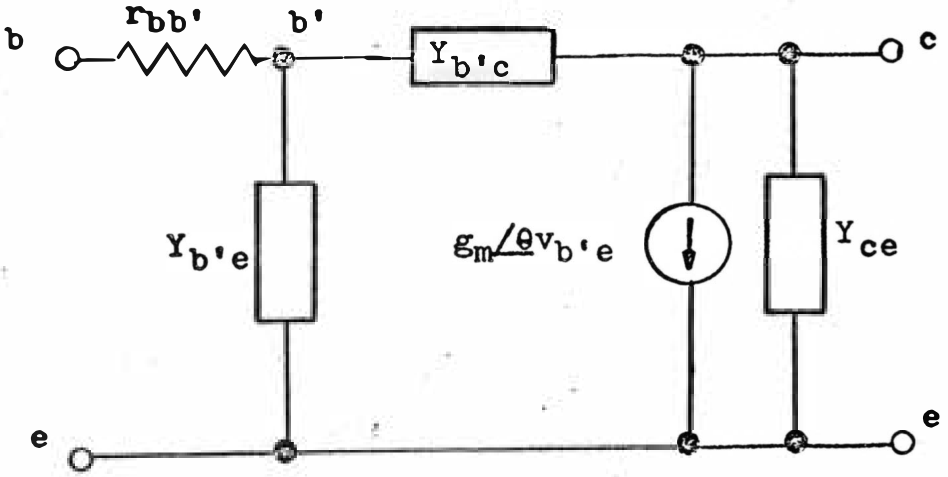

Fig. A-II. Hybrid Pi equivalent circuit for a bipolar device.

Note: $S_{12}S_{21}$ and $Y_{b'c}$ are assumed negligible in the derivations.

2. $Y_{b'e}$ $(= 1/r_{b'e} + j\omega C_{b'e})$

$$Y_{b'e} = 1/(Z_i - r_{bb'}) \qquad \text{(II-1)}$$

where Z_i is input impedance obtained from Smith Chart plot of S_{11}.

3. g_m

$$\underline{g_m/\theta} = -\tfrac{1}{2}Y_{b'e}S_{21}/(1 - S_{11})(1 + S_{22})$$

(II-2)

θ is the phase shift due to minority carrier transit time.

4. $Y_{b'c}$ $(= 1/r_{b'c} + j\omega C_{b'c})$

$$Y_{b'c} = \tfrac{1}{2}Y_{b'e}S_{12}/(1 - S_{11})(1 + S_{22})$$

(II-3)

5. Y_{ce} $(= 1/r_{ce} + j\omega C_{ce})$

$$Y_{ce} = Y_o - Y_{b'c} \qquad \text{(II-4)}$$

where Y_o is output admittance obtained from Smith Chart plot of S_{22}.

APPENDIX III

FURTHER DISCUSSIONS ON REFERENCE PLANE

A. The Effect of Improper Reference Plane

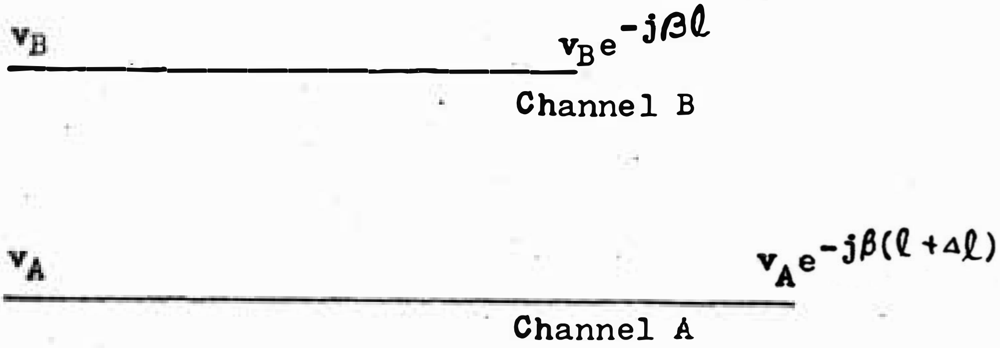

Fig. A-III-1. Phase relation of incident and scattered waves at the measurement point.

If the ratio of the voltage waves v_B/v_A gives a desired S-parameter, then the effect of remote measurements for the parameters will be as follows:

$$S_{BA}' = \frac{v_B e^{-j\beta\ell}}{v_A e^{-j\beta(\ell+\Delta\ell)}} = \left(\frac{v_B}{v_A}\right) e^{j\beta\Delta\ell} = S_{BA} e^{j\beta\Delta\ell}$$

since $\beta = 2\pi/\lambda = 2\pi f/v$ (III-1)

where v is the velocity of a wave traveling along a transmission line and f is the frequency.

$$S_{BA}' = S_{BA} e^{j\theta f} \qquad \text{(III-2)}$$

where $\theta = (2\pi/v)\Delta\ell$

The measured S-parameter S_{BA}' will experience a linear phase error which is a function of frequency.

For positive $\Delta\ell$ (longer reference signal path) the measured S-parameter S_{BA}' will have a negative phase error corresponding to θf.

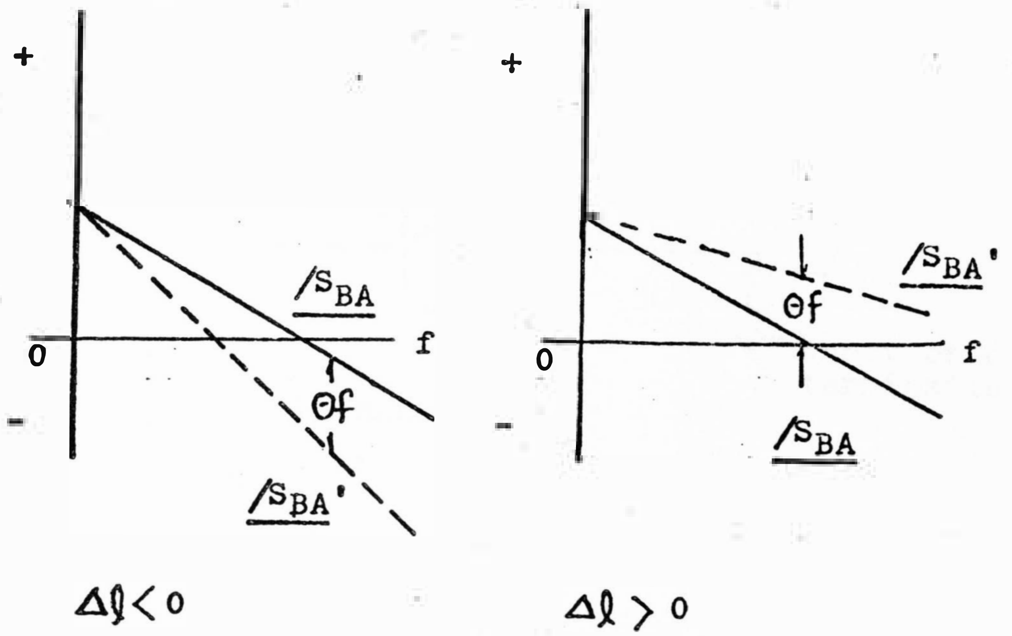

Fig. A-III-2. Phase error due to improper reference plane.

B. Fringing Effect Error - Short and Open Position Difference

This is the error due to the end effect of a transmission line. Theoretically if $\Delta\ell = 0$

$$S_{BA} = S_{BA}' = \underline{1\angle{+180^\circ}} \qquad \text{for short end,}$$
$$= \underline{1\angle{0^\circ}} \qquad \text{for open end.} \qquad \text{(III-3)}$$

But in actual case the open and short termination positions differ from each other by a small angle.

To study this relationship a measurement is performed as follows:

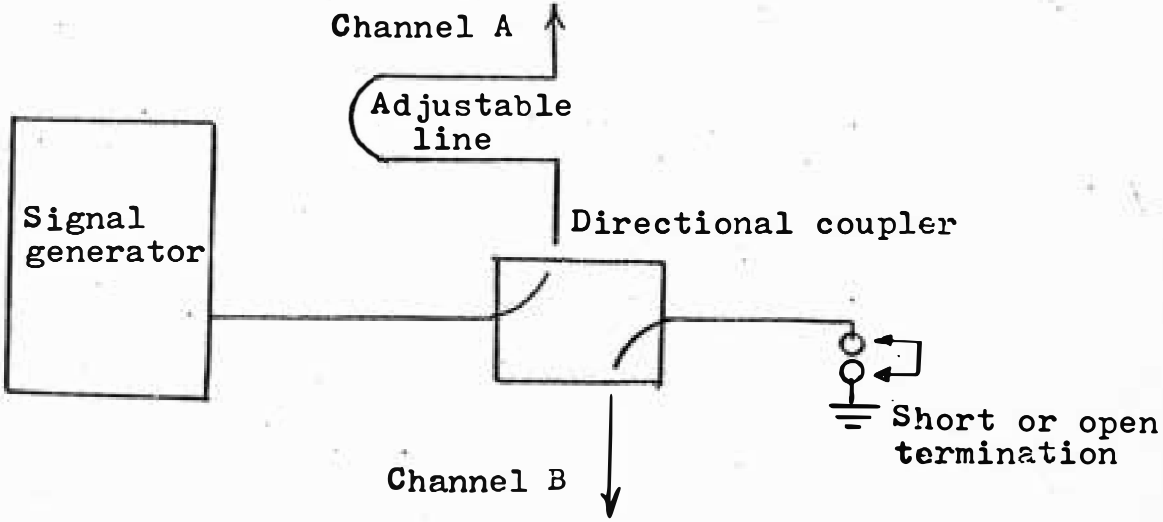

Fig. A-III-3. Measurement of fringing effect error.

The adjustable line is adjusted for a short termination such that VVM shows 180° over a wide range of frequencies. Then the short is removed and the phase deviation from 0° is measured. The general curves are as follows:

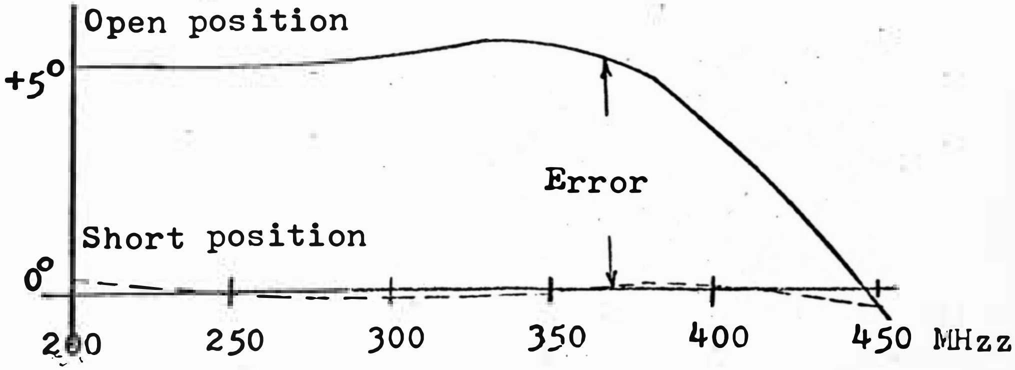

Fig. A-III-4. An example of fringing effect.

So if reference plane is set at a point using the short termination method, the high impedance (open condition) termination will show significant position errors depicted in the figure. For high impedance measurements the angular error should be subtracted from the measured values.

APPENDIX IV

COMMON-GATE S-PARAMETERS OF SINGLE-GATE MOSFET (S-V_{DG} CURVES)

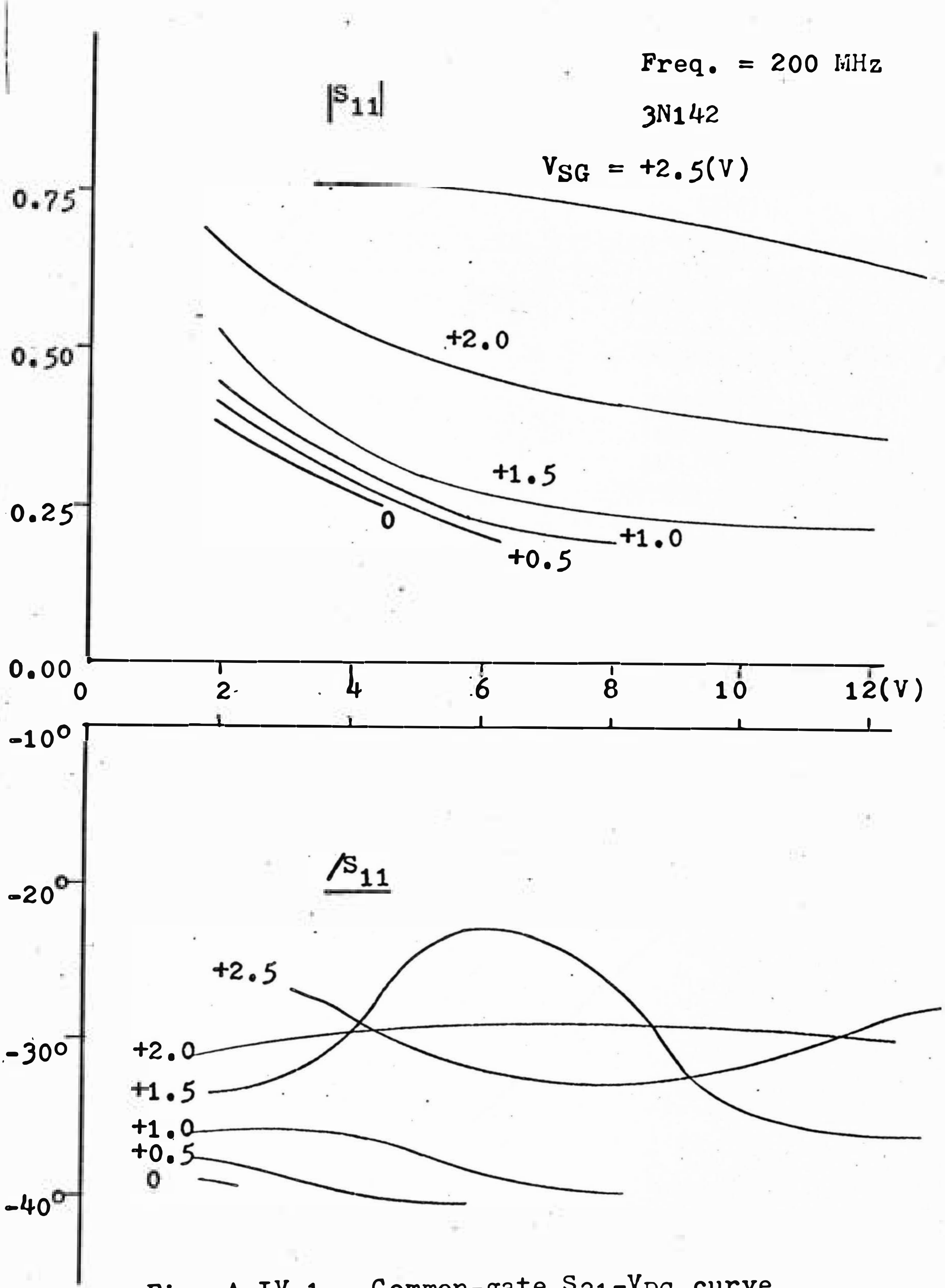

Fig. A-IV-1. Common-gate S_{21}-V_{DG} curve (Single-gate MOSFET)

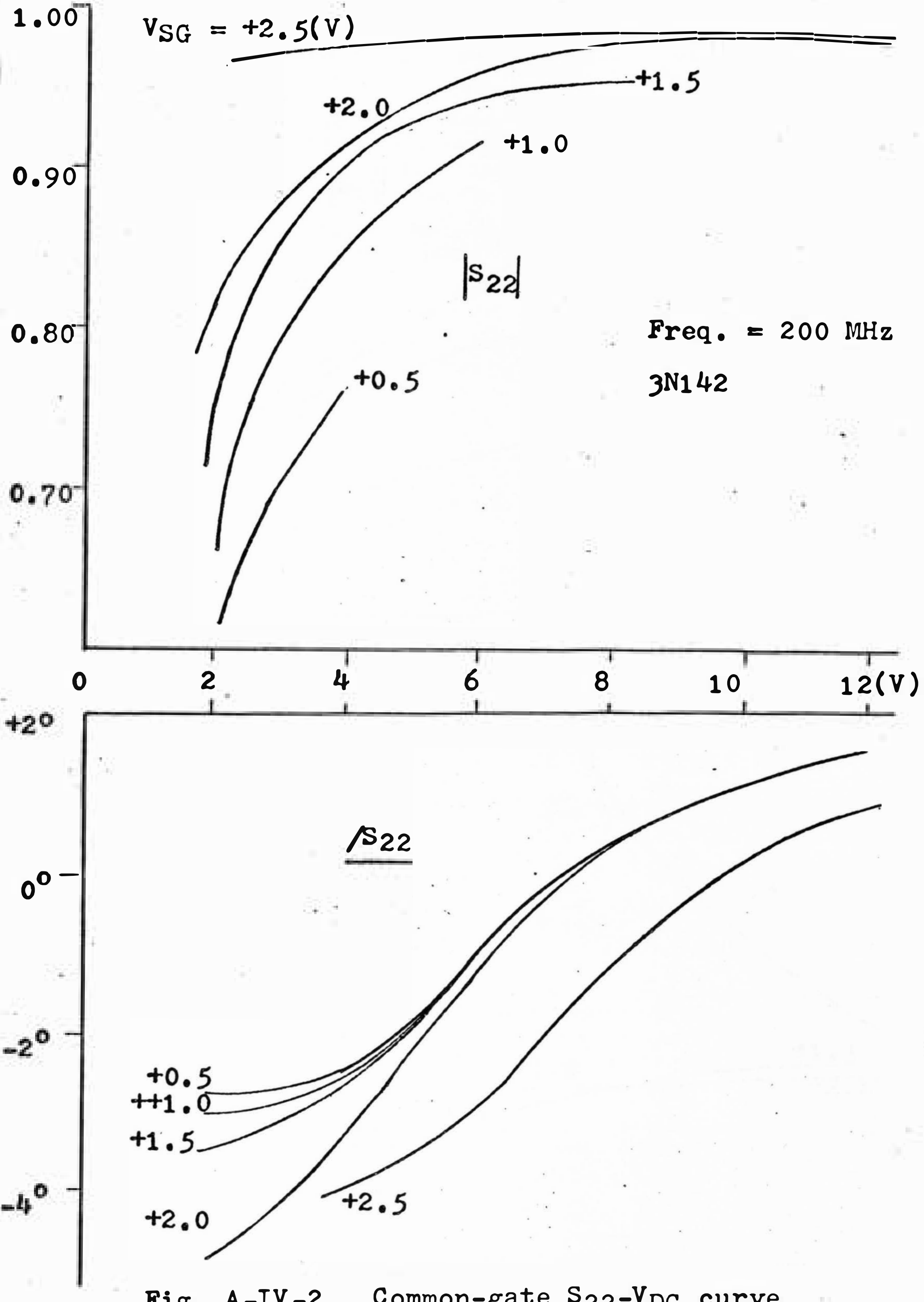

Fig. A-IV-2. Common-gate S_{22}-V_{DG} curve (Single-gate MOSFET)

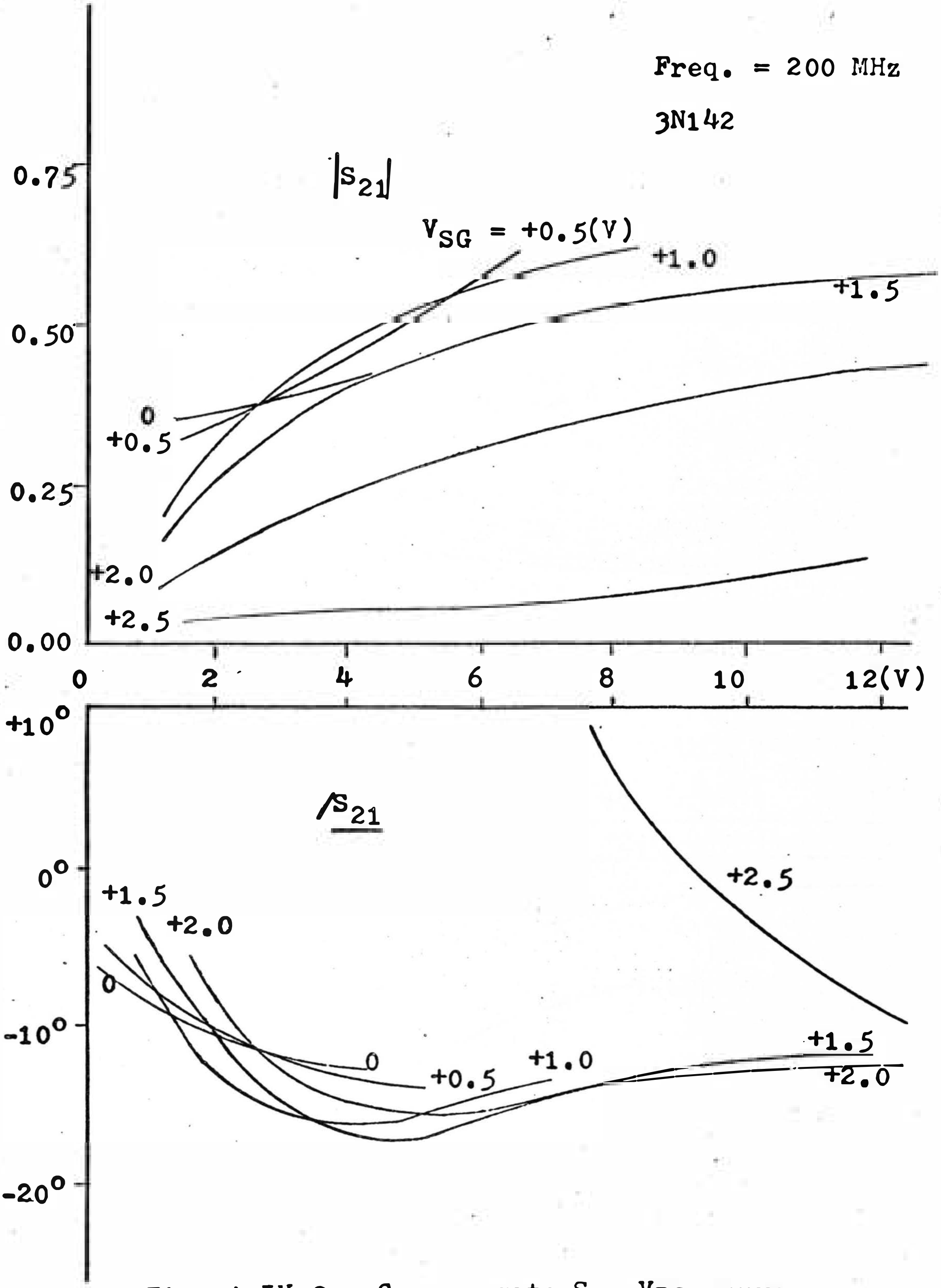

Fig. A-IV-3. Common-gate S_{21}-V_{DG} curve (Single-gate MOSFET).

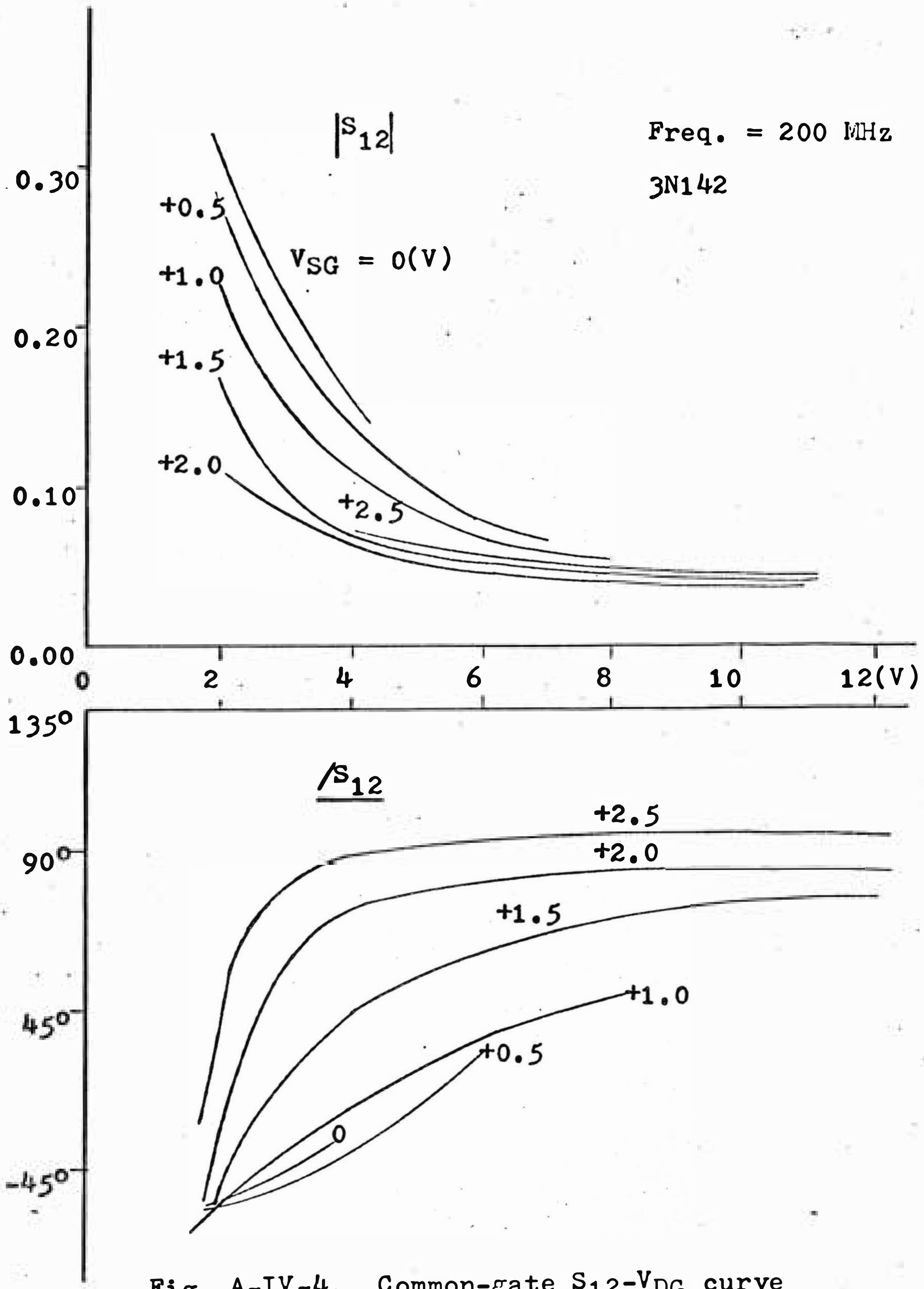

Fig. A-IV-4. Common-gate S_{12}-V_{DG} curve (Single-gate MOSFET)

APPENDIX V

FREQUENCY RESPONSE OF DUAL-GATE MOSFET COMMON-SOURCE S-PARAMETERS BEYOND VHF

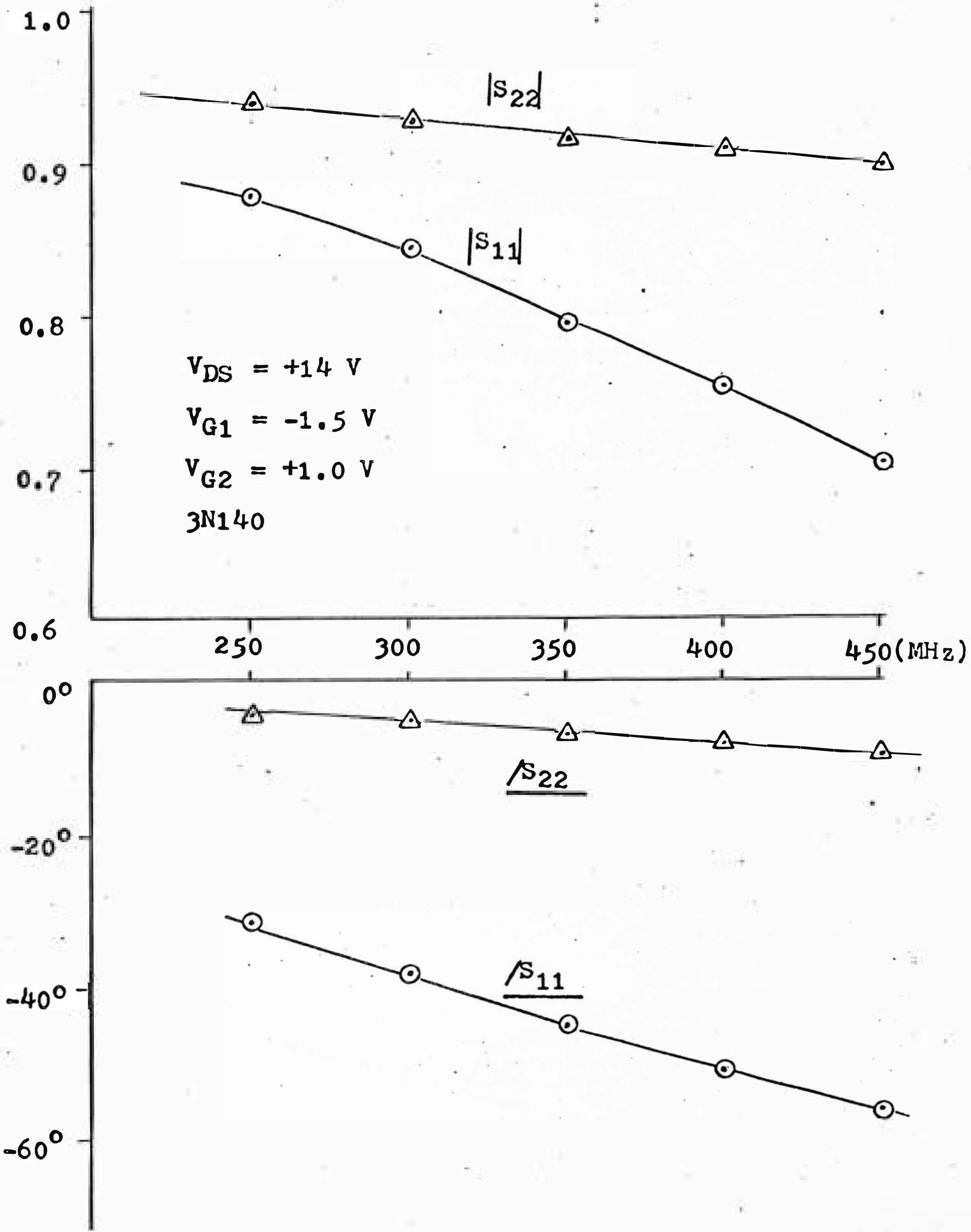

Fig. A-V-1. Frequency response of dual-gate MOSFET common-source S-parameters beyond VHF.

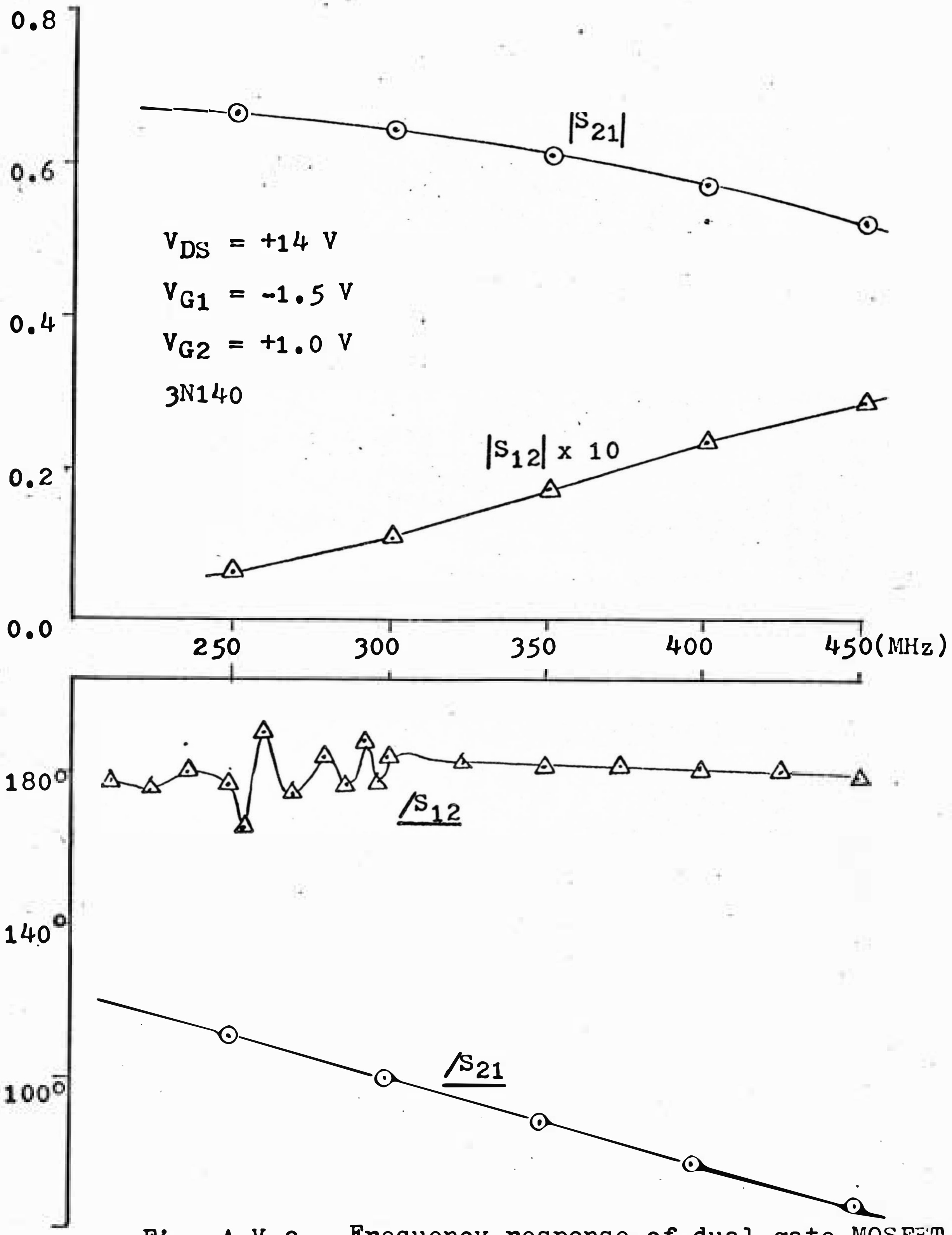

Fig. A-V-2. Frequency response of dual-gate MOSFET common-source S-parameters beyond VHF

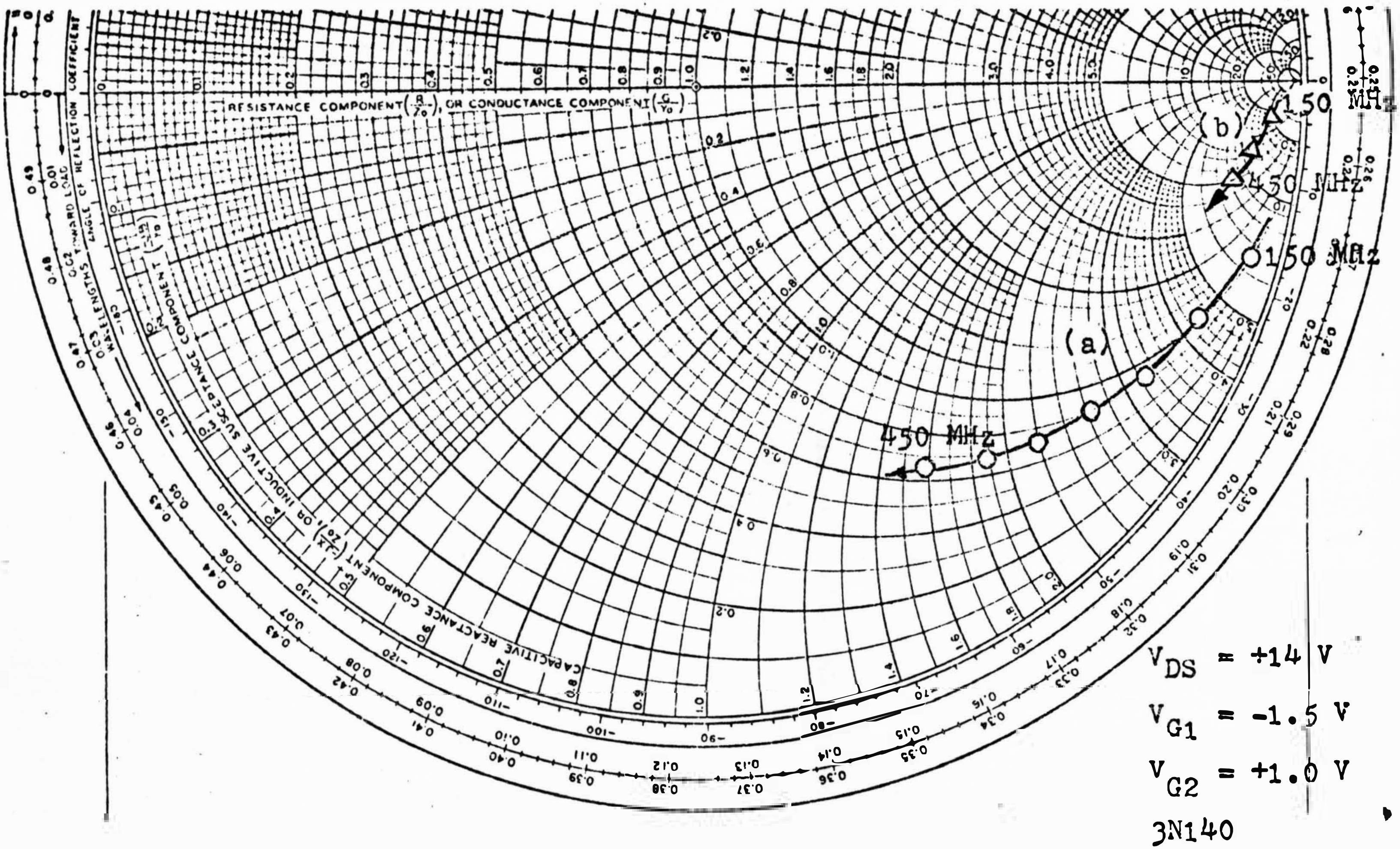

Fig. A-V-3. Smith Chart plot of frequency response for dual-gate MOSFET common-source S-parameters beyond VHF: (a) S_{11} and (b) S_{22} versus frequency curves.

APPENDIX VI

MAXIMUM UNILATERAL GAIN AND UNILATERAL FIGURE OF MERIT VERSUS FREQUENCY CURVES

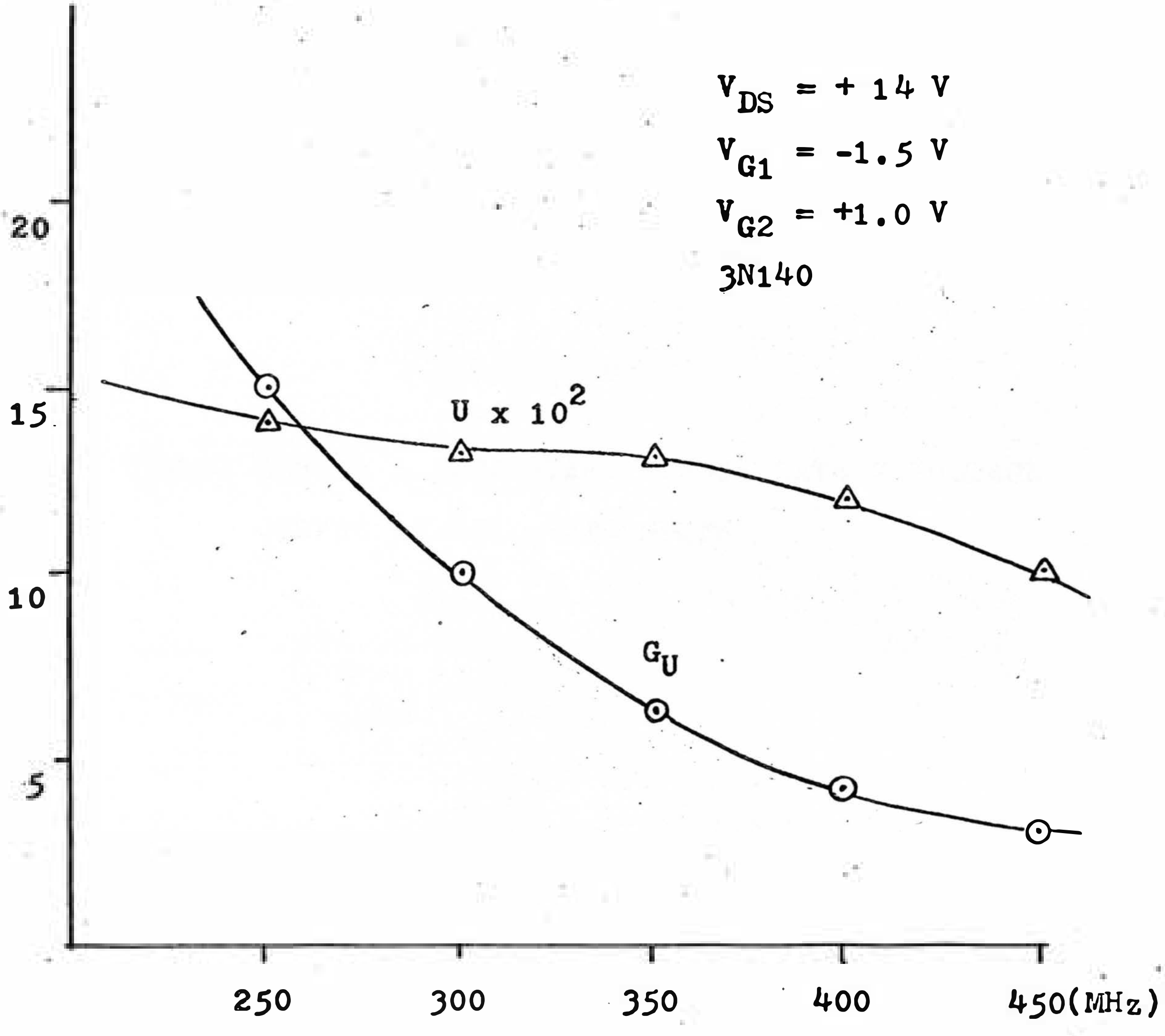

Fig. A-VI. Maximum unilateral gain G_U and unilateral figure of merit U versus frequency curves of dual-gate MOSFET common-source stage beyond VHF.

APPENDIX VII

COMMON-SOURCE S-PARAMETERS VERSUS GATE 2 VOLTAGE CURVES OF DUAL-GATE MOSFET

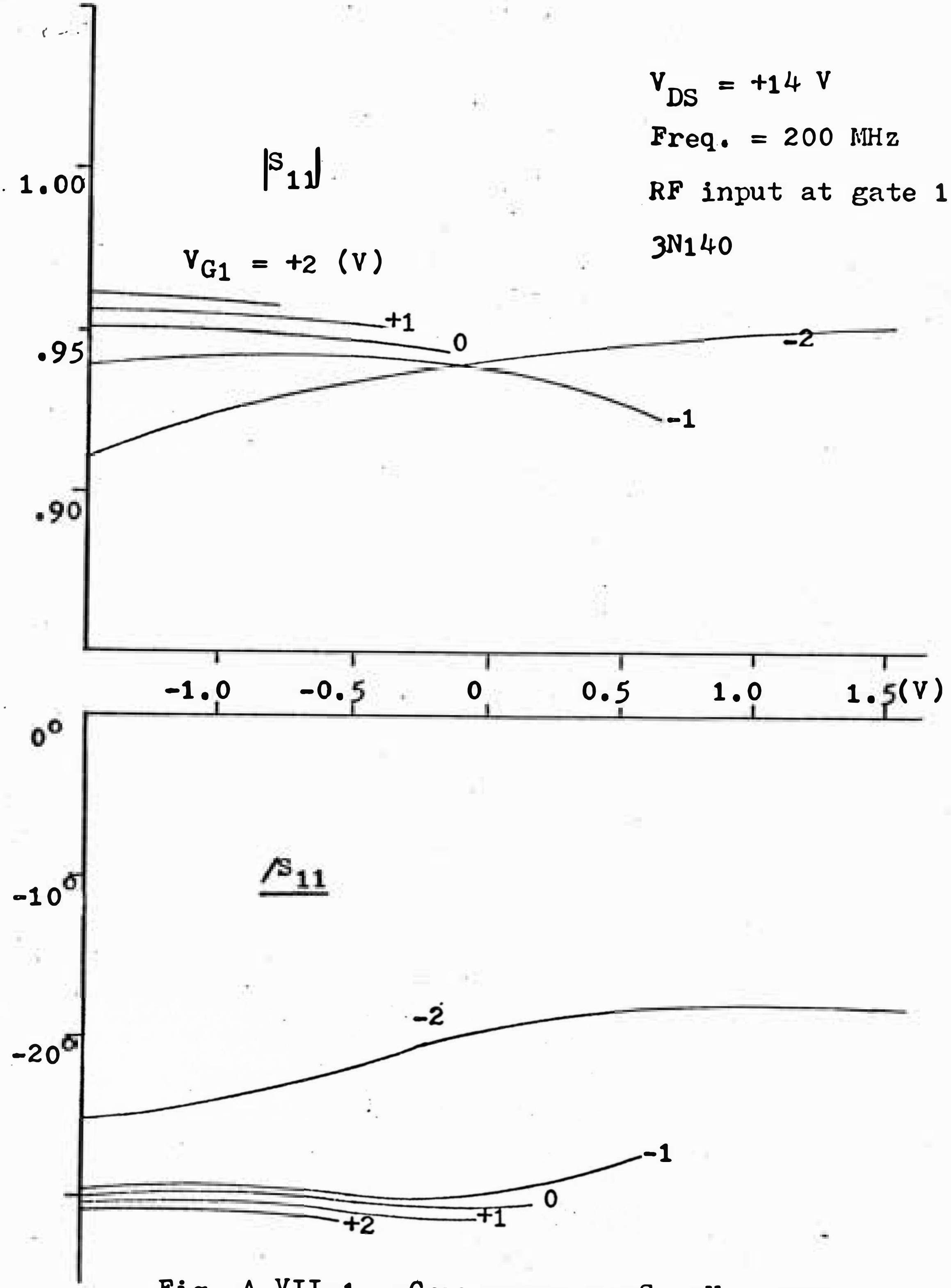

Fig. A-VII-1. Common-source S_{11}-V_{G2} curves (Dual-gate MOSFET).

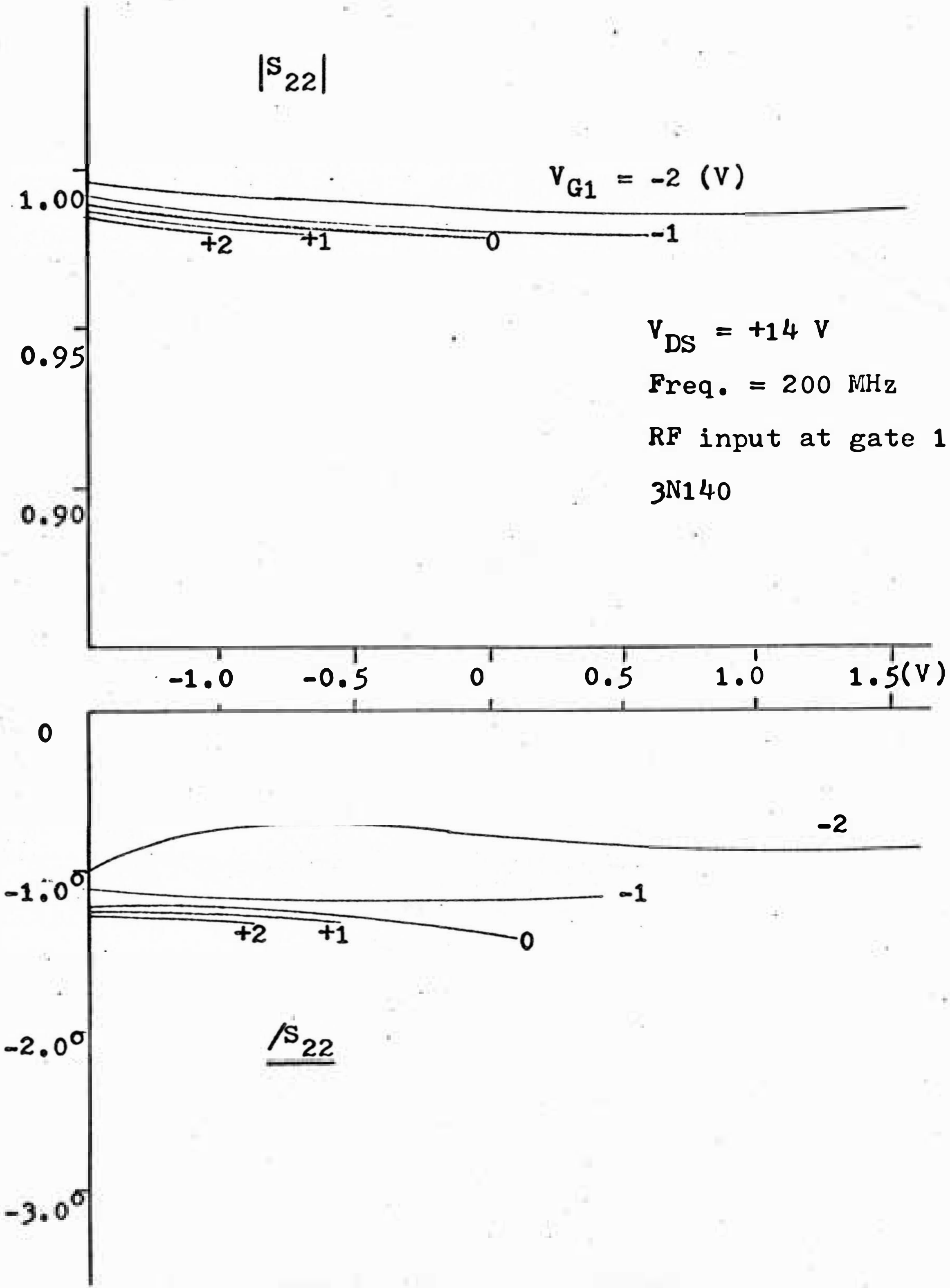

Fig. A-VII-2. Common-source S_{22}-V_{G2} curves (Dual-gate MOSFET)

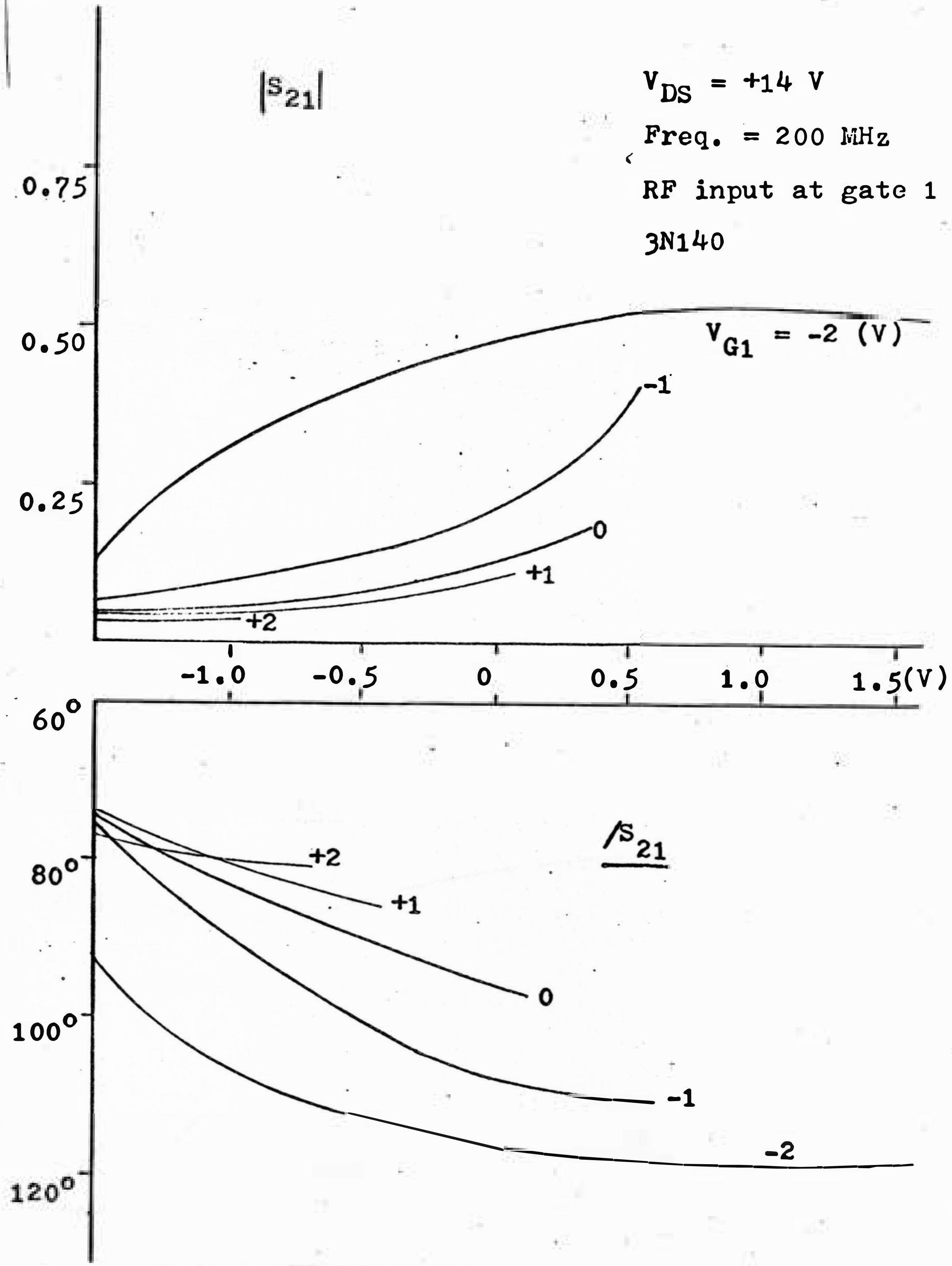

Fig. A-VII-3. Common-source S_{21}-V_{G2} curves (Dual-gate MOSFET)

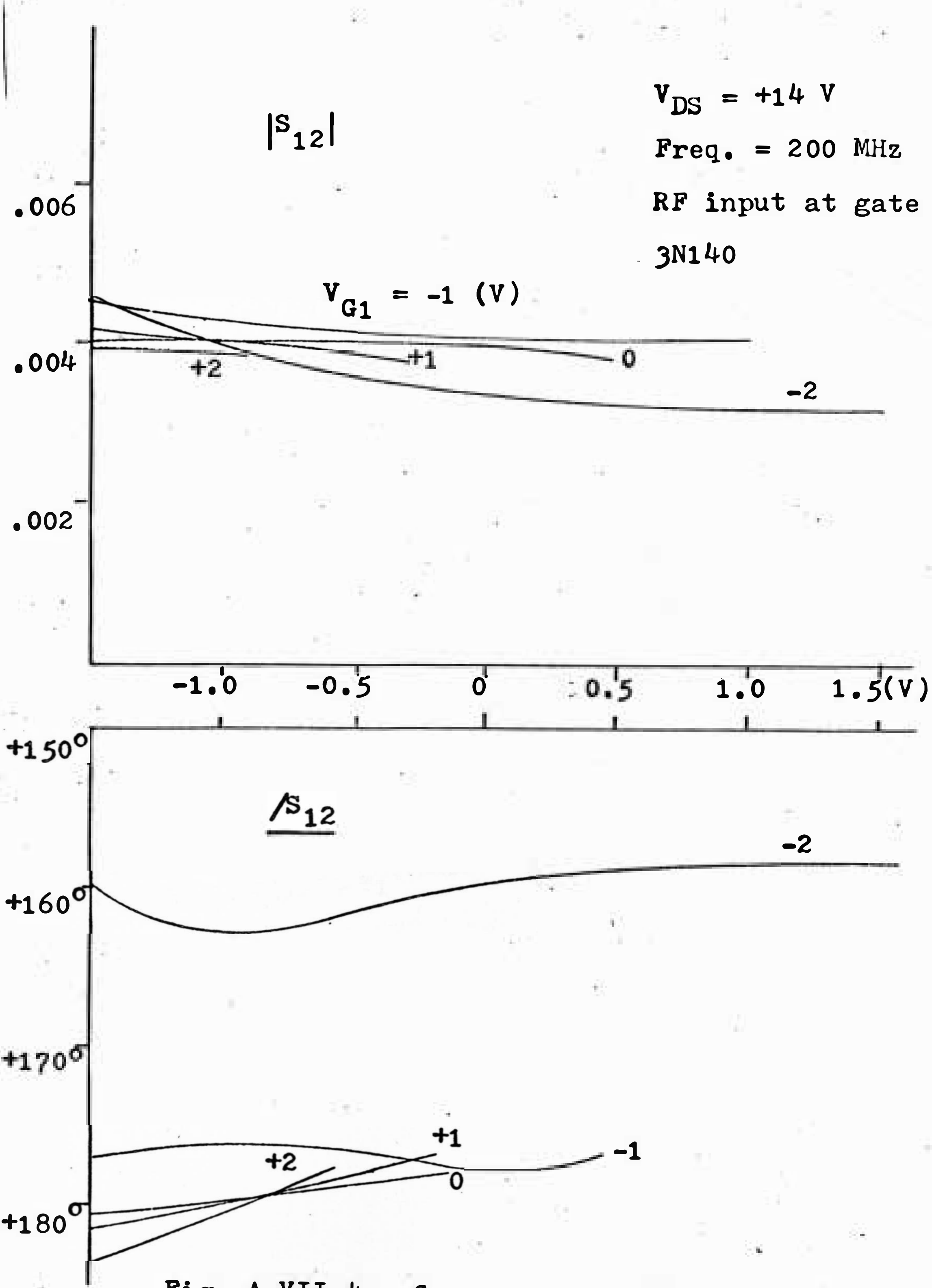

Fig. A-VII-4. Common-source S_{12}-V_{G2} curves (Dual-gate MOSFET).

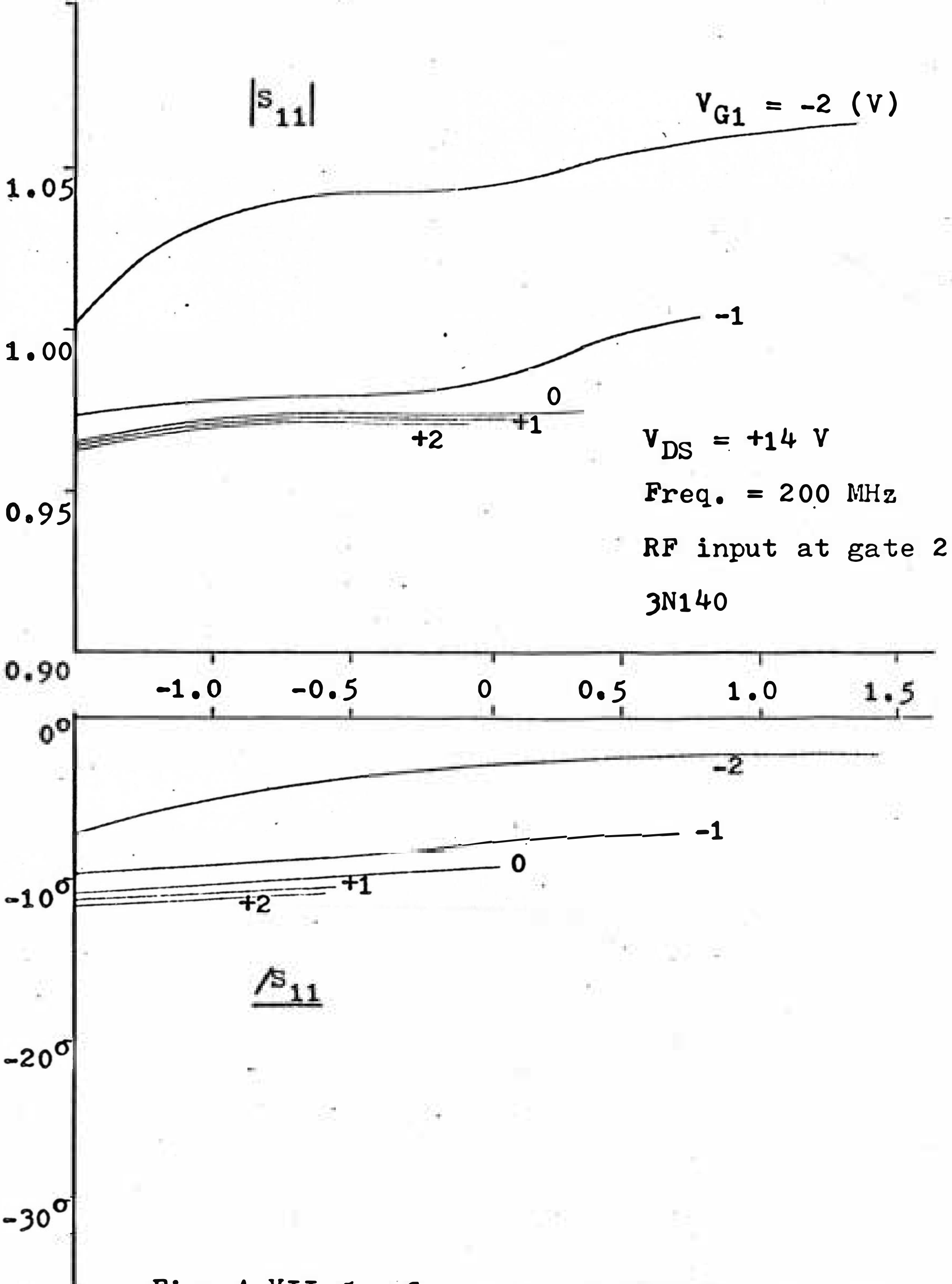

Fig. A-VII-5. Common-source S_{11}-V_{G2} curves (Dual-gate MOSFET).

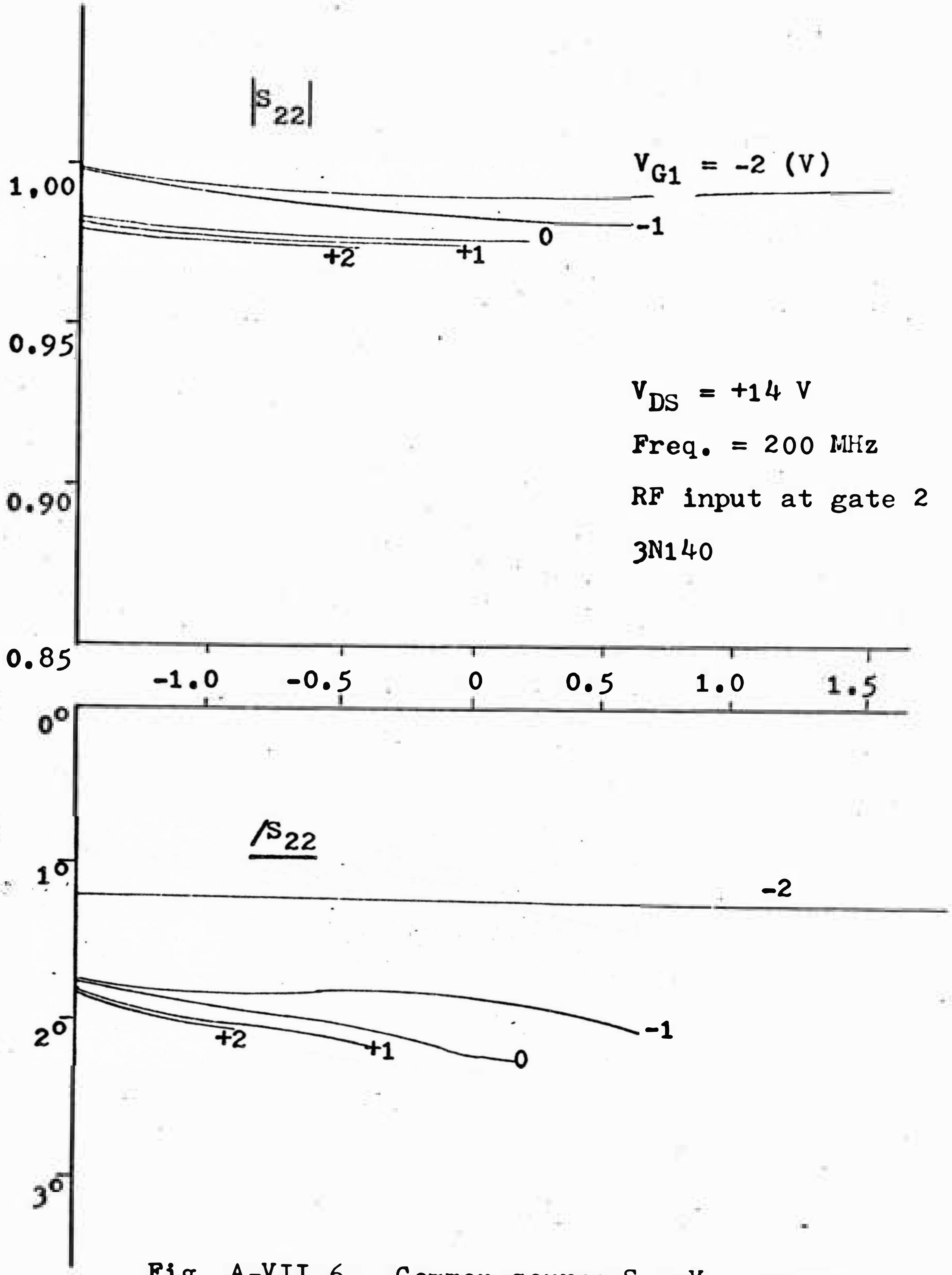

Fig. A-VII-6. Common-source S_{22}-V_{G2} curves (Dual-gate MOSFET).

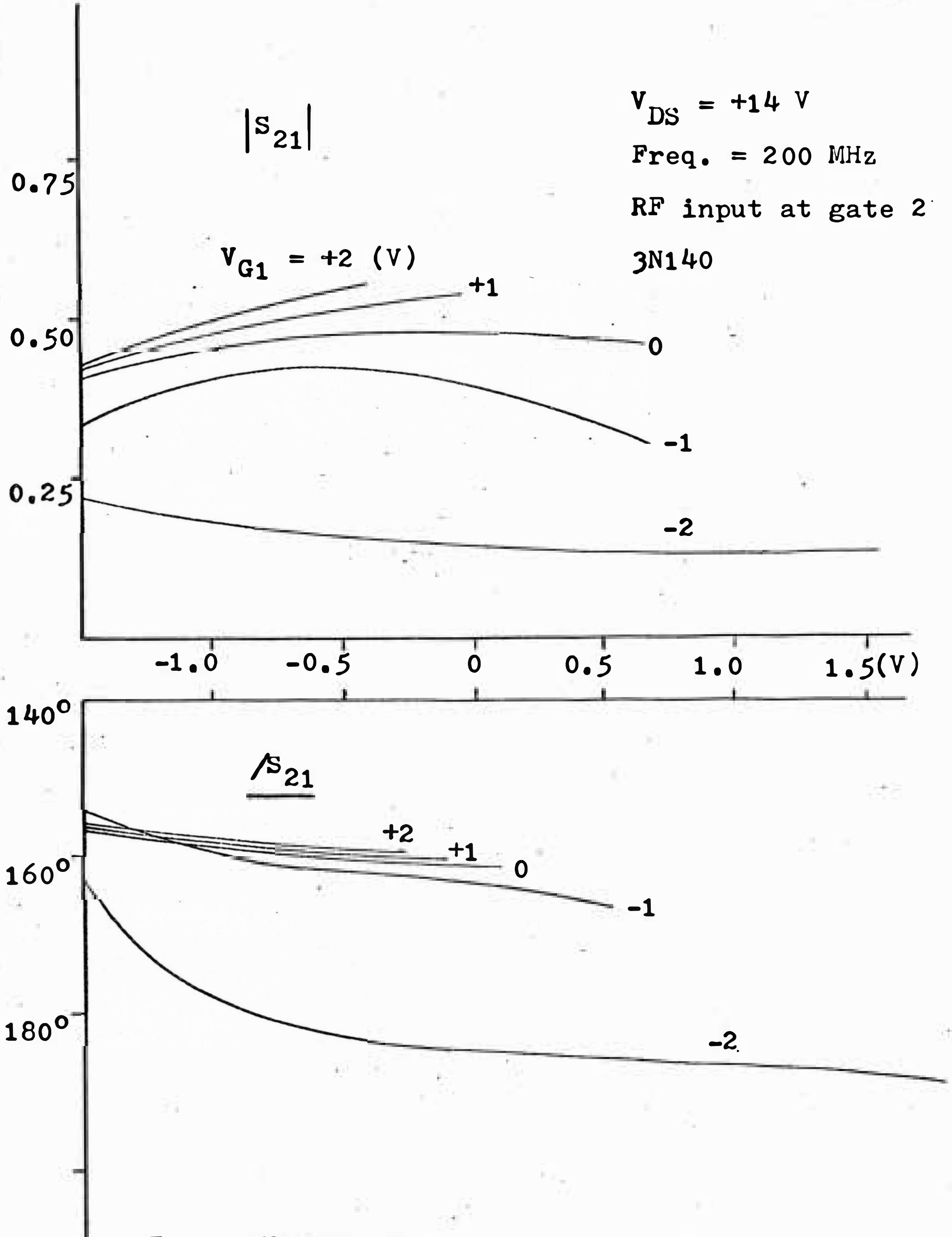

Fig. A-VII-7. Common-source S_{21}-V_{G2} curves (Dual-gate MOSFET)

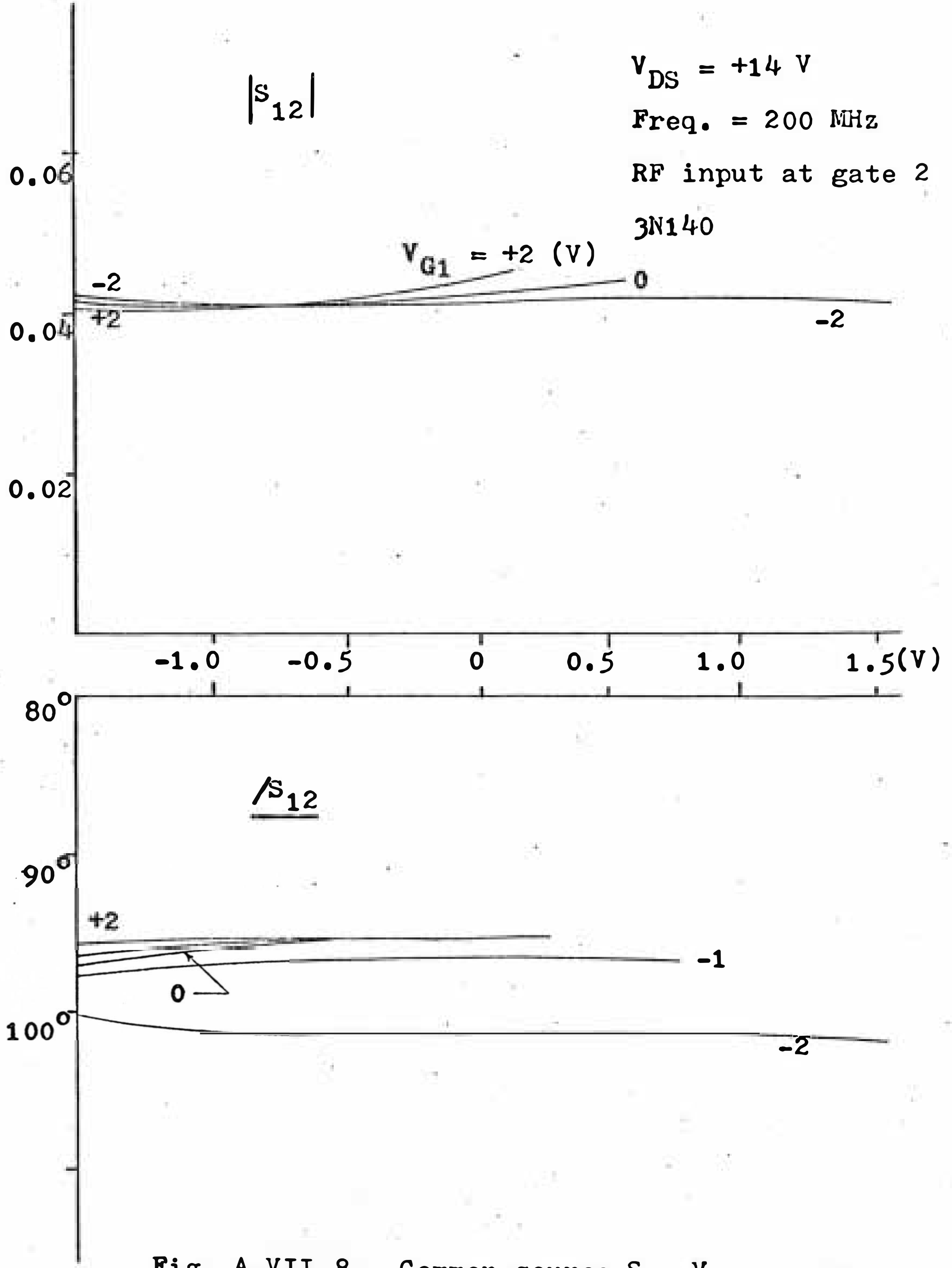

Fig. A-VII-8. Common-source S_{12}-V_{G2} curves (Dual-gate MOSFET).